GKSS
FORSCHUNGSZENTRUM
in der HELMHOLTZ-GEMEINSCHAFT

Comparison of measured and simulated wind speed data in the North Atlantic

(Vom Department Geowissenschaften der Universität Hamburg als Dissertation angenommene Arbeit)

Author:

J. Winterfeldt

ISSN 0344-9629

HELMHOLTZ
| GEMEINSCHAFT

wissen
schafft
nutzen

GKSS 2008/2

GKSS 2008/2

Comparison of measured and simulated wind speed data in the North Atlantic

(Vom Department Geowissenschaften der Universität Hamburg als Dissertation angenommene Arbeit)

Author:

J. Winterfeldt

(Institute for Coastal Research)

GKSS-Forschungszentrum Geesthacht GmbH · Geesthacht · 2008

Die Berichte der GKSS werden kostenlos abgegeben.
The delivery of the GKSS reports is free of charge.

Anforderungen/Requests:

GKSS-Forschungszentrum Geesthacht GmbH
Bibliothek/Library
Postfach 11 60
D-21494 Geesthacht
Germany
Fax.: (49) 04152/871717

ISSN 0344-9629

GKSS-Forschungszentrum Geesthacht GmbH · Telefon (04152) 87-0
Max-Planck-Straße 1 · D-21502 Geesthacht / Postfach 11 60 · D-21494 Geesthacht

GKSS 2008/2

Comparison of measured and simulated wind speed data in the North Atlantic

(Vom Department Geowissenschaften der Universität Hamburg als Dissertation angenommene Arbeit)

Jörg Winterfeldt

113 pages with 36 figures and 6 tables

Abstract

A systematic investigation and comparison of near-surface marine wind speed obtained from in situ and satellite observations, atmospheric reanalyses and regional atmospheric hindcasts with reanalysis driven regional climate models (RCMs) is presented for the eastern North Atlantic and the North Sea.

Wind speed retrievals from two remote sensing data sets, namely QuikSCAT and the Hamburg Ocean Atmosphere Parameters and Fluxes from Satellite (HOAPS) data set, are found to give good representation of observed near-surface wind speed. The value of the root mean squared error (RMSE) for all co-located HOAPS and in situ wind speed data is 2 m/s, while it is 1.8 m/s for QuikSCAT demonstrating that QuikSCAT's mission requirement of providing wind speed with an RMSE of 2 m/s is met for the eastern North Atlantic and the North Sea. QuikSCAT shows a slightly better agreement with observed instantaneous wind speed and its frequency distribution than HOAPS. In contrast, HOAPS wind speed is available for a much longer period and is therefore the more suitable product for climatic studies or investigations of trends in wind speed.

The capability of two state-of-the-art RCMs (with and without spectral nudging applied) to add value for surface marine wind fields in comparison to the reanalysis wind speed forcing is assessed by the comparison with in situ wind speed observations in the eastern North Atlantic in 1998. The comparison of the 10 m wind speed forecasts from the NCEP/NCAR and NCEP/DOE-II reanalyses with in-situ observations demonstrates the implausibility of the latter forecast resulting in its non-consideration in the added value assessment. The added value is investigated for instantaneous wind speeds (relevant for case studies) and their frequency distribution (relevant for e.g., extreme value statistics and estimations of wind potential). The observations are discriminated into groups according to their proximity to land and assimilation status, meaning whether they are assimilated into the reanalysis or not.

For open ocean areas no value added to the reanalysis forcing is found by the use of the RCMs neither for instantaneous wind speed nor its frequency distribution. The RCMs add value in the wind speed frequency distribution in coastal areas, especially for higher wind speed percentiles. In case of rough coastal areas with a complex orography added value is indicated also in the instantaneous wind speeds. In comparison to the unnudged simulation the spectrally nudged simulations better represent both observed instantaneous wind speed and its frequency distribution. An influence of the observations' assimilation status on these findings can not be seen.

Windgeschwindigkeit im Nordatlantik – Vergleich von Messungen und Modellen

Zusammenfassung

Für das Gebiet des östlichen Nordatlantiks und der Nordsee werden oberflächennahe marine Windgeschwindigkeiten von in situ- und Satellitenbeobachtungen, atmosphärischen Reanalysen und regionalen atmosphärischen Rekonstruktionen mit Regionalklimamodellen (RCMs) untersucht und systematisch miteinander verglichen.

Die fernerkundeten Windgeschwindigkeiten von QuikSCAT und HOAPS (Hamburg Ocean Atmosphere Parameters and fluxes from Satellite data) zeigen eine gute Übereinstimmung mit in situ-Beobachtungen. Der RMSE zwischen in situ- und HOAPS-Windgeschwindigkeiten liegt bei 2 m/s, für QuikSCAT liegt er bei 1,8 m/s. QuikSCAT zeigt eine leicht bessere Übereinstimmung mit dem beobachteten „instantanen" Wind und dessen Häufigkeitsverteilung. HOAPS ist für einen längeren Zeitraum erhältlich als QuikSCAT und damit eher geeignet für die Untersuchung von Trends der Windgeschwindigkeit und Klimastudien.

Die Fähigkeit zweier RCMs (mit und ohne Verwendung des spektralen Nudgings), im Vergleich zur antreibenden Reanalyse einen Mehrwert für marine Windgeschwindigkeiten zu erzeugen, wird durch den Vergleich mit in situ-Messungen untersucht. Die Mehrwertuntersuchung wird für „instantane" Windgeschwindigkeiten (relevant für Einzelfallstudien) und deren Häufigkeitsverteilungen (relevant z. B. für Extremwertstatistiken und die Abschätzung des Windpotentials) durchgeführt. Auf Grund der unplausiblen 10-m-Windvorhersage der NCEP/DOE-II-Reanalyse wird die NCEP/NCAR-Reanalyse für die Mehrwertanalyse herangezogen. Die in situ-Beobachtungen werden im Zuge der Untersuchung bezüglich ihrer Küstennähe und der Assimilation in die Reanalyse unterteilt.

An küstenfernen Stationen ergibt sich mit der gewählten Untersuchungsmethode für die bodennahe Windgeschwindigkeit kein Mehrwert durch die Benutzung von RCMs. In küstennahen Gebieten generieren die RCMs allerdings einen Mehrwert in der Häufigkeitsverteilung, insbesondere für die höheren Perzentile. In Küstengebieten mit stark gegliederter und komplexer Orographie wird ein Mehrwert auch für den „instantanen" Wind sichtbar. Im Vergleich zur ungenudgten Simulation zeigen die spektral genudgten Simulationen eine bessere Übereinstimmung mit dem beobachteten „instantanen" Wind und dessen Häufigkeitsverteilung. Diese Resultate sind unabhängig davon, ob die jeweils betrachtete Windbeobachtung in die Reanalyse assimiliert wurde.

Manuscript received / Manuskripteingang in TKP: 26. Februar 2008

Danksagung - Thanks

I would like to acknowledge the assistance of the following people. I am deeply grateful to

- My advisory panel with the principal advisor Hans von Storch, Co-Advisor Ralf Weisse and panel chair Stephan Bakan for the scientific discussions, valuable suggestions and ideas and the close guidance. Their experience helped me to limit my pool of ideas to what is possible within the time frame agreed upon and necessary for a sound thesis layout.
- the IMPRS-ESM for establishing the advisory panel system, which I consider as an ideal tool to reduce the time burden on a PhD student, which is, as far as I am concerned, also in the student's interest.
- F. Feser for the provision of the SN-REMO and STD-REMO data and all the help and discussions.
- B. Geyer for the provision of the CLM data and the whole Atmospheric Modelling group at GKSS for the assistance.
- NCAR for supplying the NCEP/NCAR and NCEP/DOE reanalyses and Chi-Fan Shih (NCAR) for the provision of PREPBUFR files and the support.
- Wesley Ebisuzaki (Climate Prediction Center, NCEP) for fruitful comments on both reanalyses.
- Met Office UK, especially B. Hall for his help, DNMI, KNMI, DWD and BSH for supplying observation data.
- The Physical Oceanography Distributed Active Archive Center (PO.DAAC) at the NASA Jet Propulsion Laboratory for the free provision of QuikSCAT's SeaWinds data.
- A. Andersson, A. Blechschmidt, C. Klepp and K. Fennig from the HOAPS team for their help with obtaining and working with HOAPS.
- B. Gardeike for rearranging the figures making them readable and clear.

- the DFG for funding this work within the special research project 512.
- Dennis Bray, Matthias, Sebastian and Ivonne for proof reading.
- anyone I forgot.

Above all I would like to thank my family for their constant support.

Most importantly I thank my girl friend for her invaluable love, patience and support.

Contents

List of Figures

List of Tables

Chapter 1

Introduction

The scope of this work is:

- a comparison of different existing data sets of near-surface marine wind speed for European waters, namely the Northeast Atlantic and the North Sea, regarding their quality with respect to
  - instantaneous values and,
  - their frequency distribution.
- to elaborate on the added value of near-surface marine wind fields derived from regionally and dynamically downscaled global reanalyses compared to the reanalyses themselves.

Europe and the adjacent waters of the eastern North Atlantic and the North Sea lie within the mid-latitude storm track and are therefore particularly prone to mid-latitude cyclones. Extreme wind speeds and heavy precipitation linked with these cyclones can seriously affect both the adjacent coastal and inland regions. For example, Central Europe was hit by three violent storms in December 1999, which claimed more than 130 lives and caused about 13 billion Euro of total economic losses. The gust wind speeds recorded from the three winter storms 'Anatol', 'Lothar' and 'Martin' were around 50 m s^{-1} or 180 km h^{-1} (Ulbrich et al., 2001). The winter storm Lothar on 24-26 December 1999 was one of the most harmful storms in Central Europe in the last decades causing huge damage to buildings and forests in France, Southern Germany, Switzerland and Austria. More than 50 people were killed in the storm (Wernli et al., 2002).

Storms over sea cause storm surges and high waves and thus form a hazard to navigation, coasts and marine infrastructure among others. The winter gale 'Britta' on the 1 November 2006 led to individual wave height reaching up to 18 m in the North Sea, damaging the measurement platform FINO at this level. Several ships got into distress in both the North and the Baltic Sea with the freighter

"Finnbirch" capsizing. Both Anatol and Britta caused severe storm surges. Improved coastal protection measures currently reduce the damage to human life and public and private assets as compared to earlier devastating floods in Hamburg in 1962 and the Netherlands in 1953 (e.g., Gerritsen 2005; Jung et al. 2004, 2005).

For the design and the maintenance of coastal protection measures, long and homogeneous time series of wind, waves and surge are necessary, to derive their statistics (in especially extreme value statistics) and to analyse long-term changes and trends. Additionally, these time series are needed for a variety of applications, e.g. the design and maintenance of offshore installations such as platforms and wind farms.

However for marine areas, long and homogeneous data sets are rare, also for the Northeast Atlantic and the North Sea. Time series of in-situ wind speed measurements (e.g. from buoys, platforms, rigs, lightships) are usually short and local. While wind speed retrievals from satellites can give a broader spatial picture of the wind field, they are available only for even shorter periods. Alternatively, global reanalyses or regional atmospheric hindcasts driven by reanalyses are frequently used as a reality substitute, but they are limited to periods for which reliable weather analyses can be provided (typically since about the 1950's).

Despite their shortcomings, all data sets are commonly used to assess e.g. statistics of extreme events. However, a systematic investigation and comparison of near-surface marine wind speed from all these products is lacking for European waters. The first major outcome of this study will be the comparison of different existing products of near-surface marine wind speed regarding their quality with respect to instantaneous values and their frequency distribution in the Northeast Atlantic and the North Sea. Emphasis is given to a comparison of the wind speed retrievals of two remote sensing data sets, namely QuikSCAT and the Hamburg Ocean Atmosphere Parameters and Fluxes from Satellite (HOAPS) data set, with in-situ wind, which has, it appears, not been previously attempted. Elaboration of the advantages and disadvantages of all investigated data sets will also be presented.

In the case of missing or insufficiently homogeneous data regional atmospheric hindcasts are frequently used as a reality substitute, either to analyse long-term changes and trends (e.g., Fowler and Kilsby 2007; Weisse et al. 2005) or as forcing for other, e.g. hydrologic, wave or storm surge models (e.g. Gaslikova and Weisse 2006; Sotillo et al. 2005; Federico and Bellecci 2004; Kim and Lee 2003). Regional atmospheric hindcasts are usually obtained from regional climate models (RCMs) driven by global reanalyses. This method of deriving smaller-scale information with a limited-area, high-resolution model using boundary conditions from a global model (such as a reanalysis) is called dynamical downscaling. How-

ever, it remains unclear whether or not dynamically downscaled wind speed adds value to the wind speed directly obtained from the reanalysis. Thus, a simple, but unanswered question, is addressed.

Does the dynamical downscaling approach add value for near-surface marine wind fields in comparison to the reanalysis wind speed forcing?

The question is examined using two different state-of-the-art RCMs, namely REMO (REgional MOdel) and CLM (Climate Local Model), utilizing both the conventional and the spectral nudging approach. The added value is investigated for instantaneous wind speed (relevant for case studies) and its frequency distribution (relevant for e.g., extreme value statistics and estimations of wind potential).

The definition of added value used in this study is:

- For instantaneous marine surface wind speed: The RCM adds value to the reanalysis, if the 10 m wind speed obtained from the RCM hindcast shows a better agreement with measured instantaneous wind speed at 10 m height than the wind speed of the forcing reanalysis.
- For marine surface wind speed frequency distributions: The RCM adds value to the reanalysis, if the 10 m wind speed obtained from the RCM hindcast shows a better agreement with observed 10 m wind speed frequency distributions than the wind speed of the forcing reanalysis.

To judge if a RCM provides more realistic wind fields in this respect, both RCM and reanalysis wind speed are compared with in-situ data from buoys, ships and platforms in the eastern North Atlantic and the North Sea.

The Thesis is structured as follows. The different wind speed data sets are introduced in Chapter 2. First the set of in-situ surface marine observations is described. The second part of this chapter discusses the basic concepts of remote sensing focusing on wind speed retrieval from SSM/I and the SeaWinds radiometer, the instruments used in the HOAPS and QuikSCAT data sets. Finally the reanalyses and hindcasts with the RCMs REMO and CLM are presented.

In Chapter 3 the wind speed from QuikSCAT and HOAPS are compared to observations. In Chapter 4 the concept of added value is introduced and the method to determine it is explained. Following that, the added value of the hindcasts in comparison to the reanalysis forcing is assessed including a discussion of the results. In Chapter 5 an outlook on how QuikSCAT and HOAPS can be used in the added value assessment is presented.

Section A in the appendix introduces some properties of the wind field in the

North Atlantic considered to be helpful for the understanding of this thesis. The different scales of motion are introduced and the composition of the Planetary Boundary Layer and the effects of stability on the vertical wind profile are explained. Some effects of ocean-atmosphere and land-sea interaction are described.

Section B.1 introduces the spectral nudging technique after von Storch et al. (2000) which is applied in the SN-REMO and CLM hindcasts used in this study. Due to an unresolved compatibility issue between the NCEP/NCAR Reanalysis and the REMO preprocessor, both STD-REMO and SN-REMO hindcasts are forced with the NCEP/DOE-II Reanalysis from March 1997 onwards. This change in reanalysis forcing may cause inhomogeneities. Elaboration on this issue is made in Chapter B in the appendix.

Chapter 2

Data Sets

This Chapter introduces the different marine surface wind speed data sets used in this study. In-situ surface marine wind speed is typically measured at a height of 10 m or, if measured at other heights, is usually converted to 10 m, especially in wind speed comparison studies. Furthermore, wind speed retrieval algorithms of satellite products are tuned to provide 10 m wind speed. Consequently, 10 m wind speed is employed in this analysis as measure for surface marine wind speed.
Wind speeds at 10 m height obtained from the following sources are used:

- in-situ observations,
- two satellite wind speed sources: the Hamburg Ocean Atmosphere Parameters and Fluxes from Satellite (HOAPS) data set and retrievals from the QuikSCAT mission satellite,
- the NCEP/NCAR-Reanalysis (NRA_R1) and NCEP-DOE Reanalysis II (hereafter: NRA_R2),
- two regional atmospheric hindcasts with the Regional Climate Model (RCM) REMO, one standard simulation without spectral nudging applied (STD-REMO) and one with spectral nudging applied (SN-REMO),
- one regional atmospheric hindcast with the RCM CLM, with spectral nudging applied,

The temporal and spatial dimensions of these surface marine wind products are given in Table 2.1.

The wind speeds given by the different products are averages over certain time intervals, which for the reanalyses and the RCMs are equivalent with the model's integration time step. While HOAPS and QuikSCAT measure microwave radiation almost instantly, the incoming radiation is averaged over a wide area as

Table 2.1: *Description of the different wind speed data sets: The time interval and the area over which the wind speed is averaged is given. The temporal resolutions with which the data are submitted and the periods for which the data were available for this study are also listed. For further explanations see text.*

Data	time interval for averaging	Resolution spatial	temporal	Availability
in-situ	10-17 min	point	1h	1998, 2002
HOAPS	inst.	≈ 50 km	0-6/day	1987 - 2005
QuikSCAT	inst.	12.5x12.5 km	0-2/day	1999 - present
NRA_R1	20 min	1.875x1.875°	6h	1948 - present
NRA_R2	20 min	1.875x1.875°	6h	1979 - present
SN-REMO	5 min	0.5°x0.5°	1h	1948 - 2006
STD-REMO	5 min	0.5°x0.5°	1h	1989 - 1999
CLM	4 min	0.44°x0.44°	1h	1998

depicted by the spatial resolution. Thus HOAPS and QuikSCAT wind speed retrievals cannot be considered as instantaneously measured wind speeds. Furthermore HOAPS' resolution is dependent on the detected frequencies within the different microwave channels, as will be described later (see Table 2.3). The wind speed comparison is limited to the periods of the data sets with the lowest data availability, which are the in-situ observations (measurements from all considered in-situ stations were available for 1998 only, for some in 2002 in addition). In 1998 and 2002 the multi-satellite product HOAPS combines up to six overflights per day, which, depending on the amount of rain contaminated measurements, can result in between zero and six wind speed measurements per day. The QuikSCAT satellite only delivers two overflights per day, but it's wind speed product has a much finer resolution than HOAPS. While the spatial resolutions of the RCMs are comparable to HOAPS, their temporal resolution is higher, as they deliver one wind speed value per hour. The 10 m wind speed forecast of both reanalyses have, by far, the coarsest resolution both in space and time, their integration time step of 20 min is also considerably larger than those of the RCMs. Nevertheless, they have the highest availability periods and the RCMs depend on them for boundary conditions and forcing.

The different data sets will be described in detail hereafter.

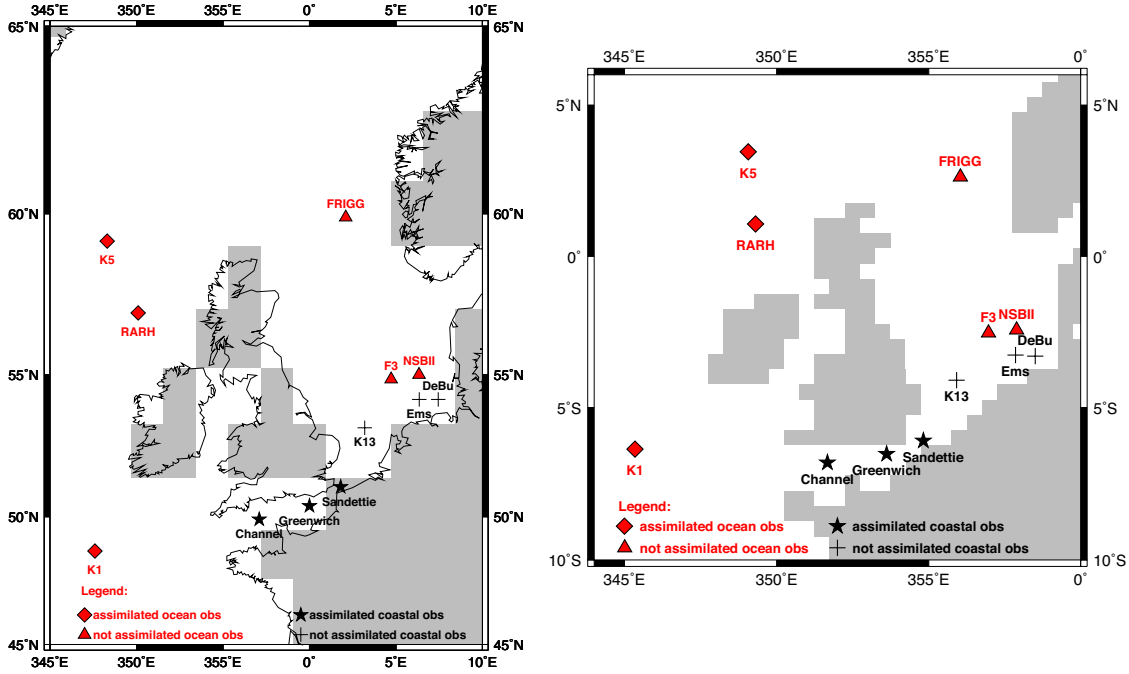

Figure 2.1: *Locations of wind speed observations (obs) over land sea masks of NRA_R1 (left) and REMO (right, rotated coordinate system).*

2.1 In-situ surface marine observations

The in-situ surface marine wind speed observations used in this study are depicted in Figure 2.1 over the underlying land sea masks of the NCEP/NCAR Reanalysis and the RCM REMO. The discrimination of the observations, as illustrated by the different symbols and colours, are discussed in detail in Chapter 4. The wind speed data from the buoys K1, K5 and RARH and the light ships Channel (Chan), Greenwich (GRW) and Sandettie (Sand) were obtained from the UK Meteorological Office (Met Office). Wind speed measurements at the oil rigs F3 and K13 came from the Dutch Koninklijk Nederlands Meteorologisch Instituut (KNMI), at the oil rig Frigg from the Norwegian Meteorologisk institutt (DNMI). The German institutions Deutscher Wetterdienst (DWD) and Bundesamt für Seeschifffahrt and Hydrographie (BSH) delivered data from the light ships Ems and Deutsche Bucht (DeBu) and the North Sea Buoy II (NSBII). The observations are described in Table 2.2.

It is important to note that more surface marine wind speed observations exist for the North Sea and the eastern North Atlantic. Obtaining this data, however, is difficult and time consuming as it has to be ordered from different institutions of the adjacent countries. Furthermore each institute uses different measurement

Table 2.2: *Marine wind speed observations, their location, platform type and measurement height z_{obs}.*

Name	lon °E	lat °N	Type	z_{obs}
K1	-12.4	48.7	buoy	3 m
K5	-11.7	59.2	buoy	3 m
RARH	-9.9	57.0	buoy	3 m
Frigg	2.1	59.9	rig	95 m
F3	4.73	54.85	rig	59 m
NSBII	6.33	55.0	buoy	10 m
K13	3.2	53.2	rig	74 m
Ems	6.35	54.17	ship	10 m
DeBu	7.45	54.17	ship	10 m
Chan	-2.9	49.9	ship	14 m
GRW	0.0	50.5	ship	14 m
Sand	1.8	51.1	ship	14 m

systems and data formats. In most cases the obtained data were not checked for errors. Despite all these drawbacks the data are, depending on the institution, often not without cost for scientific use. The combined effect of these handicaps is that the marine surface wind speed measurements in the eastern North Atlantic and the North Sea have been rarely considered in any wind speed comparison studies. Consequently this study is perhaps the first that combines marine surface wind speed measurements from the five institutions from four countries mentioned for a detailed wind speed comparison in the eastern North Atlantic.

These limitations meant only 12 wind speed observations were used in this study. Furthermore, data from all 12 stations were available only for 1998. The year 1998 was chosen, simply because the wind speed observations available prior to this study had a maximum temporal overlap in 1998. Obtaining both additional wind speed observations or more measurement years was considered an disproportionate effort due to the reasons mentioned above. Additional data was acquired solely for 2002 for the comparison with wind speed retrievals from the QuikSCAT mission satellite which started operations in 1999. The year 2002 was also chosen for data availability reasons.

All in-situ data were checked for errors. Unplausible wind speed data were replaced by error values. As listed in Table 2.2, most in-situ wind speeds were measured at heights other than 10 m. As it was decided upon that wind speed

be at 10 m height as measure for surface marine wind, these wind speeds had to be converted from the anemometer height to 10 m height. The wind speed data obtained from KNMI and DNMI (K13, F3 and Frigg) were already converted to 10 m with constant factors based on the logarithmic wind profile and a constant sea roughness. For this study wind measurements from the Met Office buoys and light ships were converted using the COARE bulk flux algorithm in version 3.0b after Fairall et al. (2003). Bulk flux algorithms represent the interfacial turbulent fluxes of momentum, sensible heat, and latent heat in terms of the bulk meteorological, near-surface variables of wind speed, air temperature, humidity, and the sea surface temperature through empirical transfer coefficients. Consequently, in addition to the wind speed, air temperature, relative humidity and sea surface temperature data were obtained for the Met Office buoys and light ships for the conversion of the wind speed to 10 m height after Fairall et al. (2003). Records with unplausible wind speed, air and sea temperature were not converted and thus not considered in the analyses. The influence of the relative humidity on the wind speed conversion is minor as compared to the air-sea temperature difference (e.g. Babin and Thompson 2000, their Figure 2). Therefore, if relative humidity data was missing, a relative humidity of 75 % was assumed, which is a typical value given by the in-situ observations.

2.2 Satellite Data

Surface marine wind speeds from two satellite data sets are used in this study, stemming from the Hamburg Ocean Atmosphere Parameters and Fluxes from Satellite (HOAPS) data set and from retrievals from the QuikSCAT mission satellite. HOAPS's and QuikSCAT's wind speed are based on measurements with several Special Sensor Microwave/Imagers (SSM/I's) and the SeaWinds scatterometer, respectively. Both HOAPS and QuikSCAT retrieve the wind speed by measuring the sea surface roughness, either directly (QuikSCAT) or indirectly (HOAPS). The next sections describe the basic principles and methodologies behind these conversions.

In general, satellite marine surface wind speed data are transformations of electromagnetic radiation signals detected by sensors onboard of satellites. The electromagnetic radiation received at the antenna has three principal sources: black body radiation emitted from the earth surface, reflected solar radiation and energy pulses emitted by satellite radars. The spectral radiance L_ν emitted by a black body is given by Planck's equation

$$L_\nu(\nu, T) = \frac{2h\nu^3}{c^2} \cdot \frac{1}{\exp(h\nu/k_B T) - 1}. \tag{2.1}$$

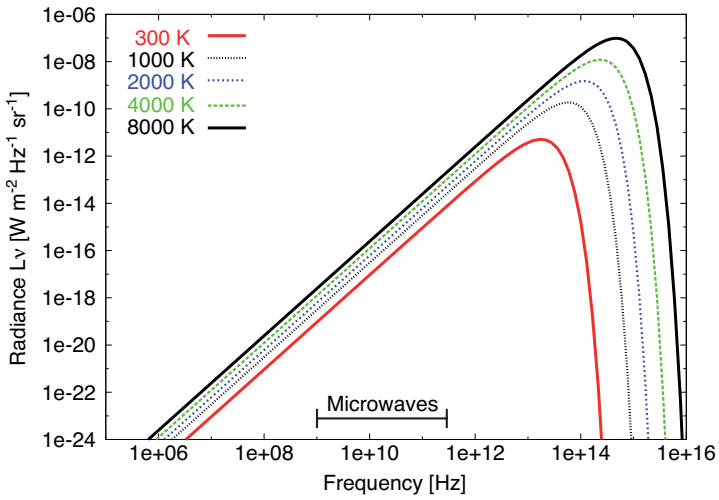

Figure 2.2: *Spectral Radiance L_ν emitted from black bodies at different temperatures. For microwaves L_ν depends linearly on temperature (Rayleigh-Jeans approximation), the frequency of maximum radiance follows Wien's displacement law.*

where ν is the frequency, T is the absolute temperature, c is the speed of light, h and k_B are the Planck and Boltzmann constants, respectively. Three important quantities can be derived from Planck's equation, which is depicted in Figure 2.2. First the total emitted radiance increases with T^4, known as Stefan-Boltzmann Law. Second, by setting the first derivation of Planck's equation to zero, Wien's displacement law can be derived. Thus, λ_{max} and ν_{max}, the wavelength and frequency of maximum radiance can be determined for any black body with $\lambda_{max} = 2879\ \mu\text{m K} / T$ and $\nu_{max} = 5.87 \cdot 10^{10}\ \text{Hz K}^{-1} \cdot T$ respectively. The maximum black body radiance of the earth with $T = 300$ K is therefore emitted at wavelengths around 10 μm (at frequencies around 20 THz) which is in the thermal infrared.

Third, for long wavelengths λ satisfying the inequality $hc/\lambda k_B T \ll 1$, which is the case for microwaves emitted from the earth, the spectral radiance L_ν is a linear function of temperature and the Rayleigh-Jeans approximation holds:

$$L_\nu = \frac{2\nu^2 k_B}{c^2} \cdot T. \tag{2.2}$$

The Rayleigh-Jeans approximation enables the radiative transfer equation to be written in form of brightness temperatures instead of radiances.

The properties of the received radiation also depend on the way it is altered

by its propagation through the atmosphere. Due to reflection and absorption within the atmosphere, remote sensing is conducted in certain bands in the visible (VIS), infrared (IR) and microwave wavelength range. Remotely sensed wind speed data is only obtained within the microwave bands, where microwaves occupy the part of the electromagnetic spectrum between 1 - 500 GHz in frequency, or 0.3 m - 1 mm in wavelength.

The main advantage of microwave instruments is that microwave radiation naturally emitted or reflected from the Earth's surface and lower layers of its atmosphere is only minimally influenced by non-precipitating clouds. This permits sea surface roughness to be evaluated, and with it, wind speed to be retrieved under all weather conditions except heavy rain (e.g. Executive Summary in Barrett et al. 1997).

Microwave instruments are classified as active or passive instruments. Passive instruments, such as the Special Sensor Microwave/Imager (SSM/I) observe either reflected solar radiation or the naturally emitted blackbody radiation. In contrast, active measurements are made by radars that transmit pulses of energy towards the ocean surface, then receive the backscatter, so that the radar provides its own illumination. Active microwave instruments include imaging radars (the Synthetic Aperture Radar or SAR), directed, pulsed vertical beams (altimeter), several pulsed fan beams or rotating pulsed beam (scatterometers).

Microwave instruments, such as the passive SSM/I and the active SeaWinds instrument on the QuikSCAT mission satellite, directly or indirectly measure the small scale roughness of the ocean surface, which is assumed to be in equilibrium with the wind stress at the ocean surface. The same wind speed at a given height z above the sea surface can result in varying wind stress at the surface. This difference is due to the turbulence occurring between z and the surface, which is determined by the stability of the atmosphere. The same wind speed at z would lead to a higher (lower) near surface wind speed in an unstable (stable) atmosphere as turbulence is increased (suppressed) and the momentum is more easily (heavily) transferred from z to the surface.

In-situ observations measure the actual wind speed at the height of the anemometer. Since the direct comparison with microwave winds is erroneous, the in-situ winds are usually converted to a 10-m equivalent neutral-stability wind (e.g. Freilich and Dunbar 1999; Ebuchi et al. 2002; Pickett et al. 2003; Chelton and Freilich 2005). This is the wind speed, that for a given surface stress, would be observed at a height of 10 m, assuming that the atmosphere is neutrally stable. Thus it can be considered to be a measurement of surface stress expressed in units of wind speed (Mears et al. 2001, p. 7ff). The model functions of SSM/I and QuikSCAT are directly or indirectly tuned to the 10-m equivalent neutral-

stability winds determined from buoy measurements. Therefore HOAPS and QuickSCAT wind measurements represent neutral stability 10-m wind.

The SSM/I and QuikSCAT's SeaWinds instrument are introduced in more detail in the following sections, their capabilities and limitations in providing information on wind speed are discussed.

2.2.1 SSM/I & HOAPS

Table 2.3: *The channel abbreviation includes the information about its capability to measure vertically or horizontally polarized radiation (V=Vertical, H=Horizontal), e.g. the channel "19V" measures vertically polarized radiation at frequencies around 19.35 GHz. Its integration time of 7.95 ms results in footprint sizes of 70 km cross-scan and 45 km along-scan.*

Channel	Center Frequency (GHz)	Center Wavelength (mm)	Integration Time (ms)	Footprint Size Cross-Scan (km)	Along-Scan (km)
19V	19.35	15.49	7.95	70	45
19H	19.35	15.49	7.95	70	45
22V	22.235	13.48	7.95	60	40
37V	37.0	8.10	7.95	38	30
37H	37.0	8.10	7.95	38	30
85V	85.5	3.51	3.89	16	14
85H	85.5	3.51	3.89	16	14

The US Special Sensor Microwave/Imager (SSM/I) has operated with a number of replacements on the US Department of Defense Meteorological Satellites Program (DMSP) satellites since June 1987. All DMSP satellites are in a near polar, sun synchronous orbit, meaning that throughout the year each orbit crosses the equator at the same local time of day, at an altitude of approximately 830 km above the earth with an orbital period of about 101 minutes. Sun-synchronous orbits are described in terms of their daytime equatorial crossing times and their inclination, which is about 98.8° for all DMSP satellites. The SSM/I is a conically scanner that operates with an incidence angle of $\theta = 53°$. The radiometric characteristics of the seven SSM/I channels are listed in Table 2.3.

The choice of the SSM/I channels was motivated by both the position of specific microwave bands, where the atmosphere is mostly transparent, and absorption bands, where the terrestrial radiation is attenuated through molecular absorption/emission. The absorption bands of oxygen and water vapour are distin-

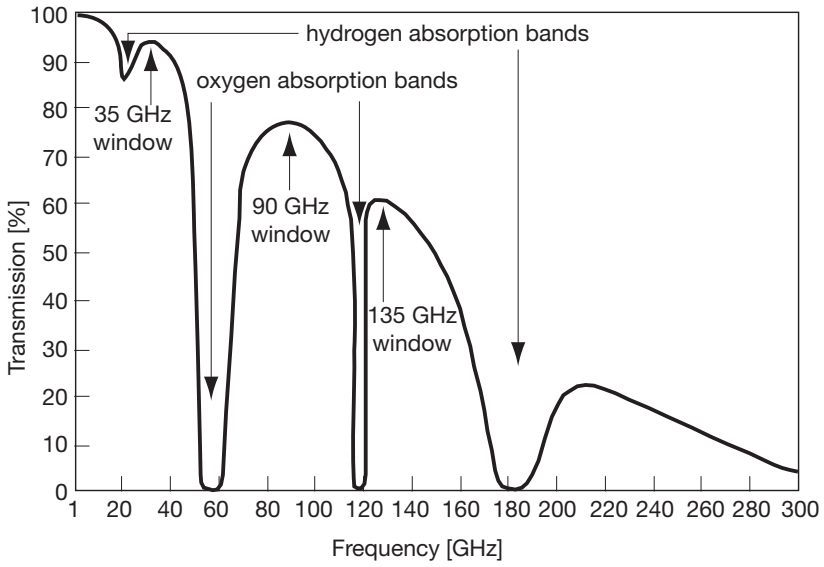

Figure 2.3: *Transmission of the atmosphere in the microwave range, taken from Ulaby et al. (1981).*

guishable in Figure 2.3. In the frequency range of 1-15 GHz and in the 35 GHz window the atmosphere is practically transparent, even in the presence of clouds and light rain (Fennig 2001, p. 8f), which allows for the measurement of surface properties such as vegetation and marine wind speed (Goodberlet et al., 1989). Furthermore the water vapour content of the atmosphere can be determined by measurements around the center of the water vapour absorption band at 22.2 GHz (Schluessel and Emery, 1990). With measurements in the 90 GHz window the columnar liquid water content can be derived, as the scatter of terrestrial radiance at cloud droplets and rain drops is very effective in this frequency range (Bauer and Schluessel, 1993). While the ocean emits polarized radiation, the emissions from the atmosphere are unpolarized. With the measurement of both horizontally and vertically polarized radiation atmospheric emissions can be identified and the original surface emissions can be derived (Schluessel and Luthardt, 1991).

One complete conical scan takes 1.899 seconds, the active scan area is limited to an angle of 102.8 degrees corresponding to scanned arcs and a 1400 km swath on the Earth's surface. Complete coverage of the earth is provided every two to three days, except for small patches near the poles. Each scan (arc) is separated by 12.5 km along the ground track direction. The footprint for each SSM/I frequency is an ellipse with the cross scan axis (being parallel to the satellite ground track only in the precise center of the SSM/I scan) and the along-scan axis as major and semi-major axes. Their sizes are displayed in Table 2.3 (for a more

detailed description of the SSM/I please refer to Davis 1999).

The emissivity of open calm sea water is relatively low and increases with frequency from 0.4 (at 19 GHz) to 0.6 (at 85 GHz). The range of sea surface temperatures from 270 K to 310 K leads to brightness temperatures from 150 K at 19 GHz to 240 K at 85 GHz. Calm open ocean appears to the SSM/I as a cool, homogeneous, polarized background. The presence of clouds, rain, water vapor, wind or surface roughness changes the ocean signal substantially which allows their accurate measurement (Davis, 1999)

Wind blowing across the water surface roughens the surface and produces foam, both effects increase sea surface emissivities. Capillary waves cause the greatest changes in microwave emissivity as they are approximately the same size as the microwave wavelengths. They are very responsive to changes in wind speed being quickly created by small gusts and dissipated in calm winds. The sensitivity of the SSM/I to wind at low speeds is due primarily to the effect of capillary waves on microwave emissivity. The effect from capillary waves saturates at 12-15 m/s. Above these speeds the effect of foam is dominant. For wind speeds greater than 15 m/s the majority of the energy due to wind speed detected from the orbiting SSM/I may be due to foam, whose emissivity, under the right conditions, can approach unity.

As brightness temperatures are increased by surface roughness, any phenomenon that roughens the surface could result in erroneous wind speeds. Rain is the most common culprit. Wind speed is not accurate in areas of heavy rain and even light rain will degrade the signal. The degree to which wind speed estimates are degraded by rain is indicated by the rain flag (Davis, 1999).

The total amount of extinction of the surface emission caused by spherical and near-spherical water droplets as primary components of low- and mid-altitude clouds (cumulus, stratus etc.) increases with the thickness and water content of the cloud. Thick clouds with a high water content have high emissivities, too. Thus the signal from the surface is not only masked but replaced by denser clouds.

HOAPS

The Hamburg Ocean Atmosphere Parameters and Fluxes from Satellite (HOAPS) data set is a multi satellite product over the global ice free oceans (Table 2.4). All variables are derived from SSM/I measurements, except for the SST which stems from the NODC/RSMAS Pathfinder data set. To derive the HOAPS data set the different contributing SSM/I instruments were intercalibrated using F11

Table 2.4: *HOAPS is a multi satellite product consisting of measurements from all available SSM/I instruments providing utilisable data. The DMSP satellites with SSM/I instruments and the time span they are used in the HOAPS-3 data base, as determined by the start and end dates, are listed. Their equatorial crossing time (ECT) is given as Local Time (LT) or Local Solar Time (LST). NOTE: F10 did not achieve the desired orbit, as a result the equator crossing time is increasing by approximately 45 minutes per year (see* `http://daac.gsfc.nasa.gov/guides/GSFC/guide/dmsp_f10.gd.shtml`*)*

satellite	start date	end date	ECT (local solar time)
F08	1987-07-09	1991-12-31	06:17 a (LT)
F10	1991-01-07	1996-12-31	22:09 a (LT)
F11	1992-01-01	1999-12-31	18:25 a (LT)
F13	1995-09-01	2005-12-31	18:33 a (LST)
F14	1997-06-01	2005-12-31	19:08 a (LST)
F15	2000-03-01	2005-12-31	21:05 a (LST)

as reference satellite and the method described in Fennig (2001). The wind speed algorithm in the current HOAPS-3 data set uses a neural network to derive the wind speed at 10 m height above the sea surface from SSM/I measurements. It consists of 3 layers: an input layer with 5 neurons (brightness temperatures from the 19V, 19H, 22V, 37V, 37H channels, described in Table 2.3), a hidden layer with 3 neurons and an output layer with one neuron (wind speed). The network was trained with a composite data set of buoy measurements and radiative transfer simulations.

Pixels containing substantial atmospheric contamination (rain) are filtered in HOAPS to avoid mis-detection of wind speeds. The detection is done by brightness temperature thresholds for 19 and 37 GHz channels. If one of these thresholds is exceeded the corresponding pixel is flagged and wind values are not calculated. For rain rates above 6 mm/h all pixels are flagged (Andersson, personal communication).

Three HOAPS-3 data sets are available, HOAPS-G and HOAPS-C can be obtained from the CERA database at http://cera-www.dkrz.de/CERA/:

- HOAPS-G: The default spatial resolution of HOAPS-G is 0.5 degrees on a global grid. Pentade, monthly and climatological monthly means are available, consisting of multi-satellite averages including all SSM/I instruments available at the same time.

- HOAPS-C: This data set contains 1 degree twice daily globally gridded multi-satellite composite products, providing high temporal resolution. Each

grid-cell contains data from only one satellite pass, there is no average from two or more satellites

- The HOAPS-S data set contains all retrieved physical parameters in the original SSM/I scan resolution for every individual satellite. HOAPS-S data is used as input to obtain HOAPS-G and HOAPS-C and is not provided with the CERA data base but only on request via email for specified limited time periods.

Only, the HOAPS-S data set is used for direct comparisons with observation data in this study. For a more detailed description of HOAPS-3 please refer to Andersson et al. (2007a,d,c,b) or the HOAPS website at www.hoaps.org.

2.2.2 QuikSCAT

The US launched the SeaWinds scatterometer on the QuikSCAT mission satellite in 1999. The description of its working principle follows Martin (2004) and Ulaby et al. (1982). The SeaWinds scatterometer is an active microwave radar with dual-beam, conical scan 1 m diameter reflector (rotating dish) antenna, operating in Ku-band at 13.402 GHz. At this frequency the atmosphere has a very high transmissivity (as depicted in Figure 2.3). The inner beam operates at HH polarization (only horizontally polarized radiation is transmitted and detected) at an antenna look angle of 40° and an incidence angle of 47°. The outer beam operates at VV, an antenna look angle of 46° and an incidence angle of 55°. The SeaWinds instrument has a total swath width of 1800 km, with a swath width of 900 km on both sides of the satellite ground track.

Following Chelton et al. (2001) for a perfectly transmissive atmosphere and a non-emitting surface and in the special case of a narrow beam scatterometer pointed at the ocean surface and a small enough field-of-view (FOV) of area ΔA_{FOV} the radar equation can be written as

$$\sigma_0 = (\Phi_R/\Phi_T) \left[R_0^4 (4\Pi)^3\right] / \left[\lambda^2 G_0^2 \Delta A_{FOV}\right] \tag{2.3}$$

where σ_0 is the normalized radar cross section (NRCS), Φ_R/Φ_T the ratio of received to transmitted power at the antenna, R_0 the distance between antenna and surface, G_0 the boresight antenna gain and λ the wavelength of the radar pulse. With the antenna properties and the FOV known, σ_0 is a measure for surface properties as the small scale sea surface roughness which in turn is a measure for the local wind.

However, in reality Equation 2.3 is too simplified and corrections for atmospheric attenuation and the contributions from the various emission terms must be included in the σ_0 retrieval, as the received power Φ_R is the sum of the received

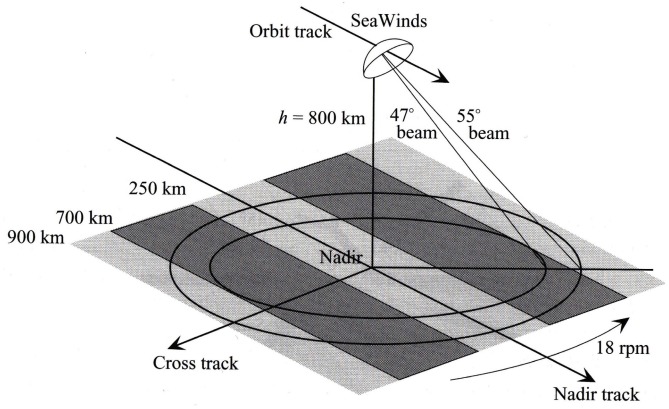

Figure 2.4: *Conceptual design of the dual-beam SeaWinds scatterometer: In the darker parts of the swath, the wind solution is determined from four looks, in the light parts from two looks. Taken from Martin (2004), who adapted it from an unpublished figure of Michael Freilich.*

power that is attenuated Φ'_σ and the thermal noise Φ_{TN}:

$$\Phi_R = \Phi'_\sigma + \Phi_{TN}. \tag{2.4}$$

Φ_{TN} is in turn the sum of the instrument noise Φ_N and the sum of environmental emissions Φ_B. As a reminder: While the latter is noise for scatterometers, it is the measured signal of passive microwave instruments such as the SSM/I.

The wavelength and incidence angles of the SeaWinds microwaves is such that they are primarily backscattered by centimeter-sized ripples (capillary waves). The density and distribution of ripples respond very quickly to changes in winds and has relatively little sensitivity to larger waves, making it very practical for determining surface winds and wind stress (Weissman et al., 2002). Furthermore a series of experiments (e.g. Jones and Schroeder 1978) had shown that small scale surface roughness and resultant σ_0 are generated locally and are independent of fetch and swell height. However, in their comparison of buoy wind speed in the range of 9 to 12 m/s with QuikSCAT Ebuchi et al. (2002) found a weak positive correlation of the wind speed residuals (QuikSCAT-buoy) with the significant wave height and the inverse wave age implying that higher and older dominant wind waves may cause enhanced radar backscattering under the same wind conditions.

While for instruments with near nadir incidence angles ($\theta <\approx 10°$) the backscatter decreases with increasing wind speed (as the increasing roughness scatters

more radiation away from the receiving antenna), the return of instruments with $\theta >\approx 15°$, such as the SeaWinds Scatterometer, increases with u due to Bragg scattering. Bragg resonance occurs if a surface wave component exists with a λ_w equal to half the surface projection of the radar wavelength λ or a multiple of it:

$$\lambda_w = n \cdot \lambda/(2 \sin\theta), \quad n = 1, 2, 3, 4, \ldots \tag{2.5}$$

Incoming radar radiation scattered incoherently at surface wave components that fulfill Equation (2.5) add coherently to a strong return at the antenna. Given that the wind generates a continuous spectrum of short ocean waves, resonant waves are generally present. As surface roughness increases with wind speed, Bragg scatter increases with u.

Wind speeds can be determined from multiple SeaWinds measurements of σ_0 if the functional relation between σ_0 and the near surface wind is known. The most general description of this relation, called the *geophysical model function* (or *model function*) gives σ_0 as a function of the polarization P (either HH or VV), wind speed u, incidence angle θ and wind direction (here as ϕ_R the azimuthal angle relative to the wind direction):

$$\sigma_0 = f(P, u, \theta, \phi_R), \tag{2.6}$$

As the two beams of the SeaWinds scatterometer have constant incident angles and polarizations, σ_0 is merely changed by u and ϕ_R. After Martin (2004) (and references therein) for constant u and fixed θ and polarization, the σ_0 dependence on ϕ_R is commonly described by an empirically derived truncated Fourier series called the two-cosine function

$$\sigma_{0P} = A_{0P}(1 + A_{1P} \cos\phi_R + A_{2P} \cos 2\phi_R + \ldots), \tag{2.7}$$

where the subscript P again stands for polarization and the coefficients are empirically derived by the comparison between the scatterometer winds and other satellite and surface data sets.

Figure 2.5 shows the dependence of σ_0 on wind speed and direction for the QuikSCAT model function. The radar return resembles a cosine function as described by Equation (2.7). The increased return with higher u due to Bragg scattering is also visible. The radar return is highest for upwind and downwind directions that coincide with the occurrence of the largest wave slopes for these directions (Cox and Munk, 1954). This difference in the upwind and crosswind σ_0, called the upwind/crosswind ratio, permits the retrieval of the wind direction. The upwind return is a bit higher than the downward return, called the upwind/downwind asymmetry. It is largest for small wind speeds and can be explained by the presence of foam and the growth of parasitic short capillary waves

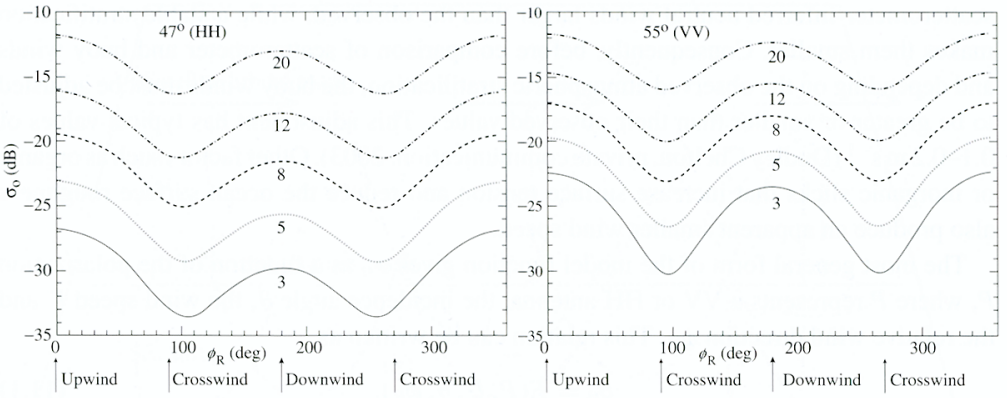

Figure 2.5: *The SeaWinds Geophysical Model Function for the inner beam (left, with incidence angle θ=47° and polarization P=HH) and outer beam (right, θ=55°, P=VV). The wind speed is given in m s^{-1} as numbers below the curves of constant wind speed. The upwind direction is at ϕ_R=0°, downwind at ϕ_R=180°.* ©*Michael Freilich*

on the downwind faces of longer waves (Martin 2004, p.280). This asymmetry makes the retrieval of a unique wind solution possible.

In this study the Level 2B 12.5 km Composite (CP12) data set is used. From σ_0 measurements the CP12 wind speed is determined in 12.5 km squares, the so called wind vector cells (WVCs). The CP12 data are provided as 152 WVCs across the satellite's path, consisting of 144 WVCs across the swath (1800 km / 12.5 km = 144) and six additional WVCs at the end of each WVC row to allow for occasional measurements outside the swath. Each WVC contains up to four possible wind vector solutions. These solutions are ranked according to a maximum-likelihood estimator based on the backscatter measurements (Long and Mendel, 1991). From this ranking, a single wind vector is then selected using an ambiguity-removal algorithm. This algorithm employs a modified median filter technique (Shaffer et al., 1991) that makes a selection based on three factors: ranking from the maximum-likelihood estimator, consistency with a NCEP numerical weather product and agreement with the surrounding (7x7) WVCs. The cross-track WVC location has an influence on the accuracy of the wind speed solution, however Ebuchi et al. (2002) found this dependence to be insignificant.

2.3 Reanalyses and hindcasts with RCMs

Three regional atmospheric hindcasts are used in this study. The SN-REMO and STD-REMO hindcasts were generated and described by Feser et al. (2001). The CLM hindcast was provided by the Regional Atmospheric Modelling group at

GKSS. All hindcasts are initialized and forced with reanalyses. The reanalyses and the models and the model setup of the hindcasts are described in the following sections.

2.3.1 Reanalyses

The global reanalysis of atmospheric fields from National Centers of Environmental Prediction (NCEP) and National Center for Atmospheric Research (NCAR) involves the recovery of land surface, rawinsonde, pibal, aircraft, satellite, surface marine (ships, buoys, oil rigs, C-man platforms) and other data (Kalnay et al. 1996, Kistler et al. 2001). These data are quality controlled and assimilated with a data assimilation scheme that is kept unchanged over the reanalysis period to eliminate perceived climatic changes due to changes in the data assimilation scheme.

In Figure 2.6 a schematic diagram of the assimilation system is represented as described in Kanamitsu (1989). In the NCEP/NCAR-Reanalysis (NRA_R1) the original optimum interpolation (OI) step is replaced by the spectral statistical interpolation (SSI), a three dimensional variational analysis after Parrish and Derber (1992) and Derber et al. (1991).

Steps	Component		Input/Output	Form of the Fields
	18Z			
			Forecast	Sigma level spherical coefficients
1.	00Z	Pre-processing		
			Observation correction	Values at obs. points (pressure)
2.	00Z	OI Analysis/SSI		
			Analysis correction	Values on analysis grids (pressure)
3.	00Z	Update		
			Analysis	Sigma level spherical coefficients
4.	00Z	Initialization		
			Initialized	Sigma level spherical coefficients
5.	00Z	Forecast		
			Forecast	Sigma level spherical coefficients
	00Z	Pre-processing		

Figure 2.6: *Diagram of the NCEP assimilation scheme, adapted from Kanamitsu (1989). In the NCEP/NCAR-Reanalysis the SSI is used instead of the OI.*

Briefly the reanalysis assimilation scheme works as follows: The 6h forecast

started from the previous analysis serves as the first-guess field. In the SSI step, differences between the assimilated observations and the first guess-field are determined, which deliver the analysis correction. The analysis is updated with the analysis correction in the next step. The initial field for the next 6h forecast is determined from the analysis in the fourth step. Finally the forecast creates the guess for the next analysis step. The forecast model used is the T62/28-level NCEP global spectral model. The details of the model dynamics and physics are described in NOAA/NMC (1988), Kanamitsu (1989) and Kanamitsu et al. (1991)

The observation data gathered for the assimilation comes from many different sources. Prior to the assimilation they are preprocessed and reformatted into a uniform BUFR-format. PREPBUFR-files (BUFR events archive) in which the assimilation status of observations into the NRA_R1 is given, were obtained from NCAR for utilization in the determination of added value in Chapter 4.

In addition two NRA_R1 data sets, provided by the NOAA-CIRES Climate Diagnostics Center (USA) from their Web site at http://www.cdc.noaa.gov/, were used:

- The global atmospheric NRA_R1 as forcing for the regional simulations.
- The forecast 10 m horizontal wind speed components valid 6 hours after the reference time on a T62 gaussian grid with a resolution of 1.875° x 1.875° for the comparison with modelled and observed 10 m wind speeds.

The NCEP-NCAR Reanalysis is available from 1948 to present, the newer reanalysis from NCEP and the Department of Energy (DOE), the NCEP-DOE Reanalysis II (NRA_R2), is available from 1979 to present. The NRA_R2 provided upgrades to the forecast model and a diagnostic package (Kanamitsu et al., 2002). Off these changes in the NRA_R2, the implementation of the Hong-Pan planetary boundary layer non-local vertical diffusion scheme (Hong and Pang, 1996), a smoothed orography and the different convective parameterizations may cause changes in the wind speed relative to NRA_R1. NRA_R2's forecasted 10 m horizontal wind components valid 6 hours after the reference time are used for the comparison with modelled and observed 10 m wind speeds, too. It is given on the same T62 gaussian grid as the NRA_R1 forecast.

2.3.2 Regional Models and Model Setup

REMO is a regional hydrostatic atmospheric model (Jacob and Podzun, 1997). It has been developed from the Europa-Modell (EM) of the German Weather Service/Deutscher Wetterdienst (DWD), its dynamics are based on the primitive equations in a terrain-following hybrid coordinate system with 20 vertical layers. The prognostic variables of the model are surface pressure, specific humidity,

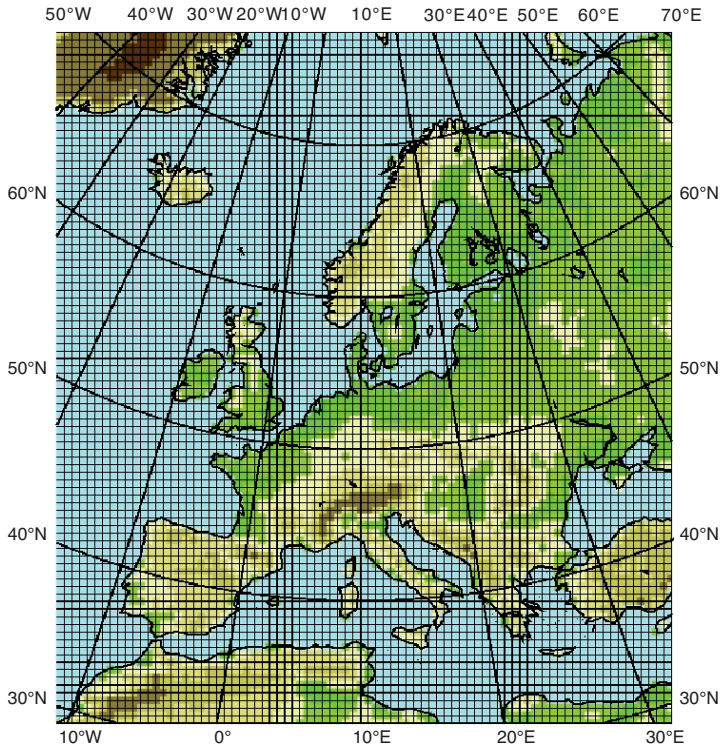

Figure 2.7: *Model domain of both SN-REMO and STD-REMO. ©B. Geyer*

liquid water, and horizontal wind components. REMO is set up in its climatic mode using the same parameterization scheme as in the global climate model ECHAM4 (Roeckner et al., 1996). Vertical diffusion and turbulent surface fluxes are resolved from Monin-Obukhov theory after Louis (1979).

To allow nearly equally spaced grid boxes the spherical coordinate system is rotated with the equator in the centre of the model area. The modelled domain consists of 81 x 91 grid boxes with a horizontal resolution of 0.5° ($\approx$ 50 km). Feser et al. (2001) generated the current 58-year (1958 - 2006) central european hindcast by forcing REMO with the NRA_R1 atmospheric global reanalysis with the spectral nudging method after von Storch et al. (2000) applied. Elaboration on the spectral nudging method is made in section B.1 in the appendix. Feser et al. (2001) applied spectral nudging from the 850 hPa level upwards with increased nudging with height. The nudging parameter was set to $\alpha = 0.05$.

In addition to this spectrally nudged REMO simulation (SN-REMO), a standard REMO simulation (STD-REMO), utilizing the conventional approach to

drive RCMs, is examined in this study. STD-REMO is available from 1989 to 1999. The North Pole for both hindcasts is at 35°N, 170°W, the modelled domain covers almost the whole eastern North Atlantic and is depicted in Figure 2.7. Apart from the spectral nudging both simulations have an identical model set up. This allows an assessment of the spectral nudging approach regarding the quality of simulated near-surface marine wind fields.

In addition, a simulation with CLM (Böhm et al., 2006) is used in this study, which allows the investigation of the effects of different RCMs on the added value assessment. CLM is the climate version of the non-hydrostatic Local Model (LM) provided by the German Weather Service (DWD). Physics and dynamics of the CLM are taken from the operational weather prediction model LM (Doms et al. 2005, Doms and Schättler 2005). The spectrally nudged CLM simulation was run with a higher nudging parameter $\alpha = 0.5$ on a rotated coordinate system with 105 x 115 grid boxes, a resolution of 0.44°x0.44° and a North Pole at 39.25°N, 162°W. It is initialized and updated at the lateral boundaries every six hours by the NRA_R2.

All three simulations deliver diagnostic 10 m wind speed, meaning that the 10 m wind speed is calculated from the prognostic wind speed at the lowest model level, being 32 m for both REMO simulations and 34 m for CLM.

Chapter 3

Comparison of in-situ wind speed with HOAPS and QuikSCAT

Marine near-surface wind speed measurements are rare, especially far offshore. For wide areas in the eastern North Atantic and the North Sea no in-situ measurements exist. Satellite wind speed retrievals are available over the global oceans and have the potential to reduce that information gap. Therefore, several national weather services started to assimilate satellite wind speed retrievals to improve weather forecasts or plan to do so. Several remote sensing instruments exist, that can deliver wind speed: e.g. altimeters, synthetical aperture radars (SAR), scatterometers, such as the SeaWinds scatterometer onboard the QuikSCAT satellite, and the SSM/I's utilized in the HOAPS data set.

However, all satellite instruments have their drawbacks. Their measurements are typically disturbed by rain. At best, two overpasses of the same satellite occur over a certain region per day. Thus, the temporal availability of wind speed retrievals is very limited. Furthermore, satellites cannot retrieve wind speed within a certain distance to the coast and in shallow seas.

This Chapter elaborates on the comparison of HOAPS and QuikSCAT with in-situ wind speed. HOAPS is chosen because it is one of the longest data sets of remotely sensed wind speed. QuikSCAT wind speed retrievals are chosen because they give a better spatial resolution than HOAPS. The direct comparison of in-situ wind speed with microwave winds is erroneous, as HOAPS and QuickSCAT wind speed retrievals represent neutral stability 10 m wind, while in-situ observations, in turn, measure the actual wind speed at the height of the anemometer. Therefore the in-situ winds are typically converted to the so called 10 m equivalent neutral-stability wind following Liu and Tang (1996).

However, this study does not follow this approach, as the focus of this study is not to judge the capability of HOAPS and QuikSCAT to measure 10 m equivalent

neutral-stability winds. The focus is on the capability of HOAPS and QuikSCAT to reproduce the measured 10 m wind, as given by the in-situ wind speed using the COARE bulk flux algorithm in version 3.0b after Fairall et al. (2003) for the stability and anemometer height correction. Thus the HOAPS and QuikSCAT 10 m neutral-stability winds are compared to 10 m winds at measured stability conditions. For this comparison it is important to note, that in case of an unstable atmosphere QuikSCAT and HOAPS would tend to overestimate real 10 m wind speed. Contrarily in the case of a stable atmosphere real 10 m wind speed is underestimated.

However, the differences should be negligible for the following reason: In their comparison of eleven years of SSM/I wind speed with 60 buoys, Mears et al. (2001) converted the buoy wind to 10 m with the 10-m equivalent neutral-stability wind method after Liu and Tang (1996) and also with the logarithmic wind profile as described in Equation A.6. They found that the wind speed error due to the stability differences in the two methods is only about 0.1 m/s. Chelton and Freilich (2005) verified this secondary importance of atmospheric stability on the comparison of scatterometer to buoy wind. Furthermore wind speed profile measurements at the metmast FINO in the North Sea showed that stability conditions are near-neutral half of the time (50% neutral, 34% unstable, 16% stable, Kay Sušelj, University of Oldenburg, ForWind, pers. comment).

3.1 Comparison of HOAPS with in-situ wind speed

The scope of this section is first to explain how HOAPS is compared to the in-situ wind speed and second, to discuss the results of the comparison.

3.1.1 Method

The HOAPS-S data set (hereafter: HOAPS) from the current HOAPS-3 version is used for the direct comparisons with in-situ wind speed in the year 1998, for which in-situ data from 12 stations are available. The in-situ wind speed at 10 m height and that of HOAPS are co-located in space and time as follows: Whenever the distance between the footprint center of a HOAPS wind speed pixel and the in-situ observation is smaller than 0.3° in longitudinal and 0.2° in latitudinal direction (approximately half the footprint size of the 37 GHz channel) and the HOAPS record time is within 10 minutes from the in-situ observation time, the HOAPS wind speed is compared to the in-situ data.

For most overflights several wind speed pixels fulfill the criterion. Typically one would choose the closest HOAPS pixel for the co-location with the in-situ wind

speed. Different to that approach all pixels fulfilling the criterion are co-located here. That means for instance if two HOAPS wind speed pixels fulfill the criterion, they are both co-located with the same in-situ wind speed. Consequently, the same in-situ measurement would enter the comparison twice.

In-situ data of the lightships GRW, Chan, Sandettie and DeBu cannot be compared with HOAPS, as all HOAPS wind speed retrievals within 50 km of any land mass are masked, due to its disturbing influence on the signal at the SSM/I. At the remaining 8 stations the instantaneous co-located wind speed data are compared in 1998, regarding their respective annual means, the standard deviation σ of each data set, as well as the correlation coefficient R and the root mean square error (RMSE) between the two data sets. The RMSE is given by

$$\mathrm{RMSE} = \sqrt{\frac{1}{n}\sum_{i=1}^{n}(x_i - y_i)^2}, \tag{3.1}$$

where x and y are the n co-located in-situ and HOAPS wind speed records. The RMSE is related to the bias and the standard deviation of the differences between the records of the two data sets σ_d by

$$\begin{aligned} \mathrm{RMSE}^2 &= \mathrm{bias}^2 + \sigma_d^2 \\ &= (\overline{x_i - y_i})^2 + (\sigma(x_i - y_i))^2. \end{aligned} \tag{3.2}$$

Henceforth the standard deviation of the differences σ_d is not used or displayed in the comparison, since it can be easily derived from the bias and the RMSE by this relation. Instead the standard deviation σ of the data sets will be compared, for a data set x it is given by:

$$\sigma = \sqrt{\frac{1}{n-1}\sum_{i=1}^{n}(x_i - \overline{x})^2}, \tag{3.3}$$

where x_i and $\overline{x}$ represent the individual records of the data set and their mean value, respectively. The correlation coefficient R between x and y is defined as:

$$R = \frac{\frac{1}{n}\sum_{i=1}^{n}(x_i - \overline{x})(y_i - \overline{y})}{\sigma_x \sigma_y}, \tag{3.4}$$

where $\overline{x}$ and $\overline{y}$ are the mean values and σ_x and σ_y are the standard deviations of x and y, respectively.

Furthermore HOAPS' capability to reflect observed wind speed frequency dis-

tributions is investigated by the means of quantile-quantile plots of the in-situ versus HOAPS' wind speed percentiles.

3.1.2 Results and Discussion

Instantaneous wind speed

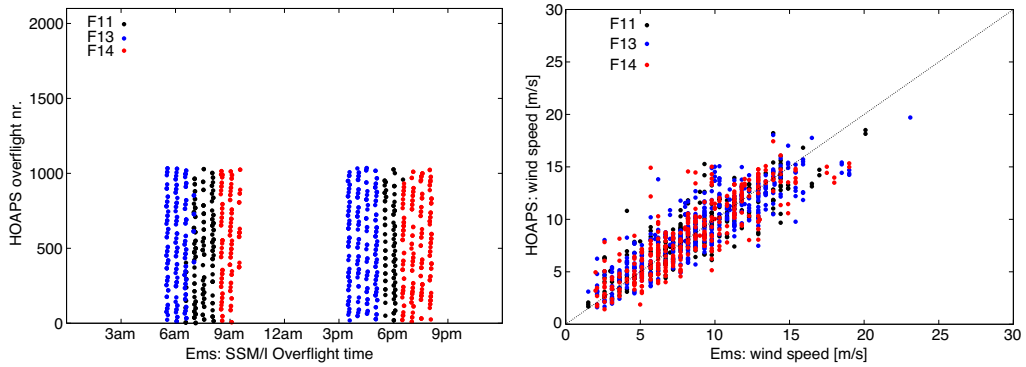

(a) (b)

Figure 3.1: *3.1(a) shows the DMSP satellites' overflight times for the co-located wind speed records at Ems in 1998. 3.1(b) is a Scatter Plot of the co-located HOAPS and in-situ wind speeds at Ems. Records originating from the different DMSP satellites are highlighted in black (F11), blue (F13) and red (F14) in both plots.*

Each DMSP satellite crosses the equator several times a day at the same local solar time, thus their overflight times are limited to certain narrow time windows. Consequently a single SSM/I instrument can not represent daily cycles in wind speed, e.g. sea breezes. Although HOAPS combines the SSM/I measurements of the DMSP satellites F11, F13 and F14 in 1998, the combined time window is larger, but still constrained to four and a half hours in the morning and four and a half hours in the evening, as shown in Figure 3.1(a). Hence there still is the probability of missing daily cycles. Figure 3.1(b) illustrates that the intercalibration of the different SSM/I instruments after Fennig (2001) successfully avoids any systematic wind speed bias between the different SSM/I instruments.

HOAPS tends to overestimate the annual mean wind speed at the open ocean stations while it gives a good representation of the mean wind speed in the German Bight (NSBII, K13 and Ems), as depicted in Figure 3.2(a). At around 1.5 to 2.5 m/s, this bias is strongest for RARH, K5 and FRIGG. There is good agreement between observed and HOAPS wind speed variability, as given by the standard deviation in Figure 3.2(a).

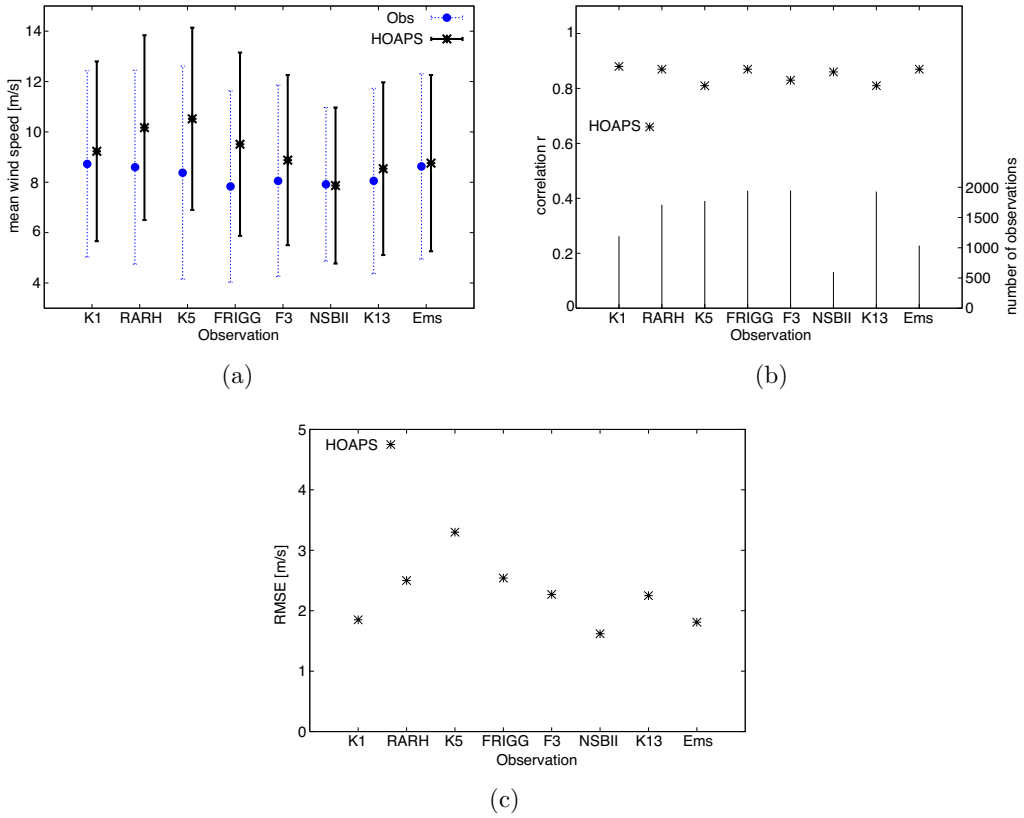

Figure 3.2: *Comparison of the co-located HOAPS and in-situ wind speed measurements in 1998. The mean wind speed is given in a) together with the standard deviation as error bars ($\pm\sigma$). b) Number of co-locations and correlation coefficient and c) RMSE between HOAPS and in-situ wind speed.*

Correlation coefficients between in-situ and HOAPS wind speed are larger than 0.8. The lowest correlations are found at K5 and K13. The RMSE varies between about 1.5 and 2.5 m/s, however at K5 the RMSE of 3.5 m/s is exceptionally high, mainly caused by a strong wind speed bias.

The average RMSE of around 2 m/s is a bit higher than the average RMSE found in earlier studies. For instance, Krasnopolsky et al. (2000) and Meng et al. (2007) used neural network multiparameter algorithms for SSM/I ocean retrievals and found RMSE values of 1.7 m/s and 1.48 m/s for wind speed. While Wentz (1992) and Wentz (1997) found RMSE of 1.6 m/s and 1.3 m/s respectively, Mears et al. (2001) found an overall bias of 0.11 m/s and RMSE of 1.25 m/s. Mears et al. (2001) compared wind speed of around hundred bouys from the National Data Buoy Center (NDBC) and the Tropical Atmosphere Ocean (TAO) project

with SSM/I retrievals for a period of 11 years showing a regional dependence of the SSM/I wind speed bias. Differentiated into several regions Mears et al. (2001) determined RMSE values of 1.49 m/s for the western North Atlantic and the Gulf of Mexico and 1.33 m/s for the North Pacific. One explanation for the higher RMSE found in this study may be that the development of SSM/I wind speed retrieval algorithms (including the HOAPS algorithm) and their tuning was realized with the help of in-situ observations from the NDBC and TAO buoy networks. As opposed to the mentioned studies, the in-situ measurements used in this study have not been used in the tuning of the HOAPS and SSM/I algorithms. Thus, the smaller RMSE found by other studies might be caused, at least in part, by the comparison with data used in the SSM/I calibration process. Another contribution to the RMSE error might stem from comparing HOAPS' neutral-stability winds to 10 m winds at measured stability conditions. However, as mentioned before, this contribution should be minor.

Wind speed frequency distribution

The wind speed frequency distribution is elaborated by means of percentile-percentile or quantile-quantile plots (qq plots). In these qq-plots, as illustrated in Figure 3.3, wind speed percentiles derived from HOAPS are plotted over observed percentiles in steps of one percent percentiles.

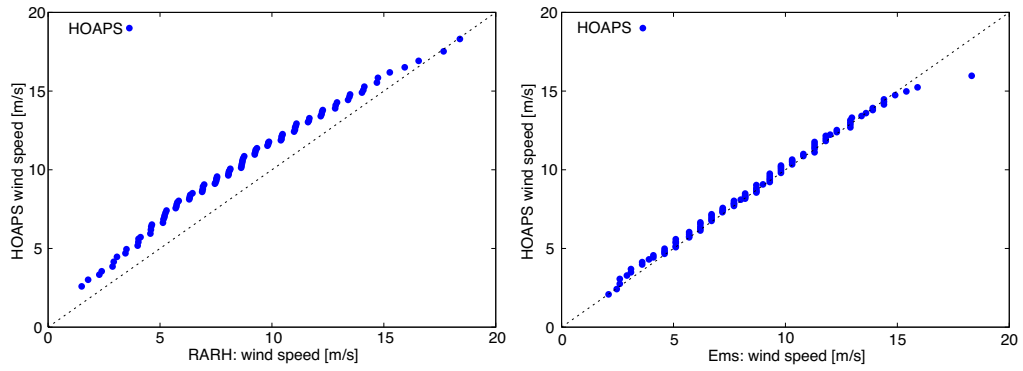

(a) (b)

Figure 3.3: *Percentile-percentile distributions of wind speed in 1998, measured (x-axis) vs. HOAPS (y-axis) at a) RARH and b) Ems. The 99 dots represent the wind speed percentiles in steps of 1 percent. Thus the first (last) dot represents the 1st (99th) percentile and the wind speed below which one (99) percent of all in-situ and HOAPS measurements can be found, respectively. In the ideal case of perfect agreement between in-situ and HOAPS wind speed frequency distributions all percentiles would lie on the bisector line.*

The positive bias of HOAPS in the open ocean is reflected in the percentile distribution, as depicted in Figure 3.3(a) for RARH, which is representative for the other open ocean stations. The wind speed percentiles of HOAPS are in general 1 to 2 m/s higher than those measured at RARH, which corresponds with the bias of around 1.5 m/s determined at RARH (Figure 3.2(a)). There is an apparent saturation for the highest wind speed percentiles, where HOAPS' wind speed bias is lower or not existing. The saturation at the upper end of the wind speed frequency distribution function is characteristic for HOAPS and may be due to emissivity saturation because of foam and wave crest blow-off in mature seas. Mears et al. (2001) found the same characteristics for a buoy in the Northwest Atlantic (NDBC bouy 44004 as depicted in their Figure 5) but not in general for their complete bouy-SSM/I intercomparison. In addition, wind speed retrievals from SSM/I measurements with a multiparameter neural network showed underestimations of high wind speeds (Meng et al. 2007, their Figure 3a).

In the North Sea at K13, NSBII and Ems HOAPS better fits the observed distributions, exemplarily shown for Ems in Figure 3.3(b). This is in agreement with the lower bias and the better representation of the wind speed variability observed at these stations.

3.2 Comparison of QuikSCAT with in-situ wind speed

This section is structured as follows: First the comparison method between QuikSCAT wind speed retrievals and in-situ wind speed is described, afterwards the results are presented and discussed.

3.2.1 Method

The wind speed of the QuikSCAT Level 2B 12.5 km Composite (CP12) dataset is compared with marine 10 m wind speed observations in 2002. They are co-located in space and time as follows. The CP12 WVC footprint is approximately 12.5 km x 12.5 km. Whenever the distance between the WVC center and the in-situ observation is smaller than 0.1° in longitudinal and 0.06° in latitudinal direction (approximately half the footprint size) and the WVC record time is within 20 minutes from the in-situ observation time, the QuikSCAT wind speed is compared to the in-situ data. If several WVC records can be co-located with one surface measurement, the WVC record closest to the in-situ data location is chosen for the comparison.

QuikSCAT, as compared to HOAPS, has the higher capability to retrieve wind speed in nearshore areas. In the presence of in-situ data the co-location of

QuikSCAT with the coastal stations Chan, GRW and DeBu is possible. This is not the case for HOAPS, due to the proximity to land and its disturbing influence on the SSM/I wind speed retrieval. However, the lightship Sand is too close to the coast to allow for comparison with QuikSCAT's CP12 data, as the latter are masked and are therefore not available, within 30 km of the coast (Pickett et al. 2003, p. 1871). Furthermore, no wind speed data from the lightships Sand, Chan, GRW and the oil rig Frigg is available for 2002 .

When rain is present the measurement of the normalized radar cross section σ_0 experiences two problems. First, the transmissivity is decreased with an increasing rain rate greatly attenuating the return. Second, the rain drops roughen the sea surface, affecting the σ_0 measurement and alter the wind solution (Martin 2004, p. 289f). The influence of rain on the quality of the wind speed solution is assessed by including and excluding rain contaminated QuikSCAT wind speed in the comparison with bouy wind speed. Rain contamination is indicated by the QuikSCAT rain impact flag (Dunbar 2006, p. 50). This rain impact flag is produced by the Impact-based Multidimensional-Histogram (IMUDH) described in Huddleston and Stiles (2000).

The comparison focusses on instantaneous wind speed and its frequency distribution, following the comparison made for HOAPS and using the statistics described in section 3.1.1.

3.2.2 Results and Discussion

Instantaneous wind speed

After the removal of rain contaminated WVCs the co-located data amounts to between 330 (K1) and 540 (F3) records for 2002, as depicted in Figure 3.4(a) for Ems. As the overflight times are limited to two time windows between 3 and 6am and 5 to 8pm, QuikSCAT can not capture any daily cycles in wind speed. Almost no records had to be removed due to rain for K1, K5 and RARH. It cannot be judged whether this is realistic or an effect of either an improper rain flagging or the small sample size. Less than 2% of the co-located data had to be removed for the North Sea stations. The effect of the elimination of rain contaminated WVCs can be seen in the scatter plot for Ems in Figure 3.4(b). As shown for Ems, the wind speed from rain contaminated WVCs generally overestimates actual wind speed, which may be attributed to the increased radar return by the rain's additional surface roughening. However, situations exist where rain flagged wind speed underestimates actual wind speed, which may be attributed to the attenuating influence of rain and, in case of smaller deviations, to differences between QuikSCAT's assumed neutral and actual stability.

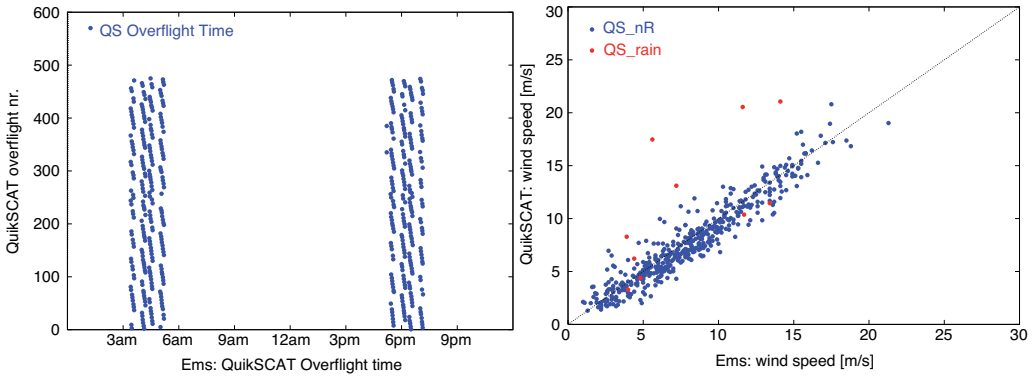

(a) (b)

Figure 3.4: *3.4(a) shows the QuikSCAT overflight times for the co-located wind speed records at Ems. 3.4(b) is a Scatter Plot of the co-located QuikSCAT and in-situ wind speeds at Ems. Rain flagged QuikSCAT data are highlighted in red.*

As depicted in Figure 3.5(a) the mean wind speed retrieved from QuikSCAT shows very good agreement with the mean co-located observed wind speed, both before (QS) and after the removal of the rain contaminated WVC from the comparison (QS_nR). The influence of rain on the mean wind speed is negligible for our case. The mean wind speed measured by K5 is much lower than that from QuikSCAT. The same was observed for HOAPS indicating irregularities in the wind speed measurement at K5.

QuikSCAT agrees very well with the observed wind speed variability (see Figure 3.5(a)) and shows high correlation coefficients around and above 0.9 with in-situ wind speed (Figure 3.5(b)). The disturbing influence of rain becomes evident in the correlation coefficients, which are higher after the removal of the rain contaminated WVCs for all stations in the North Sea. The RMSE between QuikSCAT and in-situ wind speed also reduces after the rain removal. While, neglecting the malfunctioning buoy K5, the average RMSE before the removal of the rain contaminated WVCs is approximately 2 m/s, it is approximately 1.8 m/s after the removal. A similar decrease in the RMSE due to the removal of rain flagged WVCs was observed by Pickett et al. (2003). With a RMSE of 1.8 m/s QuikSCAT's mission requirement of providing wind speed with an RMSE of 2 m/s (e.g. Pickett et al. 2003; Weissman et al. 2002) is met for the eastern North Atlantic and the North Sea.

However, the average RMSE of 1.8 m/s is somewhat higher than RMSE values between QuikSCAT and in-situ observations found in the literature. For 12 nearshore buoys between 8 to 41 km off the U.S. West Coast Pickett et al. (2003)

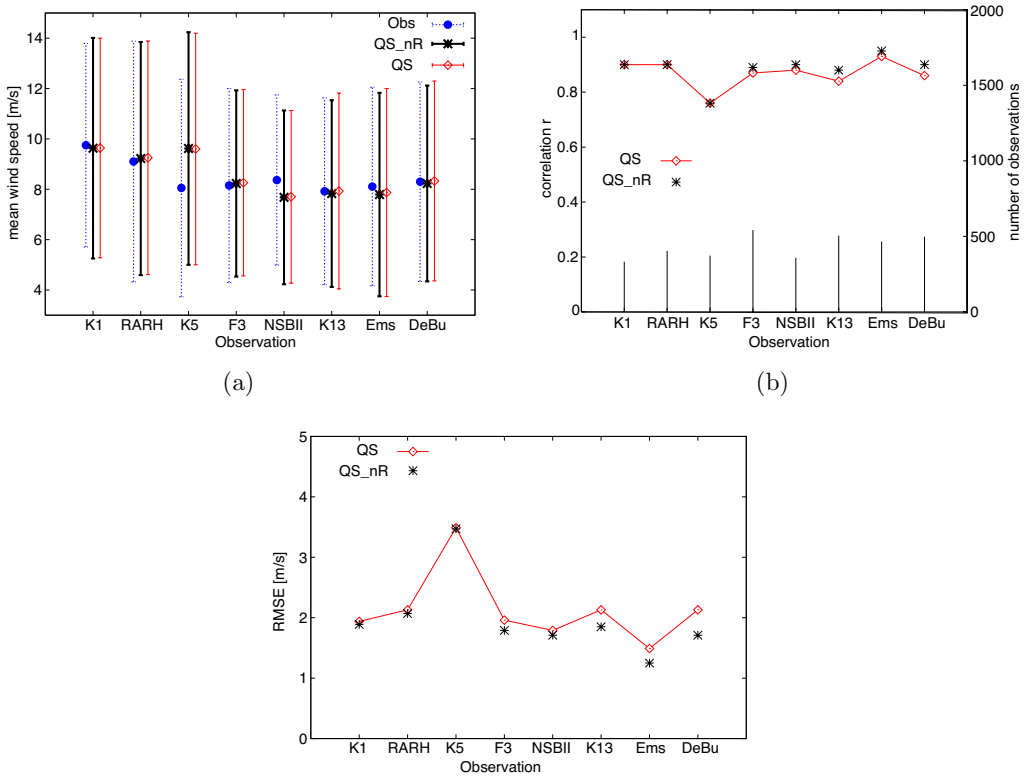

Figure 3.5: *Comparison of QuikSCAT (QS: QuikSCAT including rain contaminated WVCs, QS_nR: QuikSCAT without rain contaminated WVCs) and in-situ wind speed for 2002, as in Figure 3.2 but for QuikSCAT.*

found RMSE values of 1.6 m/s when rain flagged data and winds smaller than 3 m/s were removed and 1.3 m/s when winds lower than 6 m/s where also removed. However, the removal of low wind speeds from the comparison in this study did not lead to a reduced RMSE. Pickett et al. (2003) furthermore showed that the RMSE values dropped from 1.3 m/s near-shore to 1.0 m/s for three offshore buoys, again only taking into account wind speed data above 6 m/s. These values are similar to offshore buoy comparisons with QuikSCAT done by Ebuchi et al. (2002). They observed RMSE values of around 1 m/s using wind speed measurements of 27 NDBC buoys, 60 TAO buoys, 11 buoys by the Pilot Research Moored Array in the Tropical Atlantic (PIRATA) project and three buoys by the Japanese Meteorological Agency (JMA) in their comparison in the period from 1999 to 2001.

Goswami and Rajagopal (2003) determined RMSE values between 1.25 m/s and

2.11 m/s for the horizontal wind speed components of three buoys in the Indian Ocean in the years 1999 to 2001. For wind speeds between about 3 and 18 m/s Chelton and Freilich (2005) found very low RMS values of 1.3 m/s. They used buoy co-locations obtained in the middle 1600 km of QuikSCAT's measurement swath for which they consider the retrieved wind speed to be more accurate. Furthermore, following the selection criteria of open-ocean buoys by Freilich and Dunbar (1999), they only considered NDBC buoys far enough from land to avoid spurious wind retrievals from side-lobe contamination of the scatterometer radar measurements and to minimize the effects of small-scale orographic wind features that can render buoy measurements at point locations unrepresentative of 25-km averaged scatterometer measurements. Thus the higher RMSE found in this study may be partly due to the near shore location of some of the in-situ observations. Furthermore all mentioned studies examined a much larger amount of co-located data, as both more stations and longer time periods were available to them. Thus, it cannot be excluded that the high RMSE is partly caused by the small and unrepresentative sample.

Chelton and Freilich (2005) give another plausible reason for higher RMSE values in our investigation area. They argue that scatterometers measure the actual stress imposed on the sea surface by the wind. This stress is determined by the vector difference between the wind and the surface ocean velocity at each measurement location. Scatterometers thus measure the wind relative to the moving sea surface. In contrast, in-situ wind speed measurements are relative to fixed locations. In regions of strong currents, it has been shown that the surface ocean velocity can introduce differences of order 1 m/s between scatterometer and modelled 10-m or buoy winds (Cornillon and Park, 2001; Kelly et al., 2001; Chelton et al., 2004; Chelton and Freilich, 2005). Chelton et al. (2004) showed that the surface current modifies the mean QuikSCAT winds by nearly 1 m/s over the core of the Gulf Stream. As K1, RARH and K5 lie within the Gulf stream extensions and other stations are prone to the tidal currents in the North Sea, the high RMSE in this current study may be attributable at least in part to the fact that scatterometers measure winds relative to a moving sea surface.

The RMSE differences between buoy and QuikSCAT winds are also influenced by the surface velocity of energetic eddies associated with strong currents. In the Gulf Stream region, for example, Cornillon and Park (2001) showed that eddies generate relatively small-scale variations of order 1 m/s in the QuikSCAT winds.

Wind speed frequency distribution

Elaboration on the wind speed frequency distribution of QuikSCAT and in-situ data is made with the help of the quantile-quantile plots, illustrated in Figure 3.6 for Ems, K1 and RARH. However, the significance of these quantile-quantile

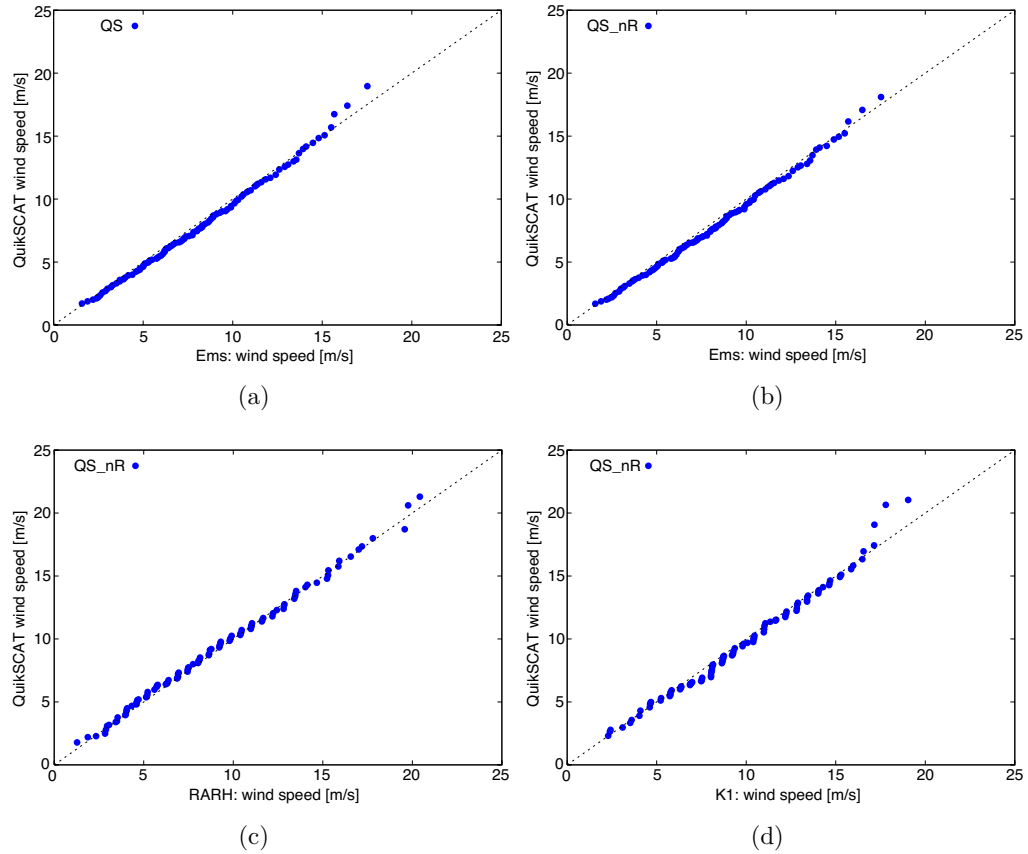

Figure 3.6: *Percentile-percentile distributions of wind speed in 2002, measured (x-axis) vs. QuikSCAT (y-axis) at a-b) Ems, c) RARH and d) K1. For Ems the wind speed percentiles of both a) QuikSCAT including rain contaminated WVCs (QS) and b) excluding them (QS_nR) are shown.*

plots is very limited, because each of the 99 percentiles stands for just three to five observations due to the small amount of co-located data. Under these constraints QuikSCAT shows good agreement with the observed wind speed frequency distributions for all stations.

After the removal of the rain flagged WVCs, the highest wind speed percentiles of QuikSCAT are in better accordance with the observed extreme percentiles at DeBu and Ems, shown exemplarily in Figure 3.6(b) for Ems. This improvement was less pronounced or not existing at K13, F3 and NSBII (not shown). At RARH and K1 an improvement in the agreement with the observed frequency distribution due to the removal of rain flagged wind speed was impossible, as almost no rain was detected at both stations. However, at K1 the highest per-

centiles are overestimated by QuikSCAT which may be caused by an improper rain flagging.

3.3 Intercomparison of HOAPS and QuikSCAT and Summary

To this point, in-situ wind speed has been compared to HOAPS in 1998 and to QuikSCAT in 2002. This raises the question as to whether the different results made for HOAPS and QuikSCAT are due to their different capabilities or at least partly due to the different years of the comparison. As HOAPS data is available in 2002, the comparison of HOAPS and in-situ wind speed was repeated for 2002 and examined as to whether the results made for HOAPS in 1998 still hold. However, a direct intercomparison of co-located HOAPS, QuikSCAT and in-situ data (triple co-location) was not considered due to the small amount of co-located overflights of SSM/I's and QuikSCAT in 2002. Therefore, only the results of the comparison of HOAPS and in-situ data in 2002 are shown and compared to the results found for QuikSCAT for the same year in the previous section. However, it should be kept in mind that the co-located in-situ data and the co-location method used are different for HOAPS and QuikSCAT. Nevertheless, it was assumed that both the co-located in-situ data in the HOAPS and QuikSCAT comparisons are equally representative for the wind speed in 2002.

This assumption is justified by Figure 3.7(a), as the means and the standard deviations of the in-situ wind speed records co-located with HOAPS in 2002 show negligible deviations to those co-located with QuikSCAT (see Figure 3.5(a) for comparison). The main results made for HOAPS in 1998 are recovered in 2002. Again, HOAPS overestimates mean annual wind speed in the open ocean. While compared to 1998 the bias is reduced at the open ocean stations K1 and RARH, with 2.6 m/s it is still exceptionally high at K5, indicating that K5 measures too low wind speeds in both 1998 and 2002 and most likely in between. As in 1998, HOAPS shows correlations values above 0.8 and RMSEs around 2 m/s (with the exception of K5 where correlation falls off and RMSE amounts to 4.6 m/s; for the RMSE see Figure 3.7(b)).

To summarize, QuikSCAT shows better agreement with mean observed wind speed than HOAPS. While HOAPS shows positive biases at open ocean stations, the bias of QuikSCAT is negligible for all stations. Furthermore, HOAPS shows an apparent "saturation" at high wind speed (see Figure 3.8) resulting in a narrower wind speed frequency distribution.

While both data sets show good agreement with the temporal development of

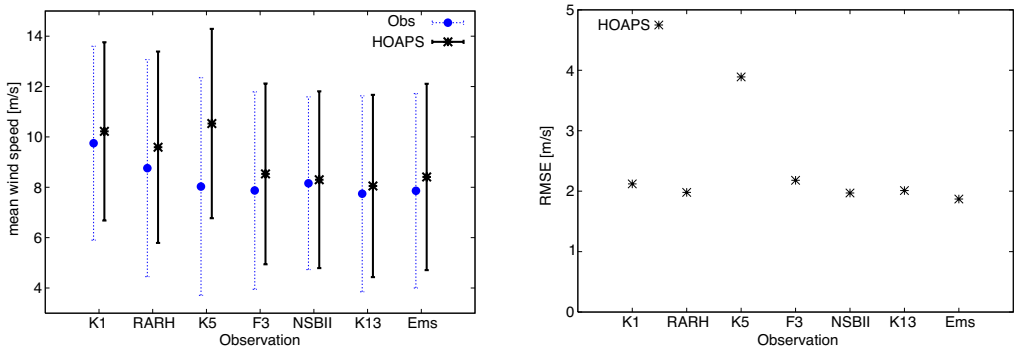

Figure 3.7: *Comparison of HOAPS and in-situ wind speed in 2002: a) mean wind speed and its standard deviation, b) RMSE.*

the observed wind speed as given by the correlation, QuikSCAT outcompetes HOAPS in that sense, too. Finally, HOAPS shows slightly higher RMSE values of around 2 m/s as compared to 1.8 m/s for QuikSCAT after the removal of rain contaminated WVCs. Both data sets give RMSE values slightly higher but consistent with those in the current literature. Possible reasons are the inclusion of low wind speeds in the current comparison, the near shore location of some of the in-situ observations, strong currents or eddies affecting scatterometers winds and the use of "real" 10 m winds instead of 10 m equivalent neutral-stability winds.

Additionally the development and tuning of SSM/I wind speed retrieval algorithms (including the HOAPS algorithm) and QuikSCAT's model function was realized with the help of in-situ observations from the NDBC and TAO buoy networks. In contrast, this study compares SSM/I and QuikSCAT wind speed retrievals with other than NDBC and TAO buoys and is assumed to be the first to compare HOAPS and QuikSCAT wind speeds with in-situ data in the eastern North Atlantic. This current study demonstrates that QuikSCAT's mission requirement of providing wind speed with an RMSE of 2 m/s is met for the eastern North Atlantic and North Sea.

Both the wind speed retrievals of HOAPS and QuikSCAT have advantages and drawbacks. They have in common that their algorithms are less effective in case of rain and close to coastlines. However, their measurements are extremely valuable for remote areas, where no in-situ data exist. QuikSCAT has higher capabilities in both error statistics and wind speed frequency distributions, the slight superiority of QuikSCAT's wind speed may be partly due to its finer spatial resolution. Furthermore, the results found for HOAPS may improve if the in-situ records are co-located with the respective closest HOAPS wind speed retrievals

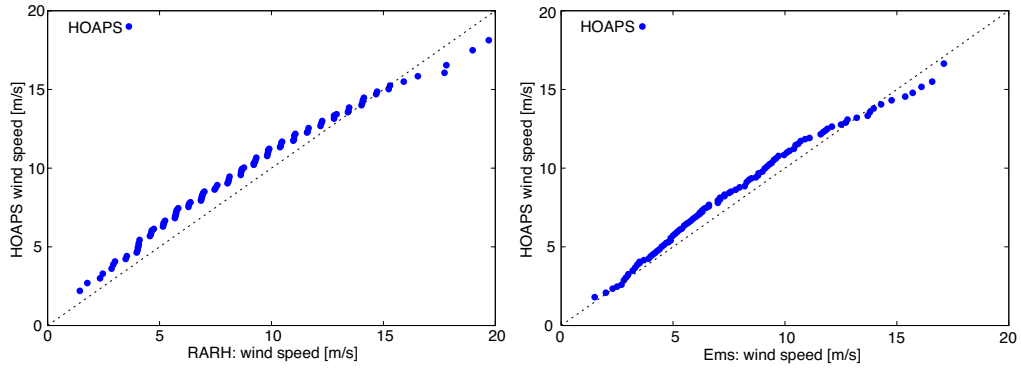

Figure 3.8: *Percentile-percentile distributions of wind speed in 2002, measured (x-axis) vs. HOAPS (y-axis) percentiles at a) RARH and b) Ems.*

only. Finally, QuikSCAT, as compared to HOAPS, allows wind speed to be retrieved much closer to the coast.

In contrast, HOAPS wind speed is available for a much longer period. Furthermore, with the higher number of daily overflights, HOAPS can deliver more wind speed data per day than QuikSCAT. Therefore, regarding climatic studies or investigations of trends in wind speed, HOAPS is the favorable product.

The results and conclusions presented are based on relatively small samples and should be reexamined when more in-situ data are available.

Chapter 4

Added value

This Chapter focuses on the question whether different state-of-the-art Regional Climate Models (RCMs), namely REMO and CLM, add value for surface marine wind fields in comparison to the reanalysis wind speed forcing in the eastern North Atlantic and the North Sea. After a short introduction of the current, relevant literature, this question is addressed by first defining the term added value. The second step describes how it is determined. After these methodological clarifications the results of the analyses are presented and discussed.

4.1 Introduction

Hindcasts with reanalysis-driven regional climate models (RCMs) are a common tool to assess the capabilities of RCMs in simulating weather statistics (i.e. climate) and recent changes and trends. Furthermore, in the case of missing or insufficiently homogeneous data, regional atmospheric hindcasts are frequently used as a reality substitute, either to analyse long-term changes and trends (e.g., Fowler and Kilsby 2007) or as forcing for other, e.g. hydrologic, wave or storm surge models (e.g. Gaslikova and Weisse 2006; Sotillo et al. 2005; Federico and Bellecci 2004; Kim and Lee 2003).

Castro et al. (2005) evaluated the value retained by dynamically downscaling the NRA_R1 using a Regional Atmosphere Model System (RAMS). By considering spectral properties they compared their RAMS simulation with the re-gridded NRA_R1 over North America. They found that for large scales, the RAMS significantly underestimates the variability as determined by the column integrated kinetic energy and integrated moist flux convergence and concluded that the RAMS could not restore the variability present in the NRA_R1. However, at smaller scales the RAMS added value compared to the driving NRA_R1, in particular when there was sufficiently strong surface boundary forcing, such as variations in topography, that could be resolved by the RAMS.

The issue of retaining or adding value at different scales by dynamical downscaling led to the development of spectral nudging techniques as proposed by Waldron et al. (1996) and von Storch et al. (2000), the latter is described in detail in section B.1. In the approach normally taken, RCMs are usually initialized and periodically provided with updated boundary conditions at the surface and the lateral boundaries only. For hindcasting, the latter are usually obtained from a reanalysis. In the interior of the model domain, the regional model can then "freely" determine the prognostic variables according to the prognostic equations. While this is desired for small scales, it is usually not in favour for large scales that are reliably reproduced in the driving reanalysis, especially when those scales are supported by data assimilation. As a result, large-scale features such as cyclone tracks or the location of pressure systems may deviate significantly from those in the reanalysis (e.g., von Storch et al. 2000), especially deep inside the model domain and far from the lateral boundaries. As an attempt to overcome these shortcomings spectral nudging techniques have been proposed by several authors (e.g., Waldron et al. 1996 and von Storch et al. 2000). Contrary to the conventional approach, the reanalysis forcing is spectrally decomposed and the large-scale components (the ones supported by data assimilation in the driving reanalysis) are in addition forced upon the regional atmosphere model in the interior of the model domain. In this philosophy, the regional model should keep close to the reanalysis at large scales and thus benefit from the data assimilation, while it is still allowed to evolve "freely" at smaller scales at which added value may be expected compared to the driving reanalysis.

A comparison of the scale-dependent skill of two RCM simulations with and without spectral nudging was provided by Feser (2006). By applying appropriate spatial filters she compared both simulations to the driving NRA_R1. The comparison was made for sea level pressure (SLP) and near-surface temperature relative to a high-resolution operational weather analysis that served as a replacement for the observations. Feser (2006) derived pattern correlation coefficients between the weather analysis and NCEP and the weather analysis and both RCM simulations. In the spectrally nudged case, significant added value in the pattern correlation was found on medium to small-scales for both SLP and temperature. In the conventional approach added value was found on these scales merely for temperature. For large scales, no added value was found for SLP in both simulations, resulting in no overall added value for SLP. The situation is different for temperature, where details of the topography not resolved in the driving NRA_R1 are more important. Here added value was found also on larger scales for the spectrally nudged but not for the conventional approach.

Summarizing current knowledge, whether a regional atmospheric hindcast can add value in representing a parameter as compared to the reanalysis forcing,

seems to be largely determined by two factors: the strength of influence of large-scale atmospheric motions on the parameter and the capabilities of the RCM in both retaining the large-scale value of the reanalysis forcing and improving the representation of smaller-scale peculiarities of the parameter.A very interesting parameter in this respect is given by near-surface marine wind fields. The latter are frequently used from regional models for driving ocean, storm surge or ocean wave models (e.g. Gaslikova and Weisse 2006; Sotillo et al. 2005). To date, the added value in dynamically downscaled near-surface wind fields has not been investigated in a systematic way. Some examples have been provided in Sotillo et al. (2005). They elaborated on the added value for near-surface marine wind fields for a RCM simulation utilizing the spectral nudging approach. For the Atlantic Basin northwest of Spain, especially far from coastal areas, they found the NRA_R1 sufficient for realistically representing near-surface marine wind fields derived from in situ observations. Consequently, the application of dynamical downscaling techniques will not substantially improve the situation there. On the other hand, Sotillo et al. (2005) found, that towards coastal regions with complex orography, NRA_R1 near-surface wind fields are significantly enhanced by dynamical downscaling using RCMs.

In contrast to Sotillo et al. (2005) this study elaborates on the added value of near-surface marine wind fields more systematically. Furthermore, while they investigate the marine surface wind speeds in the Mediterranean, the focus here is on the eastern North Atlantic and the North Sea. As they use a simulation with SN-REMO, which has, apart from the modelled domain, the same setup as the SN-REMO simulation used here, this study and the work of Sotillo et al. (2005) complement each other to give a very broad picture of the capabilities of RCMs and the NRA_R1 to represent surface marine winds for European coastal waters and the adjacent North Atlantic.

4.2 Definition of Added Value

As introduced in section 2.3.1, atmospheric reanalyses use data assimilation schemes that are kept unchanged over the reanalysis period and produce among other things a surface marine wind speed data set that is as homogeneous as possible (there are still sources of inhomogeneity, e.g. the change in data availability over time). Hindcasts with RCMs are usually initialized and forced with reanalysis data. This forcing can be a periodical provision with updated boundary conditions at the surface and the lateral boundaries only (standard approach) or in addition within the integration area (e.g., spectral nudging approach). However, the setup and production of hindcasts with RCMs is costly and a question that has to be addressed is, whether the results from hindcasts with RCMs justify their generation.

Considering marine surface wind speed, the question that is addressed by this study is:
"Do RCMs add value to the marine surface wind speed in the North Sea and the Northeast Atlantic in comparison to the reanalysis wind speed forcing to justify their usage in wind speed hindcasts?"

In this respect the conclusions that can be drawn from this study are limited, but are of big interest as such hindcasts exits for these areas and are heavily used for a large variety of subsequent studies. Wind speed is just one of many parameters in an atmospheric RCM hindcast, which means that even if the RCM does not add value to the surface marine wind speed forcing, the added value obtained in other parameters may overcompensate that drawback and still make the application of the RCM worthwhile. In contrast the value added to the surface wind speed by the RCM may be not enough to overcompensate the worse representation of other parameters to justify the RCMs usage in a hindcast. Consequently, it can only be judged whether RCMs add value in the surface marine wind speed to justify their usage in wind speed hindcasts.

It is important to stress that the meaning of our results for forecast studies and climate change simulations can not be judged, as the situation is somewhat different in hindcast studies. Under hindcast conditions the reanalysis can be seen as a perfect boundary condition due to the assimilation at all time steps. However, in the forecast mode, boundary conditions are much less perfect, thus there is a remaining chance that the regional model behaves differently for forecast purposes.

In climate change projections, with or without the usage of RCMs, the boundary conditions are based on scenarios, which are plausible socio-economic futures, which, however, may or may not happen. Thus climate change simulations with RCMs are based on purely hypothetical boundary conditions and therefore they cannot be used on their own to judge the skill of RCMs in simulating climate, as their is no truth with which to validate them. A common solution is to use hindcasts with reanalysis driven RCMs to assess the capabilities of RCMs in simulating recent climate. After showing that the RCM realistically describes recent climate, it is reasoned that the RCM will probably do so also for future climates.

Thus hindcasts with RCMs are necessary for the validation of climate projections and their generation is justified even if these hindcasts may not be suitable as a reality substitute, if they do not add value for the parameter in question.

However, here hindcasts are used as reality substitutes and the question whether RCMs add value to the "reality" as seen by the reanalysis forcing is of importance.

This question needs to be addressed for the two main applications of wind speed hindcasts, which are case studies and the derivation of wind speed frequency distributions. Case studies, e.g. of individual storms (Federico and Bellecci 2004; Keil et al. 2003; Hultquist et al. 2006; Wernli et al. 2002; Feser and von Storch 2007) help in the understanding of the atmospheric phenomena and the dynamics that govern them. The main advantage of hindcasts for case studies is that compared to buoy and satellite measurements they can deliver a spatially and temporally highly resolved picture of e.g. the wind speed within a storm. However, compared to the reanalysis forcing they have a higher skill for case studies only if the RCM used in the hindcast adds value in the instantaneous wind speed.

Marine wind speed frequency distributions derived from hindcasts can be used, for instance, for the design and maintenance of offshore installations, e.g. platforms and wind farms, and to analyse long term changes and trends (e.g. Weisse et al. 2005). For these and other purposes, hindcasts with RCMs are the product of choice, if the RCMs do add value in the wind speed frequency distribution as compared to the reanalysis forcing.

Thus our definition of added value is:

- For instantaneous marine surface wind speed: The RCM adds value to the reanalysis, if the 10 m wind speed obtained from the RCM hindcast shows a better agreement with measured instantaneous wind speed at 10 m height than the wind speed of the forcing reanalysis.
- For marine surface wind speed frequency distributions: The RCM adds value to the reanalysis, if the 10 m wind speed obtained from the RCM hindcast shows a better agreement with measured 10 m wind speed frequency distributions than the wind speed of the forcing reanalysis.

4.3 Method to determine added value

To determine whether the RCMs REMO and CLM add value for surface marine wind speed in comparison to the reanalysis forcing, the following is needed:

- a "best guess" for real 10 m wind speed,
- the 10 m wind speed obtained from the hindcasts with the RCMs REMO and CLM,
- the 10 m wind speed of the reanalysis forcing.

Possible sources of the best guess for real 10 m wind speed are the in-situ data set introduced in section 2.1 and the wind speed retrievals of HOAPS and QuikSCAT.

It has previously been demonstrated that both HOAPS and especially QuikSCAT provide an acceptable representation of 10 m wind speed. Nevertheless, in the following, only the wind speed at 10 m from the in-situ data set will be considered as best guess for real surface marine wind.

The 10 m wind speed from the SN-REMO, STD-REMO and CLM hindcasts, which were described in section 2.3.2, is available as a diagnostic parameter. However, the 10 m wind speed of the reanalysis forcing is not available. Both the NRA_R1 and NRA_R2 do not deliver reanalysed but forecast 10 m wind speed, which is used as best guess for the 10 m wind speed of the reanalysis forcing.

An issue further complicating matters is the shift in the reanalysis forcing in both SN-REMO and STD-REMO hindcasts, which was necessary for both investigated REMO simulations. Due to an unresolved compatibility issue between the NRA_R1 and the REMO preprocessor, both STD-REMO and SN-REMO are forced with the NRA_R2 from March 1997 onwards. SN-REMO and STD-REMO are driven with the NRA_R1 until February 1997 and this change in forcing may cause inhomogeneities, in especially within SN-REMO, as the origin of the large-scale horizontal wind speed components nudged in the interior also changes from NRA_R1 to NRA_R2. Elaboration on this issue is made in Chapter B in the appendix.

The value added by the RCMs REMO and CLM is assessed with the in-situ data set in 1998 when all three hindcasts are forced with the NRA_R2. Therefore, forecast 10 m wind speed of the NRA_R2 should be considered in the added value assessment. However NRA_R1 forecast wind speed had to be used, because the forecast 10 m wind speed of the NRA_R2 represents a rather unplausible data set, as will be shown in the following section.

4.3.1 Comparison of wind speed forecasts of NRA_R1 and NRA_R2

Both the NRA_R1 and NRA_R2 do not deliver reanalysed 10 m wind speed. 10 m wind speed is available from the respective forecasts, that are valid six hours after the reference time. The forecast is a step in the reanalysis system, as depicted in Figure 2.6. As explained, the forecast serves as the first-guess field for the reanalysis six hours after the forecast reference time. In the SSI step the differences between the assimilated observations and the first guess-field deliver the analysis correction on pressure levels, which leads to the updated reanalysis in the form of sigma level coefficients in the next step. These sigma level spectral coefficients are actually used for forcing the STD-REMO, SN-REMO and CLM hindcasts. However, surface wind speed can not be obtained from the spectral

coefficient data.

Instead, horizontal wind speed components on the lowest pressure level at 1000 hPa are available. In a standard atmosphere (e.g., NASA 1976) the 1000 hPa level corresponds to a height of around 100 m. Therefore, the 1000 hPa wind speed would have to be converted to 10 m height, if used in the added value assessment. However, for the conversion of the 1000 hPa wind speed to 10 m height detailed information about the stratification within the surface layer is needed, which is not available from the reanalyses and is therefore beyond the scope of this study. Thus, while the 10 m wind speed forecasts are not equivalent to reanalysed 10 m wind speed, they are the only available and best guess for the 10 m wind speed within the reanalysis forcing field.

For the assessment of added value in-situ wind speed data are available in 1998. The SN-REMO, STD-REMO and CLM hindcasts were forced by the NRA_R2 in 1998. Consequently the forecast 10 m wind speed of the NRA_R2 should be used in the added value assessment. Unfortunately the NRA_R2 10 m wind speed forecast represents a rather unplausible data set with limited agreement with in-situ wind speed, as will be demonstrated in the following.

For the comparison of the in-situ wind speed with both NRA_R1 and NRA_R2 10 m wind speed forecasts, the latter are bilinearly interpolated onto the locations of the in-situ measurements. In addition, both the NRA_R1 and NRA_R2 forecasts were time interpolated linearly to the one hour resolution given by the observations. The results of the comparison are displayed in Figure 4.1. For the locations of the in-situ observations please refer to Figure 2.1. In general a large positive bias between the NRA_R2 and the NRA_R1 in the order of 2 m s^{-1} can be inferred (see also Figure 4.2(a)). Far offshore at K1, RARH, K5, FRIGG and F3 the NRA_R1 agrees better with observed mean wind speed while the NRA_R2 overestimates 10 m wind speed by up to 2 m s^{-1} (3 m s^{-1} at K5 due to both NRA_R2 large bias and too low wind speed measurements at K5). Closer to the coast and, especially within the English Channel, the NRA_R2 shows a much better agreement with the observations.

The latter represents a highly unplausible result, because both forecasts calculate wind speed over approximately 200x200 km wide grid boxes (as depicted by the land sea mask of both reanalyses in Figure 2.1) and can therefore hardly resolve the topography within the English Channel. At each grid box within the English Channel some kind of smoothed topography, averaged over the water and adjacent land surfaces, is used in both forecasts. As a result the surface roughness will be higher and consequently the forecast wind speed within the English Channel should be lower than that measured by the English Channel lightships Chan, GRW and Sand. While this is the case for the NRA_R1, the NRA_R2 gives

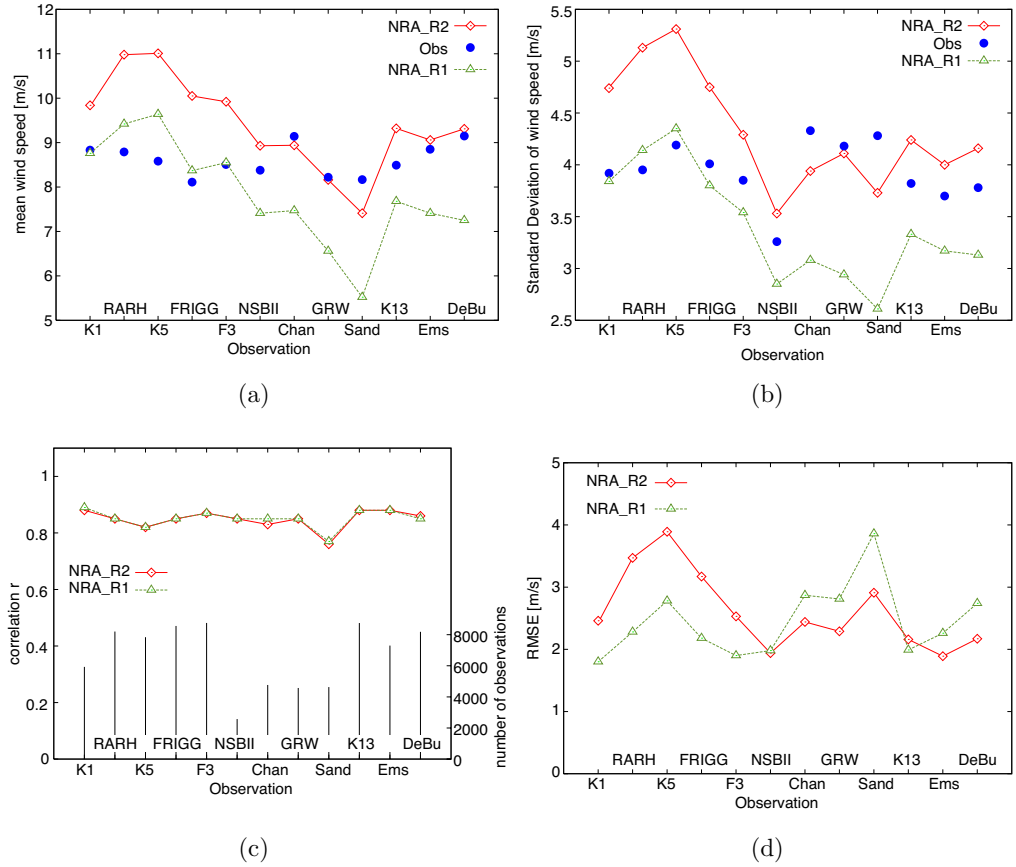

Figure 4.1: *Comparison of in-situ wind speed with 10 m wind speed forecasts of NRA_R1 and NRA_R2 in 1998: a) mean wind speed, b) its standard deviation, c) number of observations and correlation r, d) root-mean-square error.*

mean wind speeds comparable to the in-situ data. Similarly, where topographic features, averaged over a forecast grid cell, are relatively homogeneous (such as for open waters) near-surface wind speed is expected to show less variance and in-turn a better agreement between in-situ and forecast wind speed might be expected. While again this is the case for the NRA_R1, it is not for the NRA_R2. While representing an average over 200x200 km with an integration time step of 20 min, the NRA_R2 forecast gives wind speed variabilities higher than observed for 9 of 12 cases, which is highly unplausible. The RMSE of the NRA_R2 10 m forecast again shows its counterintuitive behaviour, since it gives lower RMSE values near coastlines it cannot resolve and higher RMSE for areas far offshore.

As depicted in Figure 4.2(b), the strong bias between the NRA_R2 and NRA_R1

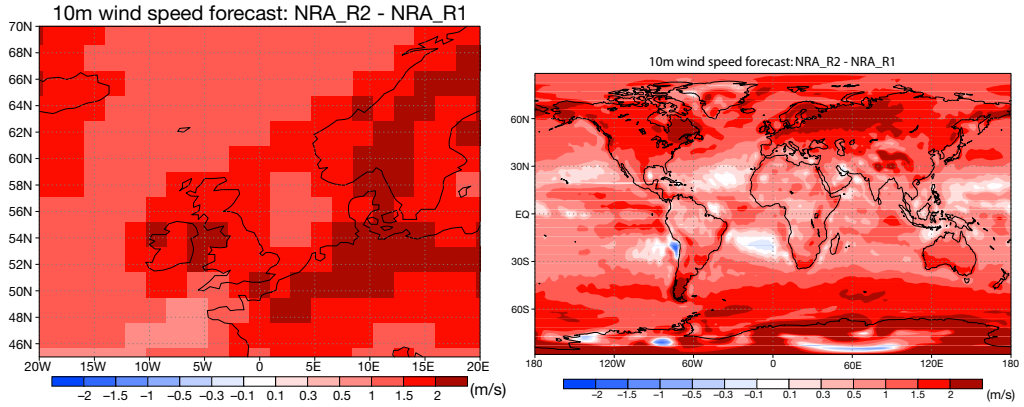

(a) (b)

Figure 4.2: *Bias between the 10 m forecast wind speed of the NRA_R2 and NRA_R1 in the eastern North Atlantic and the North Sea (left) and globally (right) in 1998 .*

10 m wind speed forecasts is not constrained to the Northeast Atlantic. With the exception of the subtropical latitudes around 30° and some patches in the Antarctic, the NRA_R2 shows too high 10 m wind speed as compared to the NRA_R1. This positive bias peaks to 1.5 m s^{-1} and above in and around the Antarctic and on the Eurasian and North American land masses.

In 1998, the mean sea level pressure in the investigated area is similar to the 1013 hPa given for the U.S. Standard Atmosphere after NASA (1976)(not shown). Thus, in agreement with the standard atmosphere, the 1000 hPa level is expected to be in average at a height of around 100 m. Consequently, according to the vertical wind speed profile in the surface layer (for details please refer to section A.2 in the appendix), the wind speed at 1000 hPa is in average higher than that at 10 m height. For 1998, the differences of the annual averages of the reanalysed 1000 hPa and forecast 10 m wind speed are depicted in Figure 4.3. While the NRA_R1 shows higher wind speeds on the 1000 hPa level (Figure 4.3(a)), the NRA_R2 forecast wind speed in 10 m height even exceeds the reanalysed wind speed at the 1000 hPa level (Figure 4.3(b)), indicating a major inconsistency in the NRA_R2 reanalysis/forecast system, as far as near-surface wind speed is concerned.

Both reanalyses show similar wind speed patterns at 1000 hPa, which is not surprising given that both reanalyses assimilate similar marine near-surface wind speed observations. In detail, the differences are much smaller than the differences between the 10 m wind speed forecasts and have the opposite sign (Figure 4.3(d)). These findings indicate on the one hand, that the NRA_R2 10 m wind speed forecast is not representative for the near-surface wind field of the NRA_R2

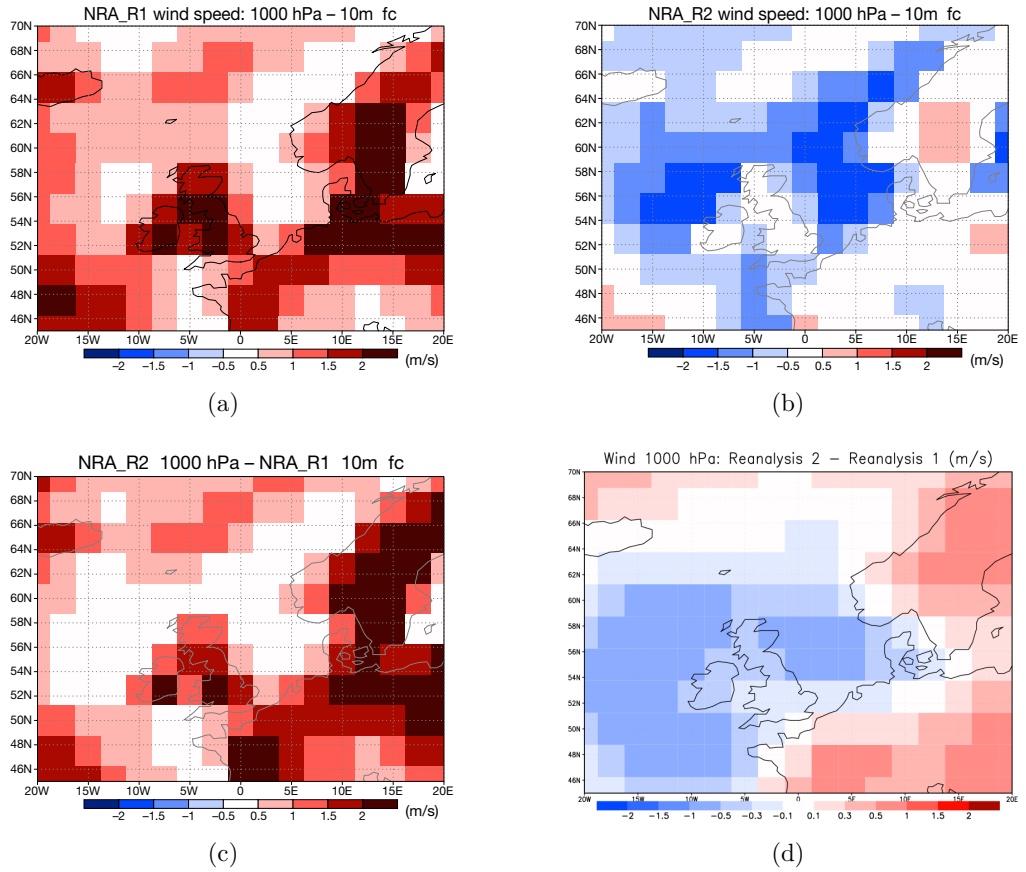

Figure 4.3: *Comparison of the reanalysed 1000 hPa and forecast (fc) 10 m wind speed of both reanalyses in 1998: a) NRA_R1: 1000 hPa - 10 m fc, b) NRA_R2: 1000 hPa - 10 m fc, c) NRA_R2 1000 hPa - NRA_R1 10 m fc, d) 1000 hPa: NRA_R2 - NRA_R1.*

reanalysis. On the other hand, a problem within the Hong-Pan planetary boundary layer non-local vertical diffusion scheme (Hong and Pang, 1996) implemented in the NRA_R2 forecast model is indicated. Additionally, the strong bias may be attributed at least in part to the different convective parameterizations leading to more intense storms in the NRA_R2 (W. Ebisuzaki (Climate Prediction Center, NCEP), pers. comment). The effects are also visible in the wind speed frequency distributions (Fig 4.4). While the bias between both forecasts is similar at all stations, the bias between the NRA_R2 forecasts and in-situ wind speed is strongest for open ocean areas (4.4(a)). The latter bias is lowered in coastal areas by the increasing influence of the surrounding land mass on the forecast wind speed, leading to apparently well matched wind speed frequency distributions in the German Bight at the light ships Ems and Debu and especially in the English Channel at Chan (Figures 4.4(b)-4.4(d)).

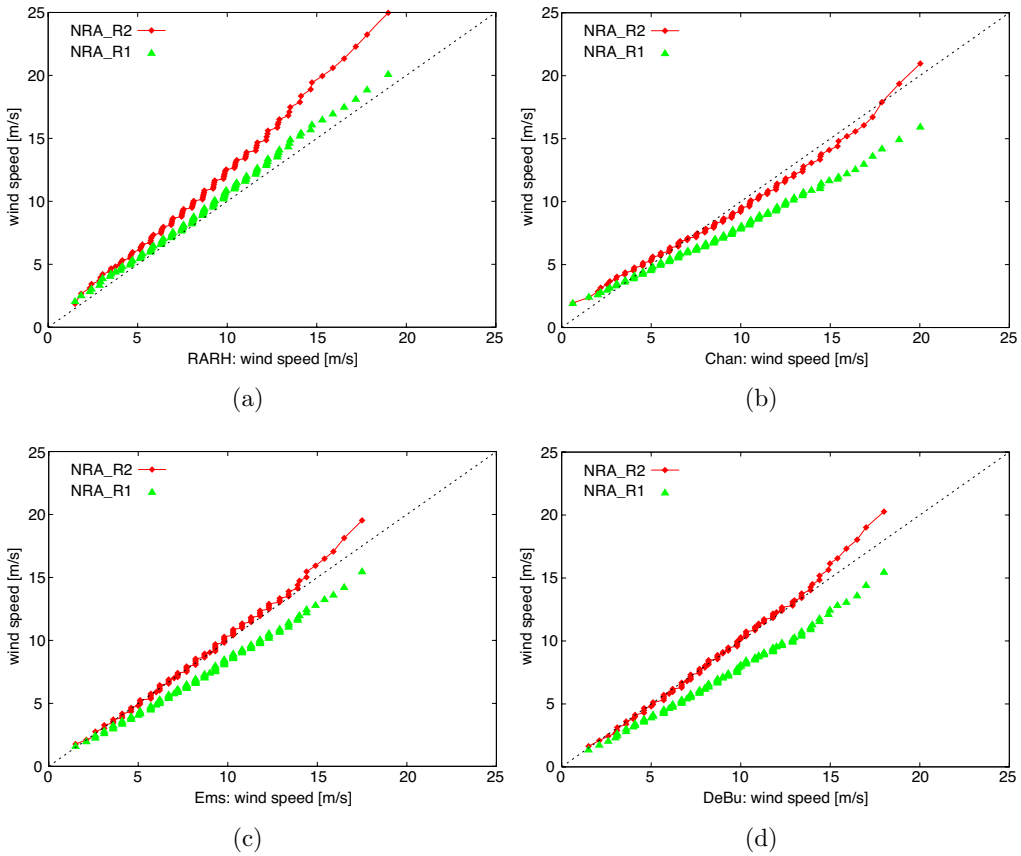

Figure 4.4: *Comparison of percentile-percentile distributions of 10 m wind speed from NRA_R1 and NRA_R2 forecasts and in-situ data at a) RARH, b) Chan, c) Ems and d) DeBu.*

Because of the plausibility arguments discussed, the NRA_R2 10 m forecast is not considered here as an appropriate product to assess the added value of RCM hindcasts. However, the difference between the NRA_R2 1000 hPa wind speed and the 10 m wind speed forecast of the NRA_R1 shows a similar spatial pattern as the difference between the NRA_R1 1000 hPa and its forecast wind speed (Figures 4.3(c) and 4.3(a)). It is therefore suggested to use the NRA_R1 10 m wind speed forecast as best guess for the 10 m wind speed within the NRA_R2 reanalysis. Still, this approach is suboptimal and the added value assessment should be redone, when in-situ data is available for periods prior to 1997, when the SN-REMO and STD-REMO hindcasts are forced with the NRA_R1.

4.3.2 Determination of added value

The following data are used for the assessment of the value added by the RCMs REMO and CLM to the surface marine wind speed obtained from the reanalysis forcing:

- the diagnostic 10 m wind speed of the STD-REMO, SN-REMO and CLM hindcasts,
- the NRA_R1 forecast 10 m wind speed as best guess of the 10 m wind speed of the reanalysis forcing of the STD-REMO, SN-REMO and CLM hindcasts
- the in-situ wind speed data at 10 m from 12 stations as best guess for real surface marine wind speed.

As listed in Table 2.1 the NRA_R1 has a computation time step of 20 minutes for dynamics and physics, therefore the NRA_R1 wind speed can be considered as a 20 minute mean. Accordingly REMO and CLM wind speeds can be seen as five and four minute means respectively. The averaging periods of the observations vary between 10 and 17 minutes. As a rough approximate it is assumed that the different means are reasonably comparable. NRA_R1 20 minute means available every 6 hours are time interpolated to one hour resolution to match the one-hour frequency prescribed by the RCMs and observations.

NRA_R1, REMO and CLM wind speeds have to be considered as spatial means over respective grid boxes, thus being spatial means over 1.875° x 1.875° ($\approx$ 200 x 200 km), 0.5° x 0.5° (50 x 50 km) and 0.44° x 0.44° (44 x 44 km) respectively. For the comparison with observed wind speeds, modelled grid box means are bilinearly interpolated to the station's location.

The different spatial and temporal resolutions of the data sets have a strong influence on their capabilities to represent actual wind speed. In-situ measurements can detect meso- and micro-scale wind flow such as sea-breezes, orographic induced wind flow, downdrafts and small-scale turbulence. Typically, in-situ wind observations are averaged over a certain time interval (here 10 to 17 min means), before they are made available. This means, while microscale turbulences are averaged out, downdrafts, sea-breezes and orographic induced wind flow leave their imprint on the available in-situ wind speed averages, e.g. by an increased wind speed variability. Their temporal and spatial resolution should allow REMO and CLM to model, at least in part, orographic induced wind flow such as near-coastal winds. Smaller scale phenomena cannot be resolved by them. Therefore, wind speed variabilities obtained from the RCMs are expected to be generally lower than those of the in-situ measurements.

The NRA_R1 has a too coarse resolution to model all of the above phenomena and can only give a reasonable representation of the large scale wind field. However, it is expected that the wind field in the open ocean is largely determined by the large scale, thus the possibilities of the RCM to add value to the NRA_R1 are expected to be limited there. In the open ocean, the RCMs may possibly enhance the wind speed delivered by the NRA_R1 by an improved representation of the pressure gradients within a cyclone, fronts and meso-scale cyclones like Polar Lows. The added value assessment with the help of in-situ measurements might give an indication whether this is actually the case. In coastal areas, especially for complex and rough coastlines, where orographic induced wind flow increases the spatial and temporal variability of the wind field, the RCMs are expected to add value to the NRA_R1.

Consequently, to discriminate whether the added value of regionally modelled wind speed is more pronounced near coastal areas with complex topographic features or strong gradients, the 12 observations are divided into coastal stations and open ocean stations. This classification is done with the help of the land sea mask of the NRA_R1 (see Figure 2.1).

- An observation is classified as an open ocean station if
    1. It is inside a NRA_R1 sea grid box,
    2. The four NRA_R1 grid boxes used to bilinearly interpolate NRA_R1 wind speed to the observation location are sea grid boxes.
- An observation is classified as a coastal station if
    1. At least one of the four NRA_R1 grid boxes used to bilinearly interpolate NRA_R1 wind speed to the observation location is a land grid box.

The only exception from this classification scheme is the station K13, which is classified as a coastal station, although the four surrounding NRA_R1 grid boxes are all sea grid boxes. K13 is regarded as a coastal station because the main westerly wind conditions are heavily influenced by the British island and eastern and southern winds by the continental land masses on both sides of the English Channel.

The comparison of reanalysis wind fields with in situ wind observations is heavily debated, e.g. Swail and Cox (2000) claim that, since the reanalysis process itself involved the assimilation of measured surface marine data into the surface wind field products, it is not possible to derive an independent assessment of the accuracy of reanalysis wind fields only from comparisons with in situ wind. Additionally, Sotillo et al. (2005) mention the dependence problem of comparing

reanalysis wind fields with assimilated observations. For three Atlantic buoys, which were assimilated into the NRA_R1, they found that the NRA_R1 already realistically characterizes the 10 m wind fields. In contrast, at the in-situ observations in the Mediterranean, which were not previously assimilated by the NRA_R1, they found an added value of their SN-REMO hindcast. These findings might on the one hand indicate that the added value is determined by the assimilation status of the observation, meaning whenever a wind speed observation is assimilated into the forcing reanalysis the dynamical downscaling with an RCM cannot add value at its position. On the other hand their result may indicate that the RCM can add value close to complex coastlines but not in the open ocean, as their in-situ observations in the Mediterranean were close to coastal areas, while the Atlantic buoys were far offshore.

To elaborate on this issue the 12 in-situ observations used in this study are discriminated according to their proximity to land and their assimilation status, meaning whether they are assimilated into the reanalysis or not. Using the NRA_R1-PREPBUFR files it was examined whether the wind speed observations are assimilated into the NRA_R1. The 12 observations can thus be divided into the four groups (see Figure 2.1):

- assimilated open ocean stations:
  K1, K5, RARH
- not assimilated open ocean stations:
  Frigg, F3, NSBII
- assimilated coastal stations:
  Chan, GRW, Sand
- not assimilated coastal stations:
  K13, Ems, DeBu

The added value for both instantaneous wind speed and its frequency distribution are elaborated. The Brier Skill Score (BSS) is used to test to what extent the regionally modelled wind gives a better reproduction of in-situ wind speed than the NRA_R1. It is defined, e.g. von Storch and Zwiers (1999), by

$$\mathrm{BSS} = 1 - \sigma_F^2 \sigma_R^{-2} \tag{4.1}$$

where σ_F^2 and σ_R^{-2} represent the error variances of the "forecast" F (the time series of regionally modelled wind speeds) and the reference "forecast" R (the time series of NRA_R1 wind speeds). The error variances are computed relative to the same predictand, here the respective time series of observed wind speeds in 1998. Therefore the BSS is equivalent to

$$\mathrm{BSS} = 1 - \frac{\mathrm{RMSE}_F^2}{\mathrm{RMSE}_R^2}, \tag{4.2}$$

where the RMSE_F and RMSE_R are the RMSE of the "forecast" F and the reference "forecast" R, respectively. Thus the Brier Skill Score is entirely determined by these two RMSE values. By definition the Brier Skill Score can vary between $-\infty$ and +1 (forecast exactly matches the observations). While negative values indicate a better performance of the reference forecast (NRA_R1), positive values indicate an added value of the regionally modelled winds in comparison to the NRA_R1 time series.

As far as the wind speed frequency distributions are concerned the wind speed percentiles and the BSS will be used to assess the value added by the RCMs.

4.4 Results

4.4.1 Instantaneous wind speed

Measured wind speeds are compared with those modelled for the year 1998. For that purpose mean wind speed, standard deviations, correlation coefficients, RMSE and Brier skill scores (BSS) have been determined. These statistics are depicted in Figure 4.5. The information of the RMSE relevant to this study is already included in the BSS (Equation 4.2). Therefore the RMSE is not shown.

Observed annual mean wind speeds vary approximately between 8 and 9 ms^{-1} (see Figure 4.5(a)). The mean wind speeds at Ems and especially DeBu are higher than the mean wind speeds at the open ocean stations, which seems unusual, although 1998 was an above average wind speed year in the German Bight. Within the English Channel mean wind speeds are highest in the broad western mouth (Chan) decreasing towards the eastern outlet (Sand). The increasing influence of the surrounding land masses may be responsible for this.

If the result of a comparison between hindcast, reanalysed and in-situ wind speed is determined by the assimilation status of the in-situ observation, it should be expected that for an assimilated observation the differences between NRA_R1 and in-situ wind speed are lower than those between hindcast and in-situ data. Similarly, the differences between the NRA_R1 and in-situ observations assimilated

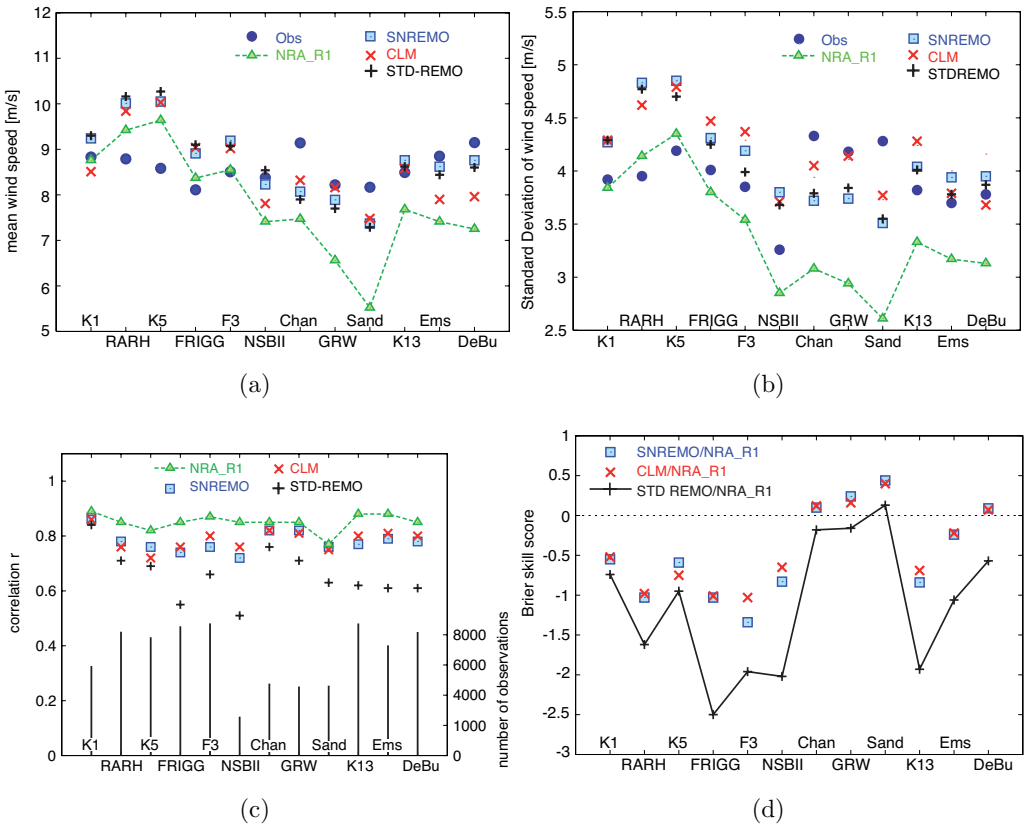

Figure 4.5: *Comparison of in-situ, reanalysed and RCM-hindcast wind speed for 1998: a) mean wind speed, b) its standard deviation, c) number of observations and correlation coefficient r and d) Brier Skill Scores using NRA_R1 time series as reference "forecast" and SN-REMO, STD-REMO and CLM time series as "forecast".*

into the NRA_R1 should be lower than those between NRA_R1 and unassimilated in-situ data. However, a dependence of the comparison of observed and modelled annual mean wind speeds on the assimilation of the observation cannot be seen in contrast to the dependence on the distance from land.

In general, the absolute difference in mean wind speed between the NRA_R1 and in-situ data is not lower, when the in-situ observation is assimilated. The differences are similar for the open ocean stations, whether they are assimilated (K1, RARH, K5) or not (Frigg, F3 and NSBII). In contrast, the absolut differences seem to be even higher for the assimilated coastal stations Chan, GRW and Sand than for their unassimilated counterparts (K13, Ems, DeBu), indicating that the complex topography in the English Channel, which the NRA_R1 cannot resolve, has a higher impact on the comparison than the assimilation status of

the observation.

At open ocean stations the regional models tend to overestimate the mean wind speed, while NRA_R1's annual mean wind speed is normally closer to the observed one. This finding is again independent of the assimilation status of the open ocean station. In contrast, the mean coastal wind is strongly underestimated by the NRA_R1, while the regional models show better agreement, although they also underestimate the mean coastal wind. Again this finding is independent of the assimilation status of the observation. Thus, while no dependence of the comparison on the assimilation status of the observation can be seen, there is a clear indication of an influence of the proximity to the coast, especially complex coastlines, on the comparison.

The mean observed wind speed at K5 is around 1.5 m s^{-1} lower than that of the NRA_R1 and all three RCM simulations. The results indicate the same low wind speed at K5 as in the comparison with HOAPS in 1998 and QuikSCAT and HOAPS in 2002 (Figures 3.2(a), 3.5(a) and 3.7(a)). Both HOAPS and QuikSCAT wind speed retrievals are not assimilated into the NRA_R1 and thus are independent from both the NRA_R1 and the hindcasts. Therefore the conclusion can be drawn that K5 measures too low wind speeds in both 1998 and 2002 and, most likely, also in between.

As expected the regionally modelled wind speeds show a higher variability than NRA_R1 at all stations (see Figure 4.5(b)). However, the regional simulations show more variability than observed at open ocean stations, which is unplausible as they give wind speed averaged over a wide area and should therefore have lower wind speed variabilities than the point observations. In coastal areas there is no consistent behaviour of modelled versus observed variability. For the light ships in the Channel, REMO and CLM underestimate the variability however, being much closer to the observed variability than the NRA_R1. Considering the coastal stations in the German Bight RCM-hindcast wind speed variability is similar to the one observed.

As depicted in Figure 4.5(c) NRA_R1 wind speeds show the highest correlation with observations approximately ranging from 0.8 to 0.9, apparently independent of observation assimilation status or proximity to coast. All regional simulations have lower correlation coefficients at all stations, however the spectrally nudged simulations (SN-REMO and CLM) always show higher correlation coefficients than the standard REMO simulation.

In order to test to which extent the regionally modelled wind speed fits the data better or worse than the NRA_R1 wind speed, the Brier skill score is computed according to Equation 4.1. While negative BSS values show a worse represen-

tation of the observations than by the reference NRA_R1 wind speeds, positive values show an improvement in comparison to the NRA_R1 time series.

As illustrated in Figure 4.5(d) the spectrally nudged simulations always have a higher BSS than STD-REMO, thus CLM and SN-REMO always reflect the measurements better than the unnudged STD-REMO. While STD-REMO has negative BSS values at all stations apart from the coastal station Sandettie, SN-REMO and CLM have positive BSS values for the four coastal stations Channel, Greenwich, Sandettie and DeBu. Thus NRA_R1 wind speed time series fit the observations better at all open ocean stations (independent of their assimilation status) and even at the two coastal stations K13 and Ems. Again the assimilation status of a coastal station is of minor importance, as SN-REMO has positive BSS values for all three assimilated light ships in the Channel, but only for one unassimilated coastal station (DeBu). Therefore the proximity to the coast and the exposition to winds affected by the land sea transition might be the determining factor for a better performance of regionally modelled winds.

Extraordinary results can be seen for the light ship Sandettie: NRA_R1 shows the biggest underestimation of the observed annual mean wind speed and its variablity and the lowest correlation coefficients. The positive Brier Skill Score at Sandettie is largely due to the strong bias of NRA_R1 wind speed. Additionally it should be noted that the light ship Sandettie is located in a NRA_R1 land grid box.

To see whether these results are similar for different years, yearly Brier Skill Scores with SN-REMO as "forecast" and NRA_R1 as "reference" were determined for several years for Frigg, F3, K13, Ems and DeBu (multiyear data were not available from CLM and the other stations). One can infer from Figure 4.6 that there is, if at all, only a small added value of SN-REMO for DeBu, for all other stations the regional model shows no added value in instantaneous wind speeds.

To judge whether the supposed added value for DeBu is significant, a T-test for comparison of the expectation value of two independent normally distributed random variables X and Y was applied. The random variables X and Y were chosen as:

$$X = |F - O|$$
$$Y = |R - O|$$

with F being the SN-REMO "forecast", R the NRA_R1 reference "forecast" and O the observation. In case of an added value of SN-REMO the expectation value of $X = \mu_X$ should be smaller than μ_Y. The null hypothesis H_0 and the alternative

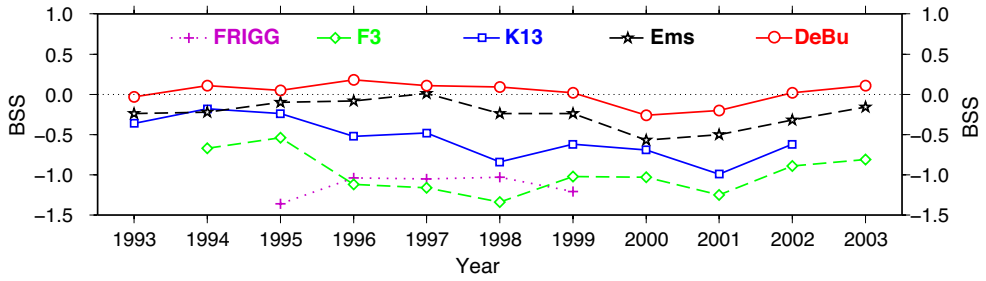

Figure 4.6: *Yearly Brier Skill Scores at five stations.*

hypothesis H_1 are therefore:

$$H_0 : \mu_X = \mu_Y$$
$$H_1 : \mu_X \leq \mu_Y$$

To allow for independence of X and Y the available realisations of X and Y were subsampled, taking into account every 161st observation which corresponds with a sampling interval of six days and 17 hours. The sampling interval was arbitrarily chosen that large to be on the safe side concerning the independence of individual observations. 17 hours were chosen to avoid an overrepresentation of daily wind cycles, which are very common in coastal regions. H_0 was tested using a t-statistic as described in e.g. von Storch and Zwiers (1999). H_0 could not be rejected with an error probability $\alpha \leq 10\%$. Thus SN-REMO has no significant added value at DeBu. The same test was applied for Frigg, F3, K13 and Ems. H_0 could be rejected with $\alpha \leq 1\%$ for Frigg, F3 and K13 and $\alpha \leq 10\%$ for Ems showing that NRA_R1 winds are statistically significantly better than their regional model counterparts.

It can be concluded, to this point, that in comparison to NRA_R1 there is no added value from regional models for instantaneous marine wind fields. However, there is an indication for an added value in the instantaneous wind speeds for rough coastal areas with a complex orography like the English Channel.

4.4.2 Wind speed frequency distribution

When wind speed distributions are concerned, the regional models always show a better representation of observed frequency distributions than the NRA_R1 for coastal areas (exemplarily shown in Figure 4.7(b) for the light ship Channel). The NRA_R1 is generally underestimating the observations variability in coastal areas, as can be expected from a mean value over 20 min and a wide area. The

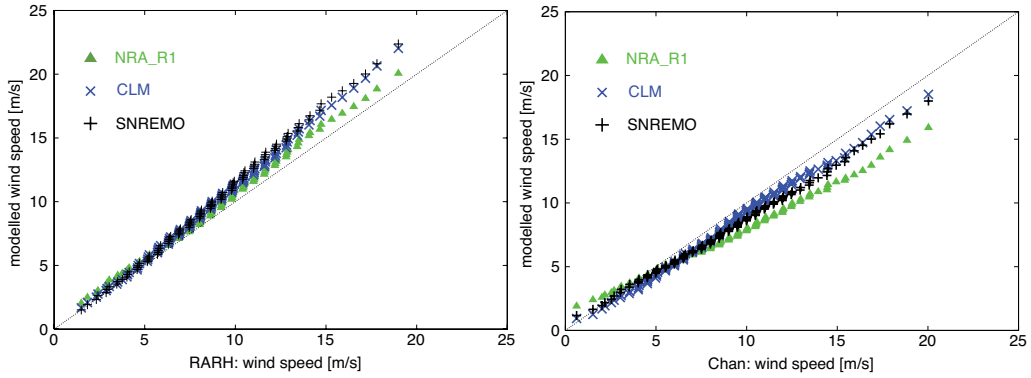

(a) (b)

Figure 4.7: *Percentile-percentile distributions of wind speed in 1998, measured (x-axis) vs. NRA_R1, SN-REMO and CLM percentiles at a) the buoy RARH as an open ocean station and b) the light ship Channel as a coastal station.*

underestimation is biggest for the English Channel stations. This underestimation of variability together with NRA_R1's strong negative wind speed bias leads to overestimations of the lowest percentiles and underestimations of higher percentiles.

For open ocean stations NRA_R1 wind speed variabilities better correspond with the observed variabilities. The regional models produce a lot of unobserved wind speed outliers for all stations (not shown). Together with the regional models' strong positive wind speed bias they lead to overestimations of higher percentiles in open ocean areas, with overestimations increasing towards the highest percentiles. Observed wind speed frequency distributions in the open ocean are better reproduced by NRA_R1, shown for RARH in Figure 4.7(a).

For coastal areas there is a clear indication of a general added value of the spectrally nudged models for wind speed frequency distributions, not limited to 1998. This can be inferred from the yearly 50, 90 and 99 percentiles determined for Frigg, F3, K13, Ems and DeBu. These percentiles are shown for F3 and DeBu in Figure 4.8. Indeed SN-REMO represents the observed 50, 90 and 99-percentiles better than the NRA_R1 at DeBu and the two other coastal stations K13 and Ems. Contrarily, NRA_R1 wind speed percentiles are closer to observed ones for the two open ocean stations Frigg and F3. Similar results were found for CLM (not shown).

Brier Skill scores have been calculated using the observed yearly 50, 90, 95 and 99 percentiles and the respective SN-REMO and NRA_R1 percentiles as "forecast"

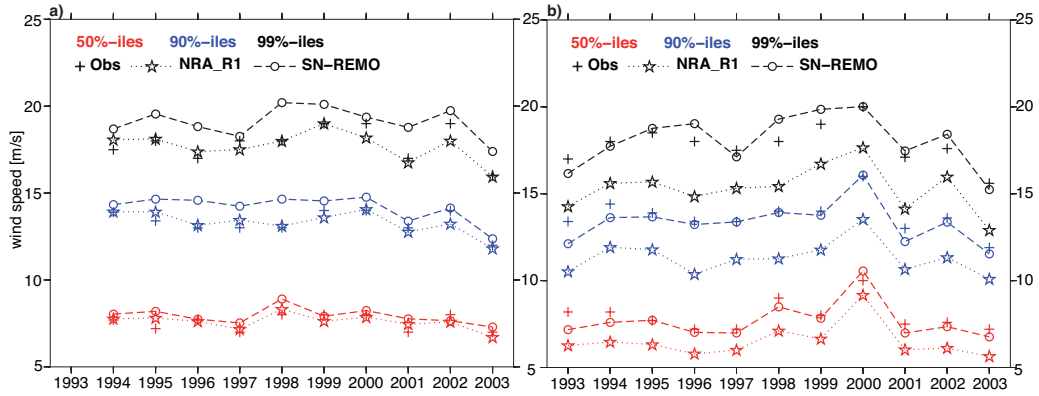

Figure 4.8: *Yearly Percentiles of wind speed for a) the platform F3 as an open ocean station and b) the light ship Deutsche Bucht (DeBu) as a coastal station: observation (cross), NRA_R1 (dotted, star) and SN-REMO (dashed, circle), red: 50%-ile, blue: 90%-ile, black: 99%-ile.*

and reference "forecast". While it can be argued, that the calculated Brier Skill Scores stem from just five (Frigg) to 11 (DeBu, Ems) available yearly percentile values and are therefore of limited value, the calculated positive and negative skills provide some indication of the general validity of the above findings. The results are displayed in Table 4.1 showing that there's an added value of SN-REMO for the distribution of higher wind speeds and their inter-annual variability in coastal areas, while NRA_R1 is better reproducing distributions of higher wind speeds in open ocean areas. The added value of NRA_R1 in the open ocean is mainly determined by the big wind speed bias of SN-REMO, but even after a bias correction the NRA_R1 has a strong positive skill for F3 and Frigg for all the mentioned percentiles.

Table 4.1: *Brier Skill Scores of yearly percentiles from Frigg, F3, K13, Ems and DeBu.*

	open ocean		coastal stations		
%-ile	Frigg	F3	K13	Ems	DeBu
99	-12.53	-6.86	0.37	0.78	0.93
95	-15.42	-2.67	0.58	0.93	0.95
90	-16.03	-6.18	0.80	0.95	0.95
50	-11.03	-1.69	0.86	0.90	0.90

4.5 Discussion and conclusions

In the eastern North Atlantic and the North Sea investigated in this study, marine wind speeds face a shift in the scale of driving processes in the transition from open ocean to coastal areas. In open ocean areas surface marine wind speed is strongly determined by large synoptic scale cyclones and pressure systems, while in coastal areas local medium to small scale wind regimes contribute more strongly to its characteristics. Therefore it was assumed that the value added by RCMs in reproducing the surface marine wind speed differs with the proximity to land. This study focuses on the confirmation of this assumption with the help of simulations of the surface marine wind speed fields from the regional atmospheric model REMO in two configurations (with and without spectral nudging applied, same simulations as used by Feser (2006)) and the regional atmospheric model CLM (Böhm et al. 2006, with spectral nudging applied). For that purpose the wind fields from these three simulations and the NRA_R1 are compared to in-situ wind speed observations. The comparison is emphasised on observed "instantaneous" wind speed and its frequency distribution.

The assumption that the added value for surface marine wind speed differs with proximity to land is confirmed by the results of this study. In detail this study shows that:

- For open ocean areas there is no value added to the reanalysis forcing by the use of the RCMs REMO and CLM neither for instantaneous wind speed nor its frequency distribution.
- In coastal areas value is added by REMO and CLM only in frequency distributions.
- However, there is an indication for added value also in the instantaneous wind speeds for rough coastal areas with a complex orography like the English Channel.
- An influence of the observations assimilation status on these findings can not be seen.

Contrarily to our results, Sotillo et al. (2005) suggested an added value of SN-REMO even for single extreme wind events in the Mediterranean linked to regional winds (i.e. Bora, Tramontana, Mistral etc.). As the area studied by Sotillo et al. (2005) has a much more complex coastline and stronger topographic gradients in the Mediterranean, it is concluded that such topographic effects are more important in the Mediterranean than in the North Sea.

Thus, combining the results of Sotillo et al. (2005) and this study, the answer

to the question "Do RCMs add value to the marine surface wind speed in comparison to the reanalysis wind speed forcing to justify their usage in wind speed hindcasts?" posed in the introduction, is that added value of regionally modelled marine wind speed fields for hindcast purposes can be seen close to very complex, rough coastal areas with a complex orography such as in the Mediterranean and the English Channel. Offshore from coastal areas with a less complex topography like in the German Bight, with its adjacent flat plains of Northern Germany and the Netherlands, there is an indication for an added value but only in the distribution and not for single events. For "open ocean" areas there is no sign of an added value of regionally modelled wind speeds.

There are several limitations to this study. In this study the analysis has been conducted for the North Sea and eastern North Atlantic, the regional models may behave differently in other areas. A part of the investigated area (North Atlantic west of the British Isles and the English Channel) was analysed for 1998 only and the behaviour may change in different years. Strictly the findings of this study only hold for hindcast studies:

- For case studies of individual storms at a certain location in the North Atlantic/North Sea the NRA_R1 is the recommended product.
- For the purpose of designing coastal and marine infrastructure when wind speed distributions are needed the NRA_R1 is recommended for open ocean areas while hindcast wind speeds from regional models may improve the results in coastal regions.
- The meaning of the results for forecast studies can not be judged, as the situation is somewhat different in hindcast studies. Under hindcast conditions NRA_R1 can be seen as a perfect boundary condition due to the assimilation at all time steps. However in the forecast mode boundary conditions are much less perfect, thus there is a remaining chance that the regional model improves for forecast purposes.
- The meaning of our results for climate change simulations is unclear.

The spectral nudging technique proposed by von Storch et al. (2000) can be interpreted as a poor man's regional data assimilation, in our case its use leads to a better reflection of instantaneous wind speeds by CLM and SN-REMO than by STD-REMO. However, the performance of CLM and SN-REMO is too poor to beat NRA_R1 wind speeds in open ocean and "less complex" coastal areas.

One of the biggest limitations of this study might be the assumption that the partly extrapolated wind speed observations represent the truth - the actual wind speeds at 10 m height. Especially for high wind speeds and a fully developed sea

the quality of buoy measurements is arguable. Wind speed measurements have their uncertainties, however the wind speed measurements at DeBu, Ems and NSBII can be considered as a good representation of the actual wind speeds as the instrumentations are mounted in 10 m height.

In coastal waters, especially in the English Channel, thermal stratification is less likely to be neutral due to effects of the land sea transition, e.g. different temperatures of water masses and winds blowing off-land, see Csanady (1974). Therefore wind speeds of the English bouys and light ships were converted using the COARE bulk flux algorithm in version 3.0b after Fairall et al. (2003) for stability correction. Additionally the same investigations were done with these observations extrapolated to 10 m using the neutral logarithmic wind speed profile with a varying roughness length according to Charnock (1955). However, the results with these two different conversions mechanisms were negligibly different, which is plausible, since for the open ocean the logarithmic wind profile is well known from observations (e.g., Edson and Fairall 1998) and the deviations at the lightships in the English Channel should be negligible due to the small difference between the measurement height of 14 m and the extrapolation height of 10 m. Furthermore, profile measurements at the metmast FINO in the North Sea showed that neutral conditions prevail during half of the time (Kay Sušelj, University of Oldenburg, ForWind, pers. comment).

The biggest deviations from actual wind speeds at 10 m should occur at the platforms Frigg, F3 and K13. They should be mainly due to the big differences between measurement and extrapolation height of up to 85 m for Frigg, the heavy influence of the oil platform structure on the measurements and the extrapolation with the logarithmic wind profile and a constant factor/a constant sea roughness.

Furthermore there are uncertainties in the diagnostic 10 m wind speed from CLM and REMO, which is calculated from the prognostic wind speed at the lowest model level, being 32 m for both REMO simulations and 34 m for CLM. It can be argued that changes in the surface layer parameterization and especially the roughness parameter or Charnock constant might lead to improvements in the surface wind speed representation by REMO and CLM in the open ocean. However, Weisse and Schneggenburger (2002) show that differences between individual realizations of different ensembles (using different parameterizations of the momentum flux after Charnock 1955; Janssen 1989, 1991 and Makin and Kudryavtsev 1999) cannot necessarily be considered as being entirely induced by the models sensitivity to the models parameterizations. Therefore any tuning of the surface layer parameterization of REMO and CLM is not considered in this study.

In 1998, the investigated SN-REMO, STD-REMO and CLM hindcast are forced

with the NRA_R2. However, no reanalysed 10 m wind speed is available. Therefore, the 10 m wind speed forecast of the NRA_R2 as buest guess for reanalysed 10 m wind speed should have been used in the added value assessment. However, the NRA_R2 10 m wind speed forecast is an unplausible data set, which can not be considered to represent neither real wind speed nor the 10 m wind speed within the NRA_R2 reanalysis, as has been demonstrated. Therefore, the only way to assess the added value for the SN-REMO, STD-REMO and CLM with the in-situ data set in 1998 is to assume that the NRA_R1 10 m wind speed forecast gives a reasonable representation for the 10 m wind speed within the NRA_R2 reanalysis forcing field.

The determination of yearly Brier-Skill Scores of the instantaneous wind speeds (Figure 4.6) and the comparison of the yearly percentiles (Figure 4.8) did not show a qualitative change of the results due to the shift in the reanalysis forcing from NRA_R1 to NRA_R2 in 1997. This might indicate, that the approach to use the NRA_R1 10 m wind speed forecast as best guess for the 10 m wind speed within the NRA_R2 reanalysis forcing field is reasonable. However, the added value assessment should be redone with in-situ data prior to 1997, when the SN-REMO and STD-REMO hindcasts are forced with the NRA_R1, to confirm the results presented. Furthermore, first preliminary results with the RCM CLM forced with the ERA40 reanalysis seem to confirm the results found in this study (not shown).

Additional uncertainties can be introduced by the different temporal and spatial resolutions of the observed, reanalysed and modelled wind speeds. The 20 minute means of the NRA_R1 forecast used in this study are available every 6 hours, modelled and observed means every hour. In the presented analysis the NRA_R1 was time interpolated to one hour resolution. Subsampling the modelled and observed wind speeds to the six-hour frequency prescribed by NRA_R1 is an alternative approach. Both methods have been tested, the resulting differences were negligible.

Chapter 5

Outlook

5.1 Feasibility of HOAPS and QuikSCAT for the added value assessment

Using HOAPS and QuikSCAT as an estimate of real surface marine wind speed makes the added value assessment possible in remote areas far offshore where in-situ wind speeds are rarely measured. Even in the North Sea, HOAPS and QuikSCAT (when gridded) may enable a cheaper, more easy and regularly spaced assessment than is possible with the in-situ observations, irregularly distributed in space. However, the assessment of added value using HOAPS and QuikSCAT as source of real surface marine wind speed is beyond the scope of this thesis. In Chapter 3 it was already shown that both HOAPS and especially QuikSCAT give good representation of real 10 m wind speed and are therefore principally suited for that task. This section elaborates on this issue by additionally comparing HOAPS and QuikSCAT with co-located NRA_R1 and RCM wind speed.

5.1.1 Comparison of HOAPS, reanalysed and RCM-hindcast wind speed

HOAPS wind speed retrievals were co-located with the 10 m wind speed obtained from the in-situ data, SN-REMO, CLM and the NRA_R1 in 1998. For that purpose SN-REMO and the NRA_R1 were bilinearly interpolated to the stations' location. Furthermore the NRA_R1 available every 6 hours is time interpolated to one hour resolution. The co-location procedure is the same as explained in section 3.1.1. The main statistics of the comparison are depicted in Figure 5.1.

Figure 5.1(a) confirms that the NRA_R1 gives the best reproduction of observed means for open ocean areas in 1998, which has already been shown in Chapter 4 (Figure 4.5(a)). However in the German Bight both HOAPS and the RCMs are closer to the observed means. In the open ocean the RCMs SN-REMO and

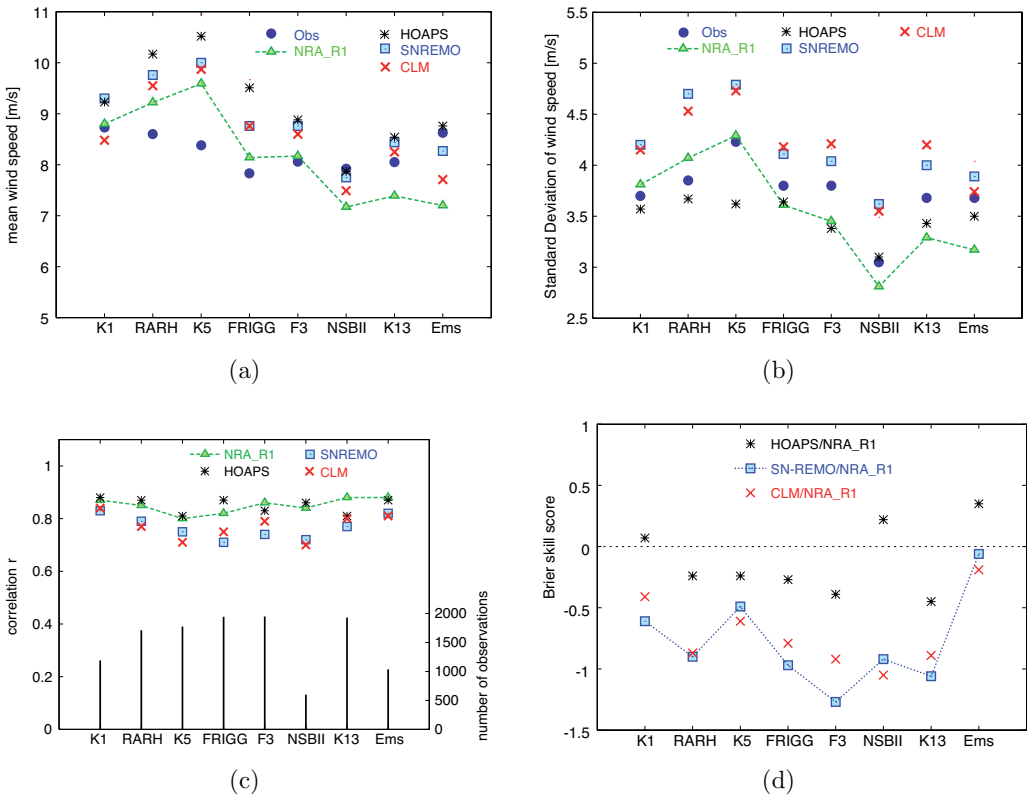

Figure 5.1: *Comparison of HOAPS, in-situ, reanalysed and RCM-hindcast wind speed in 1998: a) mean wind speed, b) its standard deviation, c) number of observations and correlation coefficient r and d) Brier Skill Scores using NRA_R1 time series as reference "forecast" and HOAPS, SN-REMO and CLM time series as "forecast".*

CLM show strong but smaller positive biases than HOAPS. HOAPS positive bias in the annual mean wind speed as compared with the NRA_R1 is in agreement with the findings of Meissner et al. (2001). They showed that the SSM/I's on F11 and F13 deliver mean biases of around 0.5 m/s as compared to the 10 m forecasted wind speed of the NRA_R1. As both F11 and F13 are incorporated in the HOAPS-S product in 1998 and F11 is the reference satellite used for the SSM/I intercalibration as described in Fennig (2001), at least part of the bias arises from the biases of these SSM/I's. While HOAPS, as a 50 km spatial average, provides a reasonable representation of observed wind speed variability as given by the standard deviation, SN-REMO and CLM tend to overestimate it.

The correlation coefficients between the observations and HOAPS are comparable to those of the NRA_R1, showing that both products give an equally good representation of the temporal development of the wind field. The RCMs

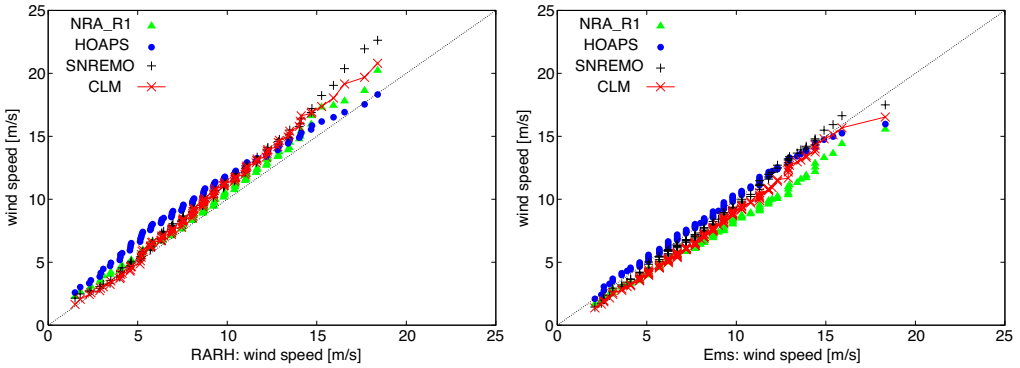

Figure 5.2: *Percentile-percentile distributions of wind speed in 1998, measured (x-axis) vs. HOAPS, NRA_R1, SN-REMO and CLM (y-axis) percentiles at a) RARH and b) Ems. The 99 dots represent the wind speed percentiles in steps of 1 percent.*

show a lower correlation with observed wind speed than both HOAPS and the reanalysis at all stations.

The BSS with HOAPS as "forecast" and NRA_R1 as reference "forecast" fluctuates around zero (Figure 5.1(d)), which means that the RMSEs between NRA_R1 and in-situ wind speed and HOAPS and in-situ wind are comparable. Furthermore, it can be deduced from that figure, that the RMSE's between the RCMs and in-situ data are higher than those between in-situ data and both HOAPS and the NRA_R1. Thus, it can be concluded, that the NRA_R1 and HOAPS give an equally good representation of instantaneous wind speed, while the RCMs can not retain the value of the NRA_R1.

Concerning wind speed frequency distributions HOAPS can reproduce the observed frequency distributions as good as the NRA_R1 in the open ocean (as depicted exemplarily for RARH in Figure 5.2(a)) and as good as the RCMs in the coastal region, as represented by the coastal station Ems in Figure 5.2(b). However, HOAPS gives no wind speed within 50 km distance from the coast, which would be a major drawback in the application of HOAPS as real wind in the added value assessment. Finally, HOAPS gives no better representation of in-situ wind speed than the NRA_R1 which limits its usefulness in the assessment.

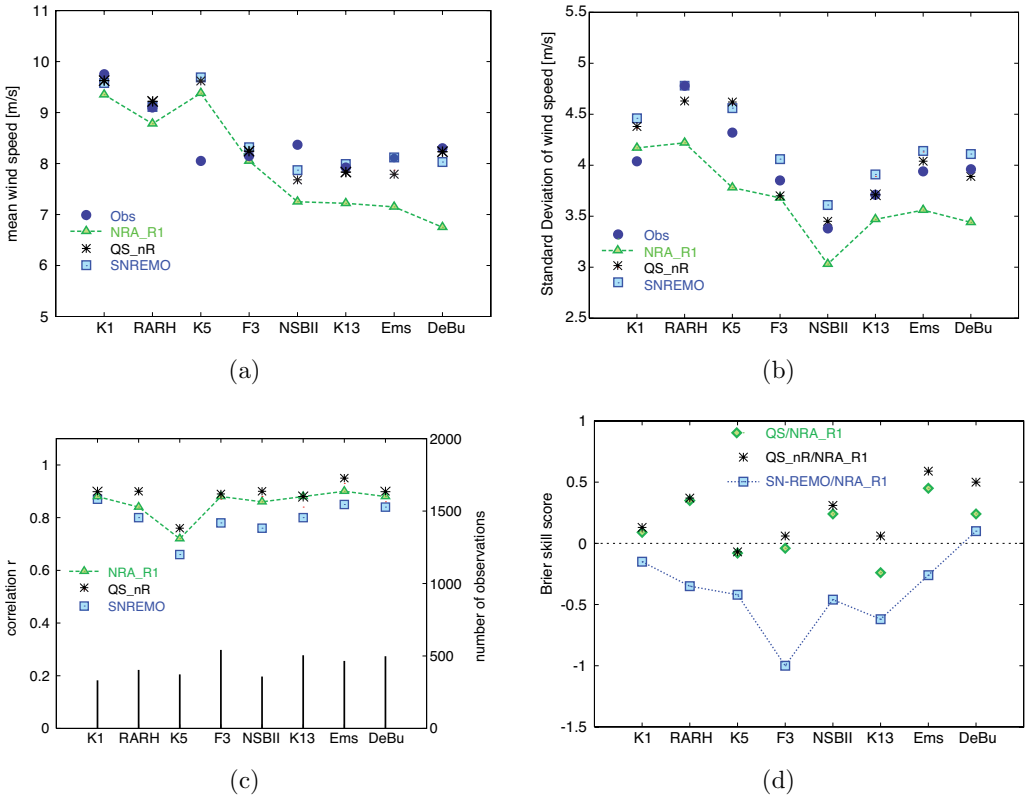

Figure 5.3: *Comparison of QuikSCAT, in-situ, reanalysed and modelled wind speed for 2002: a) mean wind speed, b) its standard deviation, c) number of observations and correlation r and d) Brier Skill Scores using NRA_R1 as reference "forecast" and QS_nR (QuikSCAT without rain contaminated WVCs), QS (QuikSCAT including rain contaminated WVCs) and SN-REMO as "forecast".*

5.1.2 Comparison of QuikSCAT, reanalysed and RCM-hindcast wind speed

QuikSCAT wind speed retrievals were co-located with the 10 m wind speed obtained from the in-situ data, SN-REMO and the NRA_R1 in 2002. For that purpose SN-REMO and the NRA_R1 were bilinearly interpolated to the stations' location. Furthermore the NRA_R1 available every 6 hours is time interpolated to one hour resolution. The co-location procedure is the same as explained in section 3.2.1. Rain contaminated WVCs are excluded from the comparison, the main statistics of the comparison are depicted in Figure 5.3.

As already mentioned, QuikSCAT and SN-REMO show a better agreement with the observed mean wind and its standard deviation than the NRA_R1 in 2002.

However, SN-REMO shows lower correlation with all observations and higher RMSE values than the NRA_R1, which is equivalent to negative Brier skill scores with SN-REMO as "forecast" and NRA_R1 as "reference forecast". Unlike SN-REMO, QuikSCAT shows higher correlations than NRA_R1 for all observations.

The RMSE values between QuikSCAT and the observations are, with the negligible exception of the malfunctioning buoy K5, always around or lower than 2 m/s. Furthermore QuikSCAT has lower RMSE values than the NRA_R1 which in turn means positive Brier Skill Scores. The positive Brier Skill Scores show an improved representation of the observed wind speed as by the reference "forecast", the NRA_R1. Even if rain contaminated WVCs are included in the comparison, QuikSCAT gives a better representation of the observed wind speed than the NRA_R1 in five of seven cases (neglecting K5, Figure 5.3(d)).

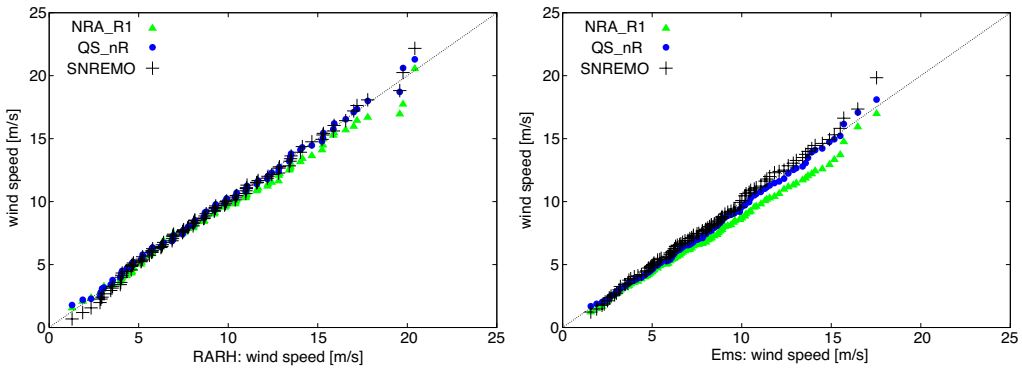

(a) (b)

Figure 5.4: *Percentile-percentile distributions of wind speed in 2002, measured (x-axis) vs. QuikSCAT, NRA_R1 and SN-REMO (y-axis) percentiles at a) RARH and b) Ems.*

The wind speed frequency distributions of QuikSCAT are compared to those of the NRA_R1, SN-REMO and the in-situ data with the help of the quantile-quantile plots illustrated in Figure 5.4 for RARH and Ems. The significance of these quantile-quantile plots is very limited as each of the 99 percentiles from the 1st to the 99th-percentile stands for just three to five observations due to the small amount of co-located data. Under these constraints QuikSCAT shows the highest agreement with the observed wind speed frequency distributions for all stations.

Thus, it is concluded that QuikSCAT gives a good representation of surface marine wind, which is better than that by the NRA_R1. Therefore QuikSCAT's wind speed retrievals enable an assessment of the added value of RCMs over a

much wider area and with a regular spatial coverage. A limitation to that assessment is the unavailability of QuikSCAT wind speed retrievals within 30 km off the coast.

The procedure of the added value assessment with QuikSCAT can be as follows: NRA_R1's forecasted 10 m wind speed is bilinearly interpolated onto the grid of the RCM hindcast. It is time interpolated to the one hour resolution of the RCM in addition. QuikSCAT is gridded taking into account wind speed retrievals within 20 min and 12.5 km (spatial resolution of QuikSCAT's Level 2B 12.5 km Composite product) of a RCM grid point wind speed record. As QuikSCAT is available since 1999, several years of gridded QuikSCAT wind speed can be compared with the NRA_R1 and RCM wind speed, allowing for a detailed statistical evaluation of the value added to the NRA_R1 wind speed forcing by the RCM at every grid point.

Bibliography

Andersson, A., Bakan, S., Fennig, K., Grassl, H., and Klepp, C. (2007a). The HOAPS-3 Climatology. In *Proceedings of the 3rd Workshop of the International Precipitation Working Group (IPWG), Melbourne, 23-27 October, 2006*. Submitted.

Andersson, A., Bakan, S., Fennig, K., Grassl, H., Klepp, C., and Schulz, J. (2007b). Hamburg Ocean Atmosphere Parameters and Fluxes from Satellite Data - HOAPS-3 - 5-days mean. Hamburg: World Data Center for Climate (WDCC), doi: 10.1594/WDCC/HOAPS3_PENTAD.

Andersson, A., Bakan, S., Fennig, K., Grassl, H., Klepp, C., and Schulz, J. (2007c). Hamburg Ocean Atmosphere Parameters and Fluxes from Satellite Data - HOAPS-3 - monthly mean. Hamburg: World Data Center for Climate (WDCC), doi: 10.1594/WDCC/HOAPS3_MONTHLY.

Andersson, A., Bakan, S., Fennig, K., Grassl, H., Klepp, C., and Schulz, J. (2007d). Hamburg Ocean Atmosphere Parameters and Fluxes from Satellite Data - HOAPS-3 - twice daily composite. Hamburg: World Data Center for Climate (WDCC), doi: 10.1594/WDCC/HOAPS3_DAILY.

Babin, S. M. and Thompson, D. R. (2000). Effects of atmospheric boundary layer moisture on friction velocity with implications for SAR imagery. *Ieee Transactions On Geoscience Remote Sensing*, 38(1):618–621.

Barrett, E., Beaumont, M., Brown, P., Taberner, M., Tait, A., and Todd, M. (1997). A satellite-based atlas of rainfall and wind speed over the eastern North Atlantic and North Sea. Report to Department of Environment, Transport and the Regions, epg 1 :9 :33, Centre for Remote Sensing, University of Bristol, UK.

Bauer, P. and Schluessel, P. (1993). Rainfall, total water, ice water, and water-vapor over sea from polarized microwave simulations and special sensor microwave imager data. *J. Geophysical Research-atmospheres*, 98(D11):20737–20759.

Böhm, U., Kücken, M., Ahrens, W., Block, A., Hauffe, D., Keuler, K., Rockel, B., and Will, A. (2006). CLM - the climate version of LM: Brief description and long-term applications. *COSMO Newsletter*, 6.

Bromwich, D. H., Fogt, R. L., Hodges, K. I., and Walsh, J. E. (2007). A tropospheric assessment of the ERA-40, NCEP, and JRA-25 global reanalyses in the polar regions. *J. Geophysical Research-atmospheres*, 112(D10).

Businger, J., Wyngaard, J., Izumi, Y., and Bradley, E. (1971). Flux profile relationship in the atmospheric surface layer. *J. Atmos. Sci. 28*, pages 181–189.

Castro, C. L., Pielke, R. A., and Leoncini, G. (2005). Dynamical downscaling: Assessment of value retained and added using the Regional Atmospheric Modeling System (RAMS). *J. Geophysical Research-atmospheres*, 110(D5).

Charnock, H. (1955). Wind stress over a water surface. *Quart. J. Roy. Meteor. Soc.*, 81:639–640.

Chelton, D. B. and Freilich, M. H. (2005). Scatterometer-based assessment of 10-m wind analyses from the operational ECMWF and NCEP numerical weather prediction models. *Monthly Weather Rev.*, 133(2):409–429.

Chelton, D. B., Ries, J. C., Haines, B. J., Fu, L. L., and Callahan, P. (2001). Satellite altimetry. In Fu, L. L. and Cazanave, A., editors, *Satellite altimetry and earth sciences*, pages 1–131. Academic Press, NY.

Chelton, D. B., Schlax, M. G., Freilich, M. H., and Milliff, R. F. (2004). Satellite measurements reveal persistent small-scale features in ocean winds. *Science*, 303(5660):978–983.

Cornillon, P. and Park, K. A. (2001). Warm core ring velocities inferred from nscat. *Geophysical Research Lett.*, 28(4):575–578.

Cox, C. and Munk, W. (1954). Statistics of the sea surface derived from sun glitter. *J. Mar. Res.*, 13:198–227.

Csanady, G. T. (1974). Equilibrium theory of the planetary boundary layer with an inversion lid. *Bound.-Layer Meteor.*, 6:63–79.

Davis, T. (1999). Special Sensor Microwave / Imager (SSM/I). User's interpretation guide fourth edition, Raytheon Systems Company.

Derber, J. D., Parrish, D. F., and Lord, S. J. (1991). The new global operational analysis system at the National Meteorological Center. *Wea. Forecasting*, 6:538–547.

Doms, G., Förstner, J., Heise, E., Herzog, H. J., Raschendorfer, M., Schrodin, R., Reinhardt, T., and Vogel, G. (2005). A description of the nonhydrostatic regional model LM Part II: Physical parameterization. Scientific documentation, Deutscher Wetterdienst, Offenbach.

Doms, G. and Schättler, U. (2005). A description of the nonhydrostatic regional model LM Part I: Dynamics and Numerics. Scientific documentation, Deutscher Wetterdienst, Offenbach.

Dunbar, R. S. (2006). Level 2B Data Software Interface Specification (SIS-2) - QuikSCAT Era. Technical report, Jet Propulsion Laboratory, California Institute of Technology, NASA.

Ebuchi, N., Graber, H. C., and Caruso, M. J. (2002). Evaluation of wind vectors observed by QuikSCAT/SeaWinds using ocean buoy data. *J. Atmospheric Oceanic Technology*, 19(12):2049–2062.

Edson, J. B. and Fairall, C. W. (1998). Similarity relationships in the marine atmospheric surface layer for terms in the TKE and scalar variance budgets. *J. Atmos. Sci 55*, pages 2311–2328.

Ekman, V. (1905). On the influence of the earth's rotation on ocean currents. Arkiv för Matematik, Astronomi och Physik, 2(1905) 1-53.

Fairall, C. W., Bradley, E. F., Hare, J. E., Grachev, A. A., and Edson, J. B. (2003). Bulk parameterization of air-sea fluxes: Updates and verification for the COARE algorithm. *Journal of Climate*, 16:571–591.

Federico, S. and Bellecci, C. (2004). Sea storms hindcast around Calabrian coasts: Seven cases study. *Nuovo Cimento Della Societa Italiana Di Fisica C-geophysics Space Phys.*, 27(2):179–203.

Fennig, K. (2001). *Interkalibration verschiedener SSM/I Mikrowellenradiometer im Hinblick auf eine gemeinsame Nutzung für eine fernerkundete Klimatologie*. Diplomarbeit, Meteorologisches Institut der Universität Hamburg, Max-Planck-Institut für Meteorologie Hamburg.

Feser, F. (2006). Enhanced detectability of added value in limited-area model results separated into different spatial scales. *Monthly Weather Rev.*, 134(8):2180–2190.

Feser, F. and von Storch, H. (2007). A dynamical downscaling case study for typhoons in SE Asia using a regional climate model. accepted for publication in Monthly Weather Review.

Feser, F., Weisse, R., and von Storch, H. (2001). Multi-decadal atmospheric modeling for Europe yields multi-purpose data. *Eos Trans. Amer. Geophys. Union*, (82):305 – 310.

Fowler, H. J. and Kilsby, C. G. (2007). Using regional climate model data to simulate historical and future river flows in northwest England. *Climatic Change*, 80(3-4):337–367.

Freilich, M. H. and Dunbar, R. S. (1999). The accuracy of the NSCAT 1 vector winds: Comparisons with National Data Buoy Center buoys. *J. Geophysical Research-oceans*, 104(C5):11231–11246.

Gaslikova, L. and Weisse, R. (2006). Estimating near-shore wave statistics from regional hindcasts using downscaling techniques. *Ocean Dynamics*, 56:26–35.

Gerritsen, H. (2005). What happened in 1953? - The big flood in the Netherlands in retrospect. *Philosophical Transactions Royal Soc. A-mathematical Phys. Engineering Sciences*, 363(1831):1271–1291.

Goodberlet, M. A., Swift, C. T., and Wilkerson, J. C. (1989). Remote-sensing of ocean surface winds with the special sensor microwave imager. *J. Geophysical Research-oceans*, 94(C10):14547–14555.

Goswami, B. N. and Rajagopal, E. N. (2003). Indian Ocean surface winds from NCMRWF analysis as compared to QuikSCAT and moored buoy winds. *Proc. Indian Acad. Sciences-earth Planetary Sciences*, 112(1):61–77.

Hong, S.-Y. and Pang, H.-L. (1996). Nonlocal boundary layer vertical diffusion in a medium-range forecast model. *Mon. Wea. Rev.*, 124:2322–2339.

Hoskins, B. J. and Hodges, K. I. (2002). New perspectives on the Northern Hemisphere winter storm tracks. *J. Atmospheric Sciences*, 59(6):1041–1061.

Hoskins, B. J. and Hodges, K. I. (2005). A new perspective on Southern Hemisphere storm tracks. *J. Climate*, 18(20):4108–4129.

Huddleston, J. N. and Stiles, B. W. (2000). Multidimensional histogram (MUDH) rain flag. Product Description Version 3.0, Jet Propulsion Laboratory, California Institute of Technology, Pasadena, CA. [Available online at http://podaac.jpl.nasa.gov/quikscat/qscat_doc.html].

Hultquist, T. R., Dutter, M. R., and Schwab, D. J. (2006). Reexamination of the 9-10 November 1975 "Edmund Fitzgerald" storm using today's technology. *Bulletin Am. Meteorol. Soc.*, 87(5):607–622.

Hurrell, J. W. (1995). Decadal trends in the North-Atlantic Oscillation - regional temperatures and precipitation. *Science*, 269(5224):676–679.

Hurrell, J. W. and van Loon, H. (1997). Decadal variations in climate associated with the North Atlantic Oscillation. *Climatic Change*, 36(3-4):301–326.

Jacob, D. and Podzun, R. (1997). Sensitivity studies with the regional climate model REMO. *Meteor. Atmos. Phys.*, (63):119–129.

Janssen, P. A. E. M. (1989). Wave-induced stress and the drag of air-flow over sea waves. *J. Phys. Oceanography*, 19(6):745–754.

Janssen, P. A. E. M. (1991). Quasi-linear theory of wind-wave generation applied to wave forecasting. *J. Phys. Oceanography*, 21(11):1631–1642.

Johnson, H. K., Hojstrup, J., Vested, H. J., and Larsen, S. E. (1998). On the dependence of sea surface roughness on wind waves. *J. Phys. Oceanography*, 28(9):1702–1716.

Jones, P. D., Jonsson, T., and Wheeler, D. (1997). Extension to the North Atlantic Oscillation using early instrumental pressure observations from Gibraltar and south-west iceland. *Int. J. Climatology*, 17(13):1433–1450.

Jones, W. L. and Schroeder, L. C. (1978). Radar backscatter from the ocean: dependence on surface friction velocity. *Boundary-Layer Meteorol.*, 13:133–149.

Jung, T., Klinker, E., and Uppala, S. (2004). Reanalysis and reforecast of three major European storms of the twentieth century using the ECMWF forecasting system. Part 1: Analyses and deterministic forecasts. *Meteorol. Applications*, 11(4):343–361.

Jung, T., Klinker, E., and Uppala, S. (2005). Reanalysis and reforecast of three major European storms of the twentieth century using the ECMWF forecasting system. Part II: Ensemble forecasts. *Meteorol. Applications*, 12(2):111–122.

Kalnay, E., Kanamitsu, M., Kistler, R., Collins, W., Deaven, D., Gandin, L., Iredell, M., Saha, S., White, G., Woollen, J., Zhu, Y., Chelliah, M., Ebisuzaki, W., Higgins, W., Janowiak, J., Mo, K., Ropelewski, C., Wang, J., Leetmaa, A., Reynolds, R., Jenne, R., and Joseph, D. (1996). The NCEP/NCAR 40-year Reanalysis Project. *Bull. Amer. Meteorol. Soc.*, (77):437–471.

Kanamitsu, M. (1989). Description of the NMC Global Data Assimilation and Forecast System. *Weather Forecasting*, 4:334–342.

Kanamitsu, M., Alpert, J. C., Campana, K. A., Caplan, P. M., Deaven, D. G., Iredell, M., Katz, B., Pan, H. L., Sela, J., and White, G. H. (1991). Recent changes implemented into the global forecast system at NMC. *Weather Forecasting*, 6(3):425–435.

Kanamitsu, M., Ebisuzaki, W., Woollen, J., Yang, S. K., Hnilo, J. J., Fiorino, M., and Potter, G. L. (2002). NCEP-DOE AMIP-II Reanalysis (R-2). *Bulletin Am. Meteorol. Soc.*, 83(11):1631–1643.

Kapala, A., Machel, H., and Flohn, H. (1998). Behaviour of the centres of action above the Atlantic since 1881. Part II: Associations with regional climate anomalies. *Int. J. Climatology*, 18(1):23–36.

Keil, C., Tafferner, A., Mannstein, H., and Schattler, U. (2003). Evaluating high-resolution model forecasts of European winter storms by use of satellite and radar observations. *Weather Forecasting*, 18(5):732–747.

Kelly, K. A., Dickinson, S., McPhaden, M. J., and Johnson, G. C. (2001). Ocean currents evident in satellite wind data. *Geophysical Research Lett.*, 28(12):2469–2472.

Kim, J. and Lee, J. E. (2003). A multiyear regional climate hindcast for the Western United States using the mesoscale atmospheric simulation model. *J. Hydrometeorology*, 4(5):878–890.

Kistler, R., Kalnay, E., Collins, W., Saha, S., White, G., Woollen, J., Chelliah, M., Ebisuzaki, W., Kanamitsu, M., Kousky, V., van den Dool, H., Jenne, R., and Fiorino, M. (2001). The NCEP-NCAR 50-year reanalysis: Monthly means CD-ROM and documentation. *Bulletin Am. Meteorol. Soc.*, 82:247–267.

Krasnopolsky, V. M., Gemmill, W. H., and Breaker, L. C. (2000). A neural network multiparameter algorithm for SSM/I ocean retrievals: Comparisons and validations. *Remote Sensing Environment*, 73(2):133–142.

Kushnir, Y. and Wallace, J. M. (1989). Low-frequency variability in the northern hemisphere winter - geographical-distribution, structure and time-scale dependence. *J. Atmospheric Sciences*, 46(20):3122–3142.

Lange, B., Højstrup, J., Larsen, S. E., and Barthelmie, R. J. (2001). A fetch dependent model of sea surface roughness for offshore wind power utilisation. In Helm, P. and A.Zervos, editors, *Wind Energy for the new millennium. Proceedings of the European Wind Energy Conference (Copenhagen 2001)*, pages 830–833. WIP, Munich and ETA, Florenz.

Lange, B., Larsen, S., Hojstrup, J., and Barthelmie, R. (2004). The influence of thermal effects on the wind speed profile of the coastal marine boundary layer. *Boundary-layer Meteorology*, 112(3):587–617.

Liu, W. T. and Tang, W. (1996). Equivalent neutral wind. Technical report, Jet Propulsion Laboratory, Pasadena, CA.

Long, D. G. and Mendel, J. M. (1991). Identifiability in wind estimation from scatterometer measurements. *Ieee Transactions On Geoscience Remote Sensing*, 29(2):268–276.

Louis, J. (1979). A parametric model of vertical eddy fluxes in the atmosphere. *Bound.-Layer Meteor.*, (17):187–202.

Makin, V. K. and Kudryavtsev, V. N. (1999). Coupled sea surface-atmosphere model - 1. Wind over waves coupling. *J. Geophysical Research-oceans*, 104(C4):7613–7623.

Martin, S. (2004). *An Introduction to Ocean Remote Sensing*. Cambridge University Press.

Mears, C. A., Smith, D. K., and Wentz, F. J. (2001). Comparison of Special Sensor Microwave Imager and buoy-measured wind speeds from 1987 to 1997. *J. Geophysical Research-oceans*, 106(C6):11719–11729.

Meissner, T., Smith, D., and Wentz, F. (2001). A 10 year intercomparison between collocated Special Sensor Microwave Imager oceanic surface wind speed retrievals and global analyses. *J. Geophysical Research-oceans*, 106(C6):11731–11742.

Meng, L., He, Y. J., Chen, J. N., and Wu, Y. M. (2007). Neural network retrieval of ocean surface parameters from SSM/I data. *Monthly Weather Rev.*, 135(2):586–597.

Monin, A. and Obukhov, A. (1954). Basic Laws of Turbulent Mixing in the Surface Layer of the Atmosphere. *Trudy Geofiz. Inst. Acad. Nauk SSSR 24*, pages 163–187.

Mostovoy, G. V., Fitzpatrick, P. J., and Li, Y. (2005). Regional accuracy of QuikSCAT gridded winds. *Int. J. Remote Sensing*, 26(18):4117–4136.

NASA (1976). *U.S. Standard Atmosphere*. NOAA, NASA and USAF.

NOAA/NMC (1988). *NOAA/NMC Development Division: Documentation of the NMC global model*. [Available from NOAA/NCEP Environmental Modeling Center, 5200 Auth Rd., Washington, DC 20233].

Onogi, K., Koide, H., Sakamoto, M., Kobayashi, S., Tsutsui, J., Hatsushika, H., Matsumoto, T., Yamazaki, N., Kamahori, H., Takahashi, K., Kato, K., Oyama, R., Ose, T., Kadokura, S., and Wada, K. (2005). JRA-25: Japanese 25-year re-analysis project - progress and status. *Quarterly J. Royal Meteorol. Soc.*, 131(613):3259–3268.

Parrish, D. F. and Derber, J. C. (1992). The National Meteorological Center's spectral statistical interpolation analysis system. *Mon. Wea. Rev.*, 120:1747–1763.

Paulson, C. (1970). The mathematical representation of wind speed and temperature profiles in the unstable atmospheric surface layer. *J. Appl. Meteor. 9*, pages 857–861.

Pickett, M. H., Tang, W. Q., Rosenfeld, L. K., and Wash, C. H. (2003). Quikscat satellite comparisons with nearshore buoy wind data off the US West coast. *J. Atmospheric Oceanic Technology*, 20(12):1869–1879.

Roeckner, E., Arpe, K., Bengtsson, L., Christoph, M., Claussen, M., Dümenil, L., Esch, M., Giorgetta, M., Schlese, U., and Schulzweida, U. (1996). The atmospheric general circulation model ECHAM4: Model description and simulation of present-day climate. Technical Report 218, Max-Planck Inst. für Meteorol., Hamburg, Germany.

Roedel, W. (2000). *Physik unserer Umwelt.* Springer-Verlag, Berlin. Dritte Auflage.

Rogers, J. C. (1997). North Atlantic storm track variability and its association to the North Atlantic Oscillation and climate variability of northern Europe. *J. Climate*, 10(7):1635–1647.

Schlünzen, K. H. and Krell, U. (2004). Atmospheric Parameters for the North Sea: a Review. *Senckenbergiana Maritima*, 34(1/2):1–52.

Schluessel, P. and Emery, W. J. (1990). Atmospheric water-vapor over oceans from SSM/I measurements. *Int. J. Remote Sensing*, 11(5):753–766.

Schluessel, P. and Luthardt, H. (1991). Surface wind speeds over the north-sea from special sensor microwave imager observations. *J. Geophysical Research-oceans*, 96(C3):4845–4853.

Shaffer, S. J., Dunbar, R. S., Hsiao, S. V., and Long, D. G. (1991). A median-filter-based ambiguity removal algorithm for NSCAT. *Ieee Transactions On Geoscience Remote Sensing*, 29(1):167–174.

Sotillo, M., Ratsimandresy, A., Carretero, J., Bentamy, A., Valero, F., and Gonzalez-Rouco, F. (2005). A high-resolution 44-year atmospheric hindcast for the Mediterranean Basin: Contribution to the regional improvement of global reanalysis. *Climate Dyn.*, (25):219–236.

Swail, V. and Cox, A. (2000). On the use of NCEP/NCAR reanalysis surface marine wind fields for a long term North Atlantic wave hindcast. *J. Atmos. Oceanic Technol.*, (17):532–545.

Taylor, P. K. and Yelland, M. J. (2001). The dependence of sea surface roughness on the height and steepness of the waves. *J. Phys. Oceanography*, 31(2):572–590.

Ulaby, F. T., Moore, R. K., and Fung, A. K. (1981). *Microwave Remote Sensing: Active and Passive, Volume 1: Fundamentals and Radiometry*. Addison-Wesley, Boston.

Ulaby, F. T., Moore, R. K., and Fung, A. K. (1982). *Microwave Remote Sensing: Active and Passive, Volume 2: Radar Remote Sensing and Surface Scattering and Emission Theory*. Addison-Wesley, Boston.

Ulbrich, U., Fink, A. H., Klawa, M., and Pinto, J. G. (2001). Three extreme storms over europe in december 1999. *Weather*, 56(3):70–80.

van der Hoven, I. (1957). Power spectrum of horizontal wind speed in the frequency range from 0.0007 to 900 cycles per hour. *Journal of Meteorology*, 14:160–164.

von Storch, H., Langenberg, H., and Feser, F. (2000). A spectral nudging technique for dynamical downscaling purposes. *Mon. Wea. Rev.*, (128):3664–3673.

von Storch, H. and Zwiers, F. (1999). *Statistical Analysis in Climate Research*. Cambridge University Press.

Waldron, K. M., Paegle, J., and Horel, J. D. (1996). Sensitivity of a spectrally filtered and nudged limited-area model to outer model options. *Monthly Weather Rev.*, 124(3):529–547.

Wallace, J. M. and Gutzler, D. S. (1981). Teleconnections in the geopotential height field during the northern hemisphere winter. *Monthly Weather Rev.*, 109(4):784–812.

Wanner, H., Bronnimann, S., Casty, C., Gyalistras, D., Luterbacher, J., Schmutz, C., Stephenson, D. B., and Xoplaki, E. (2001). North Atlantic Oscillation - Concepts and studies. *Surveys In Geophysics*, 22(4):321–382.

Wanner, H., Rickli, R., Salvisberg, E., Schmutz, C., and Schuepp, M. (1997). Global climate change and variability and its influence on Alpine climate - Concepts and observations. *Theoretical Appl. Climatology*, 58(3-4):221–243.

Weisse, R. and Schneggenburger, C. (2002). The effect of different sea-state-dependent roughness parameterizations on the sensitivity of the atmospheric circulation in a regional model. *Monthly Weather Rev.*, 130(6):1593–1600.

Weisse, R., Storch, H., and F. Feser (2005). Northeast Atlantic and North Sea storminess as simulated by a Regional Climate Model 1958-2001 and comparison with observations. *J. Climate*, 18:465–479.

Weissman, D. E., Bourassa, M. A., and Tongue, J. (2002). Effects of rain rate and wind magnitude on SeaWinds scatterometer wind speed errors. *J. Atmospheric Oceanic Technology*, 19(5):738–746.

Wentz, F. J. (1992). Measurement of oceanic wind vector using satellite microwave radiometers. *Ieee Transactions On Geoscience Remote Sensing*, 30(5):960–972.

Wentz, F. J. (1997). A well-calibrated ocean algorithm for Special Sensor Microwave/Imager. *J. Geophysical Research-oceans*, 102(C4):8703–8718.

Wernli, H., Dirren, S., Liniger, M. A., and Zillig, M. (2002). Dynamical aspects of the life cycle of the winter storm 'Lothar' (24-26 December 1999). *Quarterly J. Royal Meteorol. Soc.*, 128(580):405–429.

WMO (1998). *Clivar Initial Implementation Plan, WMO/TD No. 869.* WMO (World Meteorological Organization).

Appendix A

Wind properties in the North Atlantic

The atmosphere is a fluid on a rotating sphere, where, with differential heating near the surface, the air is constantly in motion. Winds occur on many different spatial and temporal scales ranging from the planetary scale westerlies and the North Atlantic Oscillation (NAO) to small scale downdrafts, gusts and turbulence (Figure A.1). The dominant temporal modes of wind speed linked to the

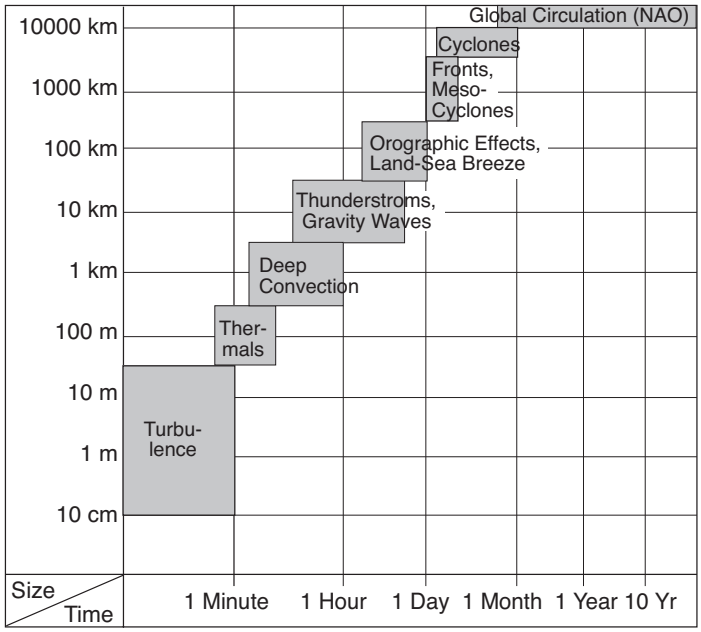

Figure A.1: *Different spatial and temporal scales of atmospheric motion.* ©*Schlünzen and Krell (2004), used with permission.*

scales of motion can be determined from frequency spectra (e.g. van der Hoven 1957).

In this Chapter the large-scale phenomena dominant in the North Atlantic are described first. Following, an elaboration of the different layers of the Planetary Boundary Layer (PBL) and the influence of stability on the vertical wind profile are presented. Finally, effects of ocean-atmosphere and land-sea interaction relevant to this study are introduced.

A.1 The large scale

Wind is generated by the sun's differential heating of the Earth's surface. The amount of radiation reaching the Earth's Surface (the radiation flux density) is highest at the equator and lowest at the poles. Due to this imbalance, heat is transported both by atmosphere and oceans from the low latitudes polewards. Air is heated in the Innertropical Convergence Zone (ITCZ) around the equator, rises and flows polewards forming winds in the upper troposphere. As the earth is rotating, the moving air is deflected on the way to the poles by the Coriolis force. On the Northern Hemisphere winds are deflected to the right, on the Southern Hemisphere winds are deflected to the left.

The air cools on it's way to the poles and sinks in the subtropics at around 30° latitude, resulting in near-surface high-pressure areas. From the high pressure regions the air flows to low pressure regions, on the one hand back to the Equatorial Low forming the Trade Winds and, on the other hand, to subpolar low pressure areas at a latitude of about 60° forming the dominating southwesterly winds in Central Europe. Large-scale meridional vacillation of the westerlies and atmospheric mass between the North Atlantic regions of the subtropical anticyclone near the Azores and the subpolar low pressure system near Iceland is described by the North Atlantic Oscillation (e.g. Wanner et al. 2001). It is a major source of seasonal to interdecadal variability in the worldwide atmospheric circulation (Hurrell, 1995) and represents one of the best studied "teleconnections" (some authors prefer the term "anomaly pattern" in this context; Wallace and Gutzler 1981; Kushnir and Wallace 1989) of the North Atlantic-European area (Hurrell and van Loon 1997; Kapala et al. 1998), where it is most pronounced in winter when the average pressure over Iceland is very low.

There are different definitions for the state of the NAO, one of them, the North Atlantic Oscillation Index (NAOI), is the sea-level pressure difference between 2 stations situated close to the "centres of action" over Iceland and the Azores. Stykkisholmur (Iceland) is often used as the northern station, whereas either Ponta Delgada (Azores, e.g. Rogers 1997), Lisbon (Portugal, Hurrell 1995) or

Gibraltar (see Jones et al. 1997) are used as the southern station for various reasons. The choice of the southern station can make some differences especially in seasons other than winter (see Jones et al. 1997).

The NAOI is widely used as a general indicator for the strength of the westerlies over the eastern North Atlantic and western Europe and, most importantly, for winter climate in Europe (Hurrell and van Loon 1997; Wanner et al. 1997; WMO 1998). The SLP distribution over the North Atlantic for the positive NAO mode (NAO+) has a well developed Icelandic Low and Azores High, associated with stronger westerlies over the eastern North Atlantic and the European continent (see Figure A.2). In the negative NAO mode (NAO-) the Icelandic Low and the Azores High are rather weak, thus giving rise to reduced westerlies over the eastern North Atlantic as depicted in Figure A.3

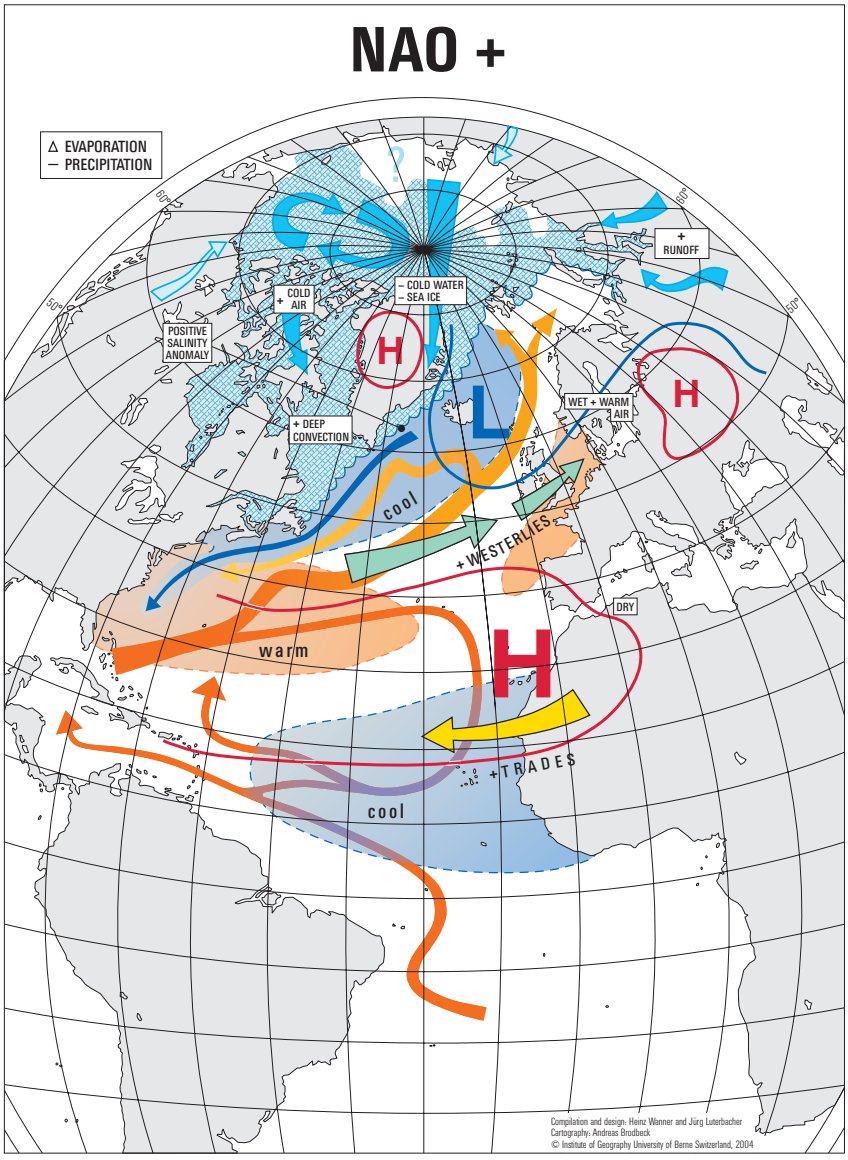

Figure A.2: *Graphical representation of the positive mode of the NAO (NAO+). Surfaces mark SSTs and sea-ice extension, arrows show the flow systems in ocean, atmosphere and rivers, blue and red lines indicate near surface sea level pressures and white rectangles describe characteristic climate conditions or important processes. (©Institute of Geography, University of Bern, Switzerland, 2004, compilation: Heinz Wanner and Jürg Luterbacher, used with permission).*

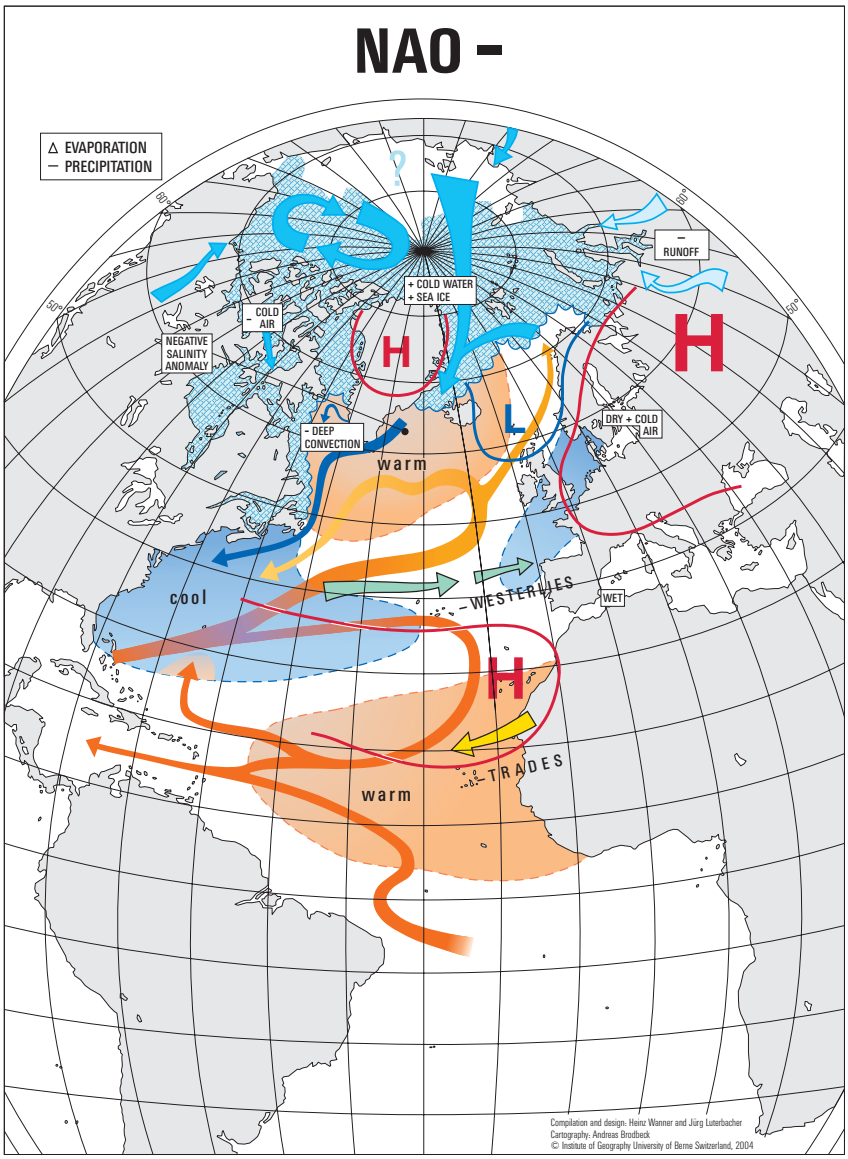

Figure A.3: *Negative mode of the NAO (NAO-), as Figure A.2*

A.2 Layers of the lower atmosphere and Stability

The layers of the lower atmosphere are derived from the equation of motion for fluids and gases, the Navier-Stokes equation. It is given by:

$$\frac{d\vec{v}}{dt} = \frac{\partial \vec{v}}{\partial t} + \left(\vec{v} \cdot \vec{\nabla}\right) \vec{v} = -\frac{1}{\rho}\vec{\nabla} p + \vec{g} - 2\vec{\Omega} \times \vec{v} + \vec{F}_R \tag{A.1}$$

where

$\frac{d\vec{v}}{dt}$	the total time derivative of the velocity vector $\vec{v}$
$\frac{\partial \vec{v}}{\partial t}$	the partial time derivative of $\vec{v}$
$\left(\vec{v} \cdot \vec{\nabla}\right) \vec{v}$	change of $\vec{v}$ due to advection
$-\frac{1}{\rho}\vec{\nabla} p$	the pressure gradient force
$\vec{g}$	gravitation
$-2\vec{\Omega} \times \vec{v}$	Coriolis force
$\vec{F}_R$	Friction

Scale analysis of synoptic scale motions, with a diameter of approximately 1000 km, shows that for the horizontal equations of motion the Coriolis force and the pressure gradient force are dominant, while the time derivative and the horizontal Coriolis-force term attached to the vertical wind speed component can be neglected. It is plausible to assume that above a certain atmospheric layer at the surface, surface friction is negligible. The friction free layer is called the Free Atmosphere and sits on top of the Planetary Boundary Layer (PBL), in which the surface friction is not negligible. Under these assumptions the horizontal wind speed in the free atmosphere can be approximated by

$$f\vec{k} \times \vec{v}_H \;\; = \;\; -\frac{1}{\rho}\vec{\nabla}_H p., \tag{A.2}$$

which is known as the geostrophic approximation. This approximation implies that the pressure gradient force is perpendicular both to the horizontal wind speed vector $\vec{v}_H$ and the vertical unity vector $\vec{k}$. Thus $\vec{v}_H$ flows parallel to the isobars and the Coriolis force acting on the wind is merely balanced by the horizontal pressure gradient force. Winds following that approximation are called geostrophic. Observations have shown that the wind in the free atmosphere follows the geostrophic approximation very closely, especially for mid- and high-latitudes (towards the equator the geostrophic balance becomes less useful as the Coriolis parameter approaches zero resulting in the collapse of the Coriolis force at the equator).

Within the PBL the flow is influenced by friction resulting from the wind speed

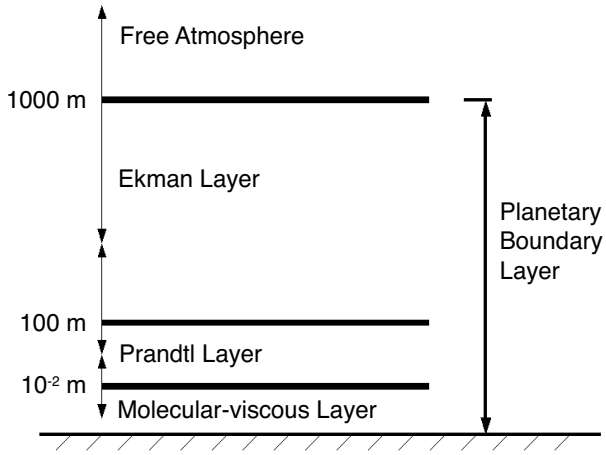

Figure A.4: *Schematic illustration of the Planetary Boundary Layer (PBL). The PBL consists of the viscous layer at the bottom and the Prandtl and Ekman layers. The heights of the layers can strongly deviate from the given average heights. The Free Atmosphere resides on top of the PBL.*

gradient between the bottom ($\vec{v} = 0$) and the geostrophic wind speed in the free atmosphere. Friction can be either molecular (viscous) or turbulent. The PBL can be divided into three layers, as depicted in Figure A.4. In the viscous layer at the ground, the dynamics of the laminar flow is determined by molecular viscosity. The thickness of the viscous layer is in the order of millimeters (Roedel, 2000). In the Prandtl Layer the dynamics are mostly governed by turbulent friction. The Ekman layer forms the transition between just friction (Prandtl Layer) and no friction (Free Atmosphere) layers.

In the Prandtl Layer (often also referred to as surface layer) the dynamics can be aproximated to be governed entirely by turbulent friction, which leads to a transfer of momentum. As the downward vertical flux of horizontal momentum due to the wind speed shear is dominant in the Prandtl Layer, the turbulent friction $\vec{F}_R$ can be approximated by

$$\vec{F}_R \approx \vec{F}_{RH} = (F_{RX}, F_{RY}, 0) = (\frac{\partial \tau_{xz}}{\partial z}, \frac{\partial \tau_{yz}}{\partial z}, 0),$$

where τ_{xz} and τ_{xz} are the vertical fluxes of the zonal and meridional components of momentum. Assuming a stationary flow and the negligibility of other forces besides the turbulent friction, $\vec{F}_{RH}$ leads to the following simplified equation of

motion for the Prandtl Layer:

$$0 = \vec{F}_{RH} = -\frac{\partial \tau}{\partial z}, \Rightarrow \tau = const$$

meaning that the downward vertical momentum flux is constant within the Prandtl Layer. As $\tau \sim const$ if

$$\Delta z \cdot \frac{\partial \tau}{\partial z} \ll \tau \tag{A.3}$$

holds, it is possible to derive an upper limit of the thickness Δz of the Prandtl Layer. According to Roedel (2000) the thickness of the Prandtl Layer is a maximum of 100 m but usually less.

The Ekman Layer forms the transition between the free atmosphere above, governed by the geostrophic approximation, and the Prandtl Layer below, governed by turbulent friction. Thus the three dominant forces in the Ekman Layer are the pressure gradient, the Coriolis and the turbulent friction forces. As the wind speed is decreasing from the geostrophic wind speed in the free atmosphere downwards, the Coriolis force, being proportional to the wind speed, decreases too, leading to a decreasing downward deflection of the wind direction. Consequently the wind direction turns, forming a spiral, which is named after Ekman who described the spiral mathematically for both the surface and bottom layers of the oceans. The mathematical description of the Ekman spiral (Ekman, 1905) is also valid for the planetary boundary layer of the atmosphere. The graphical representation is depicted in Figure A.5.

The dampening influence of the friction on the Coriolis force is therefore responsible for the surface wind direction being 45° to the left of the geostrophic wind direction in the free atmosphere. The geostrophic westerlies leave their imprint at the surface as southwesterlies, the dominating surface winds in Central Europe. This wind direction change occurs above the Prandtl Layer. Within the Prandtl Layer the Coriolis force is negligible and therefore the wind direction can be considered constant, which can also be inferred from Figure A.5.

Usually when near-surface wind speeds of different observations/products have to be compared, they have to be converted from the varying measurement heights to one comparison level. This conversion can only be done when the vertical wind speed profile is known, which most often is not the case. However, if the stability of the atmosphere can be determined, Monin-Obukhov-similarity theory (Monin and Obukhov, 1954) delivers estimations of the vertical wind speed profile within the Prandtl Layer. The stability of the atmosphere is the tendency of an air parcel to move vertically, following an initial dislocation (up or down).

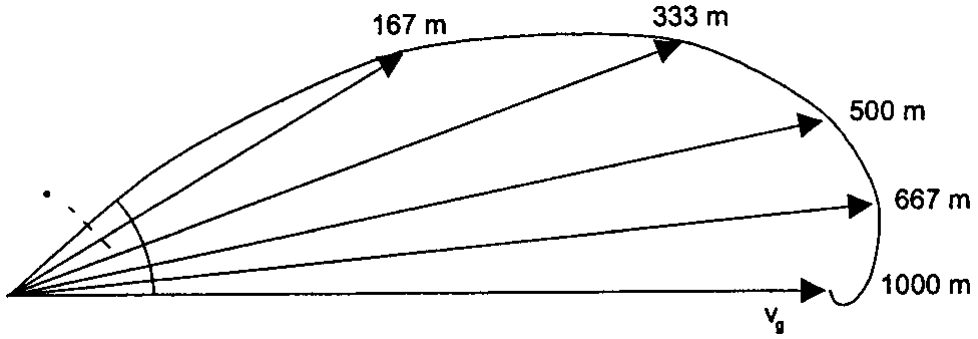

Figure A.5: *The Ekman spiral describes the wind direction deflection and wind speed decrease from the geostrophic wind speed v_g at the PBL/Free Atmosphere border ($\approx$ 1000 m) towards $\vec{v} = 0$ at the surface.*

Resulting temperature differences between an air parcel and its surrounding lead to density differences and thus to buoyancy forces in upward or downward direction. For instance, if an air parcel is dislocated upwards (e.g. by turbulance) and is denser/lighter than the surrounding, it will continue rising (sink back to its original level) and the atmosphere is said to be unstable (stable). If the air parcel stays at its new level after the vertical dislocation, the atmosphere is said to be neutrally stable. In an unstable atmosphere turbulence is amplified and thus stronger upper level wind speeds can penetrate deeper towards the surface strongly reducing the wind shear. On the other hand in case of a stable stratification of the atmosphere turbulence is suppressed and wind shear is high.

According to the similarity theory of Monin and Obukhov (1954), which is valid for the Prandtl Layer only, the vertical wind speed profile for all stratifications is given by the log-linear wind speed profile

$$u(z) = \frac{u_*}{\kappa}\left[\ln(\frac{z}{z_0}) - \Psi(\frac{z}{L})\right], \tag{A.4}$$

where $u(z)$ is the wind speed at height z above ground level, z_0 is the surface roughness length, κ is the von Kármán constant with a value of 0.40 and u_* is the so called friction velocity related to the surface stress τ through the definition

$$u_* \equiv \left(\frac{\tau}{\rho}\right)^{1/2},$$

where ρ is the air density. The stability-dependent profile function $\Psi(\frac{z}{L})$ is a function of the inverse of the Monin-Obukhov length scale L, which itself is a

measure for stability. After Paulson (1970) and Businger et al. (1971) it is given for stable and neutral stratification by

$$\Psi(\frac{z}{L}) = -4,7 \cdot \frac{z}{L} \quad \text{for} \quad z/L > 0 \quad \text{(stable)}$$
$$\Psi(\frac{z}{L}) = 0 \quad \text{for} \quad z/L = 0 \quad \text{(neutral)}. \tag{A.5}$$

In case of an unstable stratification ($\frac{z}{L} < 0$) it is

$$\Psi(\frac{z}{L}) = 2\ln\left(\frac{1+x}{2}\right) + \ln\left(\frac{1+x^2}{2}\right) - 2\arctan(x) + \frac{\pi}{2}.$$

with $x = 1/\Phi(z/L)$ and $\Phi(\frac{z}{L}) = (1 - 15z/L)^{1/4}$ after Businger et al. (1971).

In the case of a neutrally stable Prandtl Layer the log-linear wind speed profile simplifies to the logarithmic wind speed profile

$$u(z) = \frac{u_*}{\kappa} \ln \frac{z}{z_0}. \tag{A.6}$$

With its help and one known wind speed, the complete vertical wind speed profile can be calculated by

$$\frac{u(z_1)}{u(z_2)} = \frac{\ln z_1/z_0}{\ln z_2/z_0}. \tag{A.7}$$

For instance, consider a wind speed of $u = 1$ m/s in an altitude $z_2 = 10$ m and a roughness length z_0=0.03 m. The wind speed in 50 m can be calculated with Equation (A.7) as

$$u(50m) = 1\text{m/s} \cdot \frac{\ln 50/0.03}{\ln 10/0.03} \simeq 1.28\text{m/s}$$

Using the inverse Monin-Obukhov length as stability criteria, the vertical wind profile is found to be neutral during half of the time at the metmast FINO in the North Sea (Kay Sušelj, University of Oldenburg, ForWind, pers. comment). 34 % of all investigated profiles were unstable and 16% stable.

A.3 Ocean-Atmosphere and Land-Sea Effects

Usually surface roughness of the sea is low compared to land surfaces, but in contrast to land it is not constant. Instead, it depends on the wave field present, which in turn depends on wind speed, upstream fetch (distance to coast), water depth, etc. The most widely used description of z_0 at sea is the Charnock-relation

(Charnock, 1955)

$$z_0 = z_{ch}\frac{u_*^2}{g}, \tag{A.8}$$

where $z_{ch} \approx 0.01$ is the empirically derived Charnock parameter. Several other models have been proposed, relating z_0 to wave age, wave steepness or fetch in addition (e.g., Johnson et al. 1998; Taylor and Yelland 2001; Lange et al. 2001).

The stability of the marine surface layer is strongly influenced by the underlying water body. While the surface layer is most often neutrally stratified as observed from measurements (e.g., Edson and Fairall 1998), the evaporation of sea water increases air humidity and has thus a potentially destabilizing influence on the surface layer (through release of latent heat). The surface layer tends to become unstable especially if cooler air resides over comparatively warmer sea water. In contrast, warmer air over a cooler sea surface is stabilized. Thus humidity and the air and sea temperatures are important for marine surface stability and wind speed profile determination.

Diurnal variabilities in wind speed due to sea-breezes play a noticeable role in coastal regions (e.g. Mostovoy et al. 2005). A sea-breeze, or onshore breeze, is often oberved in late spring and summer and is formed by increasing temperature differences between the land and water. The air rises over the land due to its relative warmth and forces higher pressure, cooler air from the sea to move inland. The opposite phenomenon is called land-breeze and often occurs in late autumn and winter especially during nights, when air sinks over the relatively cold land and rises over the warmer sea.

According to Csanady (1974) a capping inversion might develop, when warm air is advected over colder water. The air below the capping inversion is constantly cooled by the water and gradually develops into a well-mixed layer with near-neutral stratification. The theory by Csanady (1974) offers a qualitative explanation for wind speed profiles measured at the metmast Rødsand in the Baltic Sea (Lange et al., 2004).

Appendix B

Change in Reanalysis forcing and Homogeneity

For both SN-REMO and STD-REMO hindcasts a change in the reanalysis forcing was necessary. Due to an unresolved compatibility issue between the NRA_R1 and the REMO preprocessor, both STD-REMO and SN-REMO are forced with the NRA_R2 from March 1997 onwards. SN-REMO and STD-REMO are driven with the NRA_R1 until February 1997 and this change in forcing may cause inhomogeneities.

On the one hand, the change of reanalysis forcing at the lateral boundaries may affect the homogeneity of the STD-REMO and SN-REMO hindcasts. On the other hand, the reanalysis forcing change may lead to an inhomogeneity in SN-REMO, as the origin of the large-scale horizontal wind speed components, nudged in the interior above 850 hPa, also changes from NRA_R1 to NRA_R2. However, there are arguments for both effects to be small. In general, the NRA_R1 and NRA_R2 reanalyses should show very high agreement as very similar data is assimilated. This is the case especially for the investigated area with a dense observation network. Furthermore, using the cyclone tracking algorithm by Hoskins and Hodges (2002, 2005), Bromwich et al. (2007) showed in an intercomparison of three different reanalyses (NRA_R1, ERA40 and JRA-25, for the latter see Onogi et al. 2005) that there is strong agreement throughout the full reanalysis period in the Northern Hemiphere, both for the cyclone intensity distribution and direct reanalysis-to-reanalysis cyclone matching.

After a closer look on the spectral nudging method, it is discussed to what extent SN-REMO might be affected by the change of the reanalysis forcing.

B.1 A closer look on spectral nudging

Differing from the standard approach, the forcing in the spectral nudging technique proposed by von Storch et al. (2000) is not only stipulated at the lateral boundaries, but also in the interior. The basic assumption behind the spectral nudging method is, that both the global model (the reanalysis) and the regional model have two spatial scale domains, that, due to their spatial resolution, can be modelled with different skillfulness: A large-scale spatial domain that is well resolved and a small-scale domain that is insufficiently resolved. von Storch et al. (2000) have high confidence in the large-scale domain of the reanalysis which is supported by data assimilation. Thus, where the well resolved large-scale domains of the reanalysis and the RCM overlap, the RCM should be similar to the reanalysis. For smaller scales, which cannot be resolved by the reanalysis but by the RCM, von Storch et al. (2000) believe the RCM may add value (see Figure B.1).

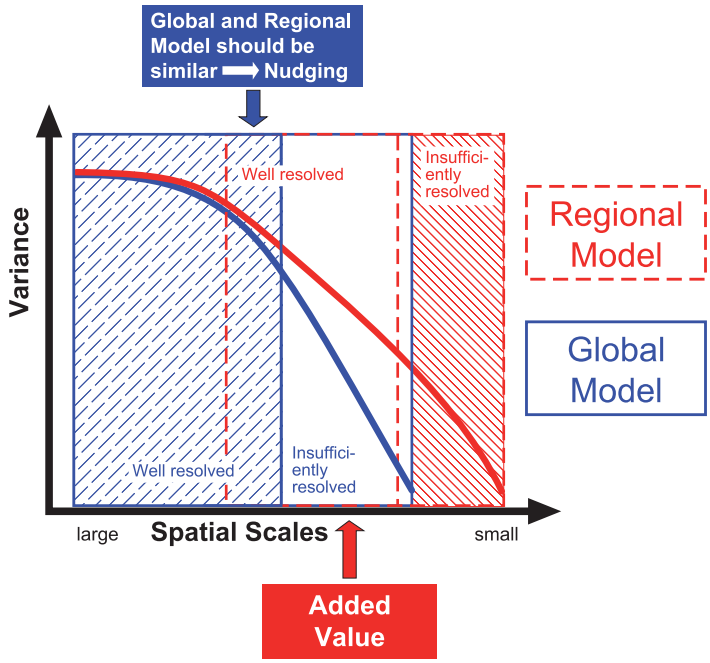

Figure B.1: *Spectral Domains of the Reanalysis and the RCM (©Frauke Feser, used with permission).*

In the spectral nudging approach the horizontal wind components above the 850 hPa level inside the integration area are forced to be close to the reanalysis for large scales, whereas smaller scales are left to be determined by the regional

model (von Storch et al., 2000). The method of von Storch et al. (2000) was applied by Feser et al. (2001) for the SN-REMO simulation used in this study. Here, this method is briefly described.

For every time step t the horizontal and vertical characteristics of the horizontal wind speed components of the SN-REMO simulation are spectrally decomposed after von Storch et al. (2000) using a Fourier expansion:

$$\Psi(\lambda,\phi,t) = \sum_{j=-J_m,k=-K_m}^{J_m,K_m} \alpha_{j,k}^{m}(t)\exp(ij\lambda/L_\lambda)\exp(ik\phi/L_\phi) \tag{B.1}$$

with zonal coordinates λ, zonal wavenumbers j and zonal extension of the area L_λ. Meridional coordinates are denoted by ϕ, meridional wavenumbers by k, and the meridional extension by L_ϕ. For REMO, the number of zonal and meridional wavenumbers is J_m and K_m and $\alpha_{j,k}^{m}$ are the Fourier coefficients (for details refer to von Storch et al. 2000 and Feser et al. 2001)

A similar expansion is done for the reanalysis. For that purpose its horizontal wind speed components are bilinearly interpolated onto the RCM grid, in the case of the SN-REMO simulation onto the 81 x 91 grid boxes with a horizontal resolution of 0.5°. Additionally the reanalysis wind speed components are time interpolated to the one hour resolution of REMO. The coefficients of the expansion are labeled $\alpha_{j,k}^{a}$. The number of reasonable zonal and meridional wavenumbers of the reanalysis J_a and K_a are smaller than the ones of REMO, as the horizontal wind speed components originate from a coarser grid.

After the determination of the Fourier coefficients, von Storch et al. (2000) nudge the SN-REMO wind speed components towards the NRA_R1 (NRA_R2 from March 1997) by adding nudging coefficients $\eta_{j,k}$ to Equation B.1:

$$\Psi(\lambda,\phi,t) = \sum_{j=-J_a,k=-K_a}^{J_a,K_a} \left(\alpha_{j,k}^{m}(t) + \eta_{j,k}\left[\alpha_{j,k}^{a}(t) - \alpha_{j,k}^{m}(t)\right]\right)\exp(ij\lambda/L_\lambda)\exp(ik\phi/L_\phi). \tag{B.2}$$

For $\eta_{j,k} = 1$ the value of the respective sinusoidal component function of SN-REMO is identical to that of the reanalysis, for $\eta_{j,k} = 0$ it will be completely determined by SN-REMO which is the desired property for small scales. In the SN-REMO simulation wave numbers of $j \geq 4$ (smaller than 90x50km/4=1125 km) in north-south direction and $k \geq 6$ (smaller than 80x50km/6=667 km) in the east-west direction were considered as small scale, thus $\eta_{j,k} = 0$.

According to von Storch et al. (2000) the confidence in the reanalysis increases with height. Additionally, they intended to leave more room to the regional model

to develop its own dynamics for lower levels, where regional geographic features become more important. Thus for large scales ($j < 4$, larger than 1500 km, $k < 6$, larger than 800 km) they have chosen a height-dependent nudging-coefficient,

$$\eta^0(p) = \begin{cases} \alpha \left(1 - \frac{p}{850hPa}\right)^2 & \text{for } p < 850hPa \\ 0 & \text{for } p > 850hPa \end{cases} \tag{B.3}$$

B.2 Effects of the change in reanalysis forcing on the SN-REMO hindcast

To judge whether an inhomogeneity in the spectrally nudged SN-REMO simulation exists due to the reanalysis change, the large-scale horizontal wind speed components of both reanalyses are compared at 500 and 850 hPa. The focus is put on the large-scale horizontal wind speed components of both reanalyses as the spectral nudging takes place for the large scales only. Furthermore, the 850 and 500 hPa levels are chosen, because the 850 hPa level forms the lower boundary of the height depending nudging scheme, while the 500 hPa level is within the spectral nudging domain (see Equation B.3).

Following the methodology of von Storch et al. (2000) the horizontal wind speed components at 850 and 500 hPa of both the NRA_R1 and NRA_R2, which were extracted from http://www.cdc.noaa.gov/, are spectrally decomposed. The spatial scale separation is carried out within the area between 20°W and 25°E and 40°N and 75°N for 1998. For that purpose a two dimensional Fourier Filter was applied on the wind speed components and the wave numbers beyond 4 (< 760 km) in the zonal and 5 (< 801 km) in the meridional domain were not considered in the Fourier composition of the spectral components.

The mean large-scale horizontal wind speed components at every grid point are averaged over the entire area (20°W - 25°E, 40°N - 75°N) and listed in Table B.1 for both reanalyses. In addition the spatial means of the standard deviation of the wind speed σ and the RMSE between NRA_R1 and NRA_R2 are given. While the mean and variances show a reasonable agreement among both reanalyses, the spatial mean of the RMSE amounts to almost 0.9 m/s. For 1998 the temporal evolution of the spatial RMSE between the low-pass filtered (large-scale) u components from NRA_R1 and NRA_R2 at 500 hPa (black) is depicted in Figure B.2. The analog time series for v is highlighted in green in the same figure. The spatial RMSE is approximately 0.9 m/s in average, with higher values during winter time. Several events with a higher spatial RMSE can be seen, with an outstanding event on 16th March 1998 at 6 am. The unfiltered wind speed (ff) and its horizontal components (u and v) are illustrated for the time of the event in Figure B.3 and for an average spatial RMSE situation one day before on the

Table B.1: *Comparison of the horizontal wind speed components u and v from both the NRA_R1 and NRA_R2 at 500 and 850 hPa within 20° W - 25° E, 40° N - 75° N in 1998. The spatial average of the means and standard deviations σ at every grid point is listed. The RMSE between NRA_R1 and NRA_R2 is given as spatial average, too.*

	500 hPa		850 hPa	
	u [m s^{-1}]	v [m s^{-1}]	u [m s^{-1}]	v [m s^{-1}]
NRA_R1: mean	8.25	-0.46	3.20	0.12
NRA_R2: mean	8.27	-0.46	3.16	0.23
bias	0.03	0.00	-0.05	0.11
NRA_R1: σ	10.96	10.81	7.39	6.86
NRA_R2: σ	10.95	10.80	7.29	6.86
spatial mean of RMSE	0.86	0.86	0.87	0.87

15th March 1998 at 6am in Figure B.4. On the 16th of March at 06:00 large differences of up to 10 m/s occur for the wind speed and its horizontal components, with the wind speed of the NRA_R2 at 500 hPa being up to 10 m s^{-}1 stronger than that of the NRA_R1 north of Scotland due to a stronger horizontal pressure gradient in that area (not shown).

Although these single events occur in the large-scale horizontal wind components above 850 hPa, it is unclear how they affect the circulation pattern and the surface marine wind speed of the spectrally nudged hindcasts. So far, it cannot be fully assessed whether SN-REMO is inhomogeneous due to the change in reanalysis forcing. A more detailed investigation with two SN-REMO hindcasts, one driven with the NRA_R1 and the other with the NRA_R2 for an overlapping period, is necessary but beyond the scope of this thesis.

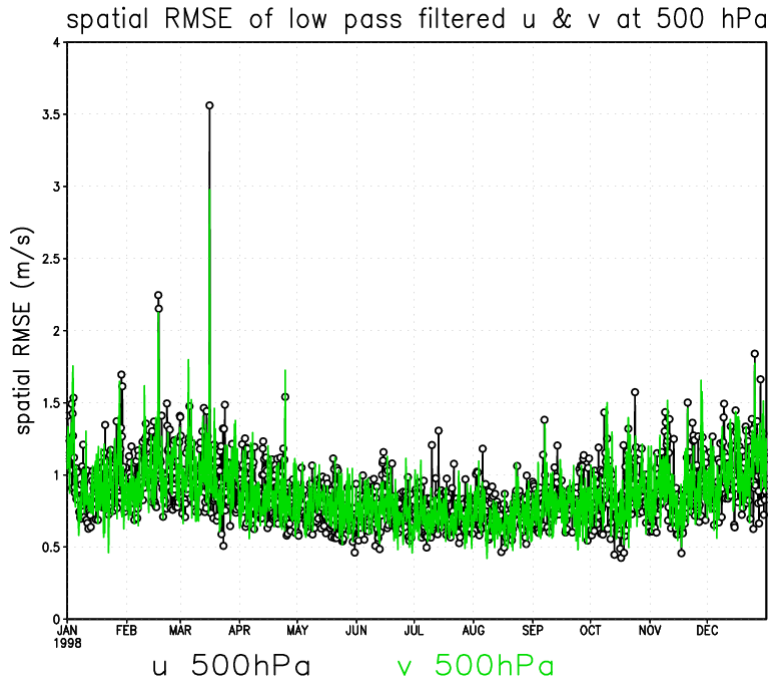

Figure B.2: *time series of spatial RMSE between u (black) and v (green) components from NRA_R1 and NRA_R2 reanalyses at 500 hPa for low pass filtered u and v components. High RMSE event on 16th March at 6am.*

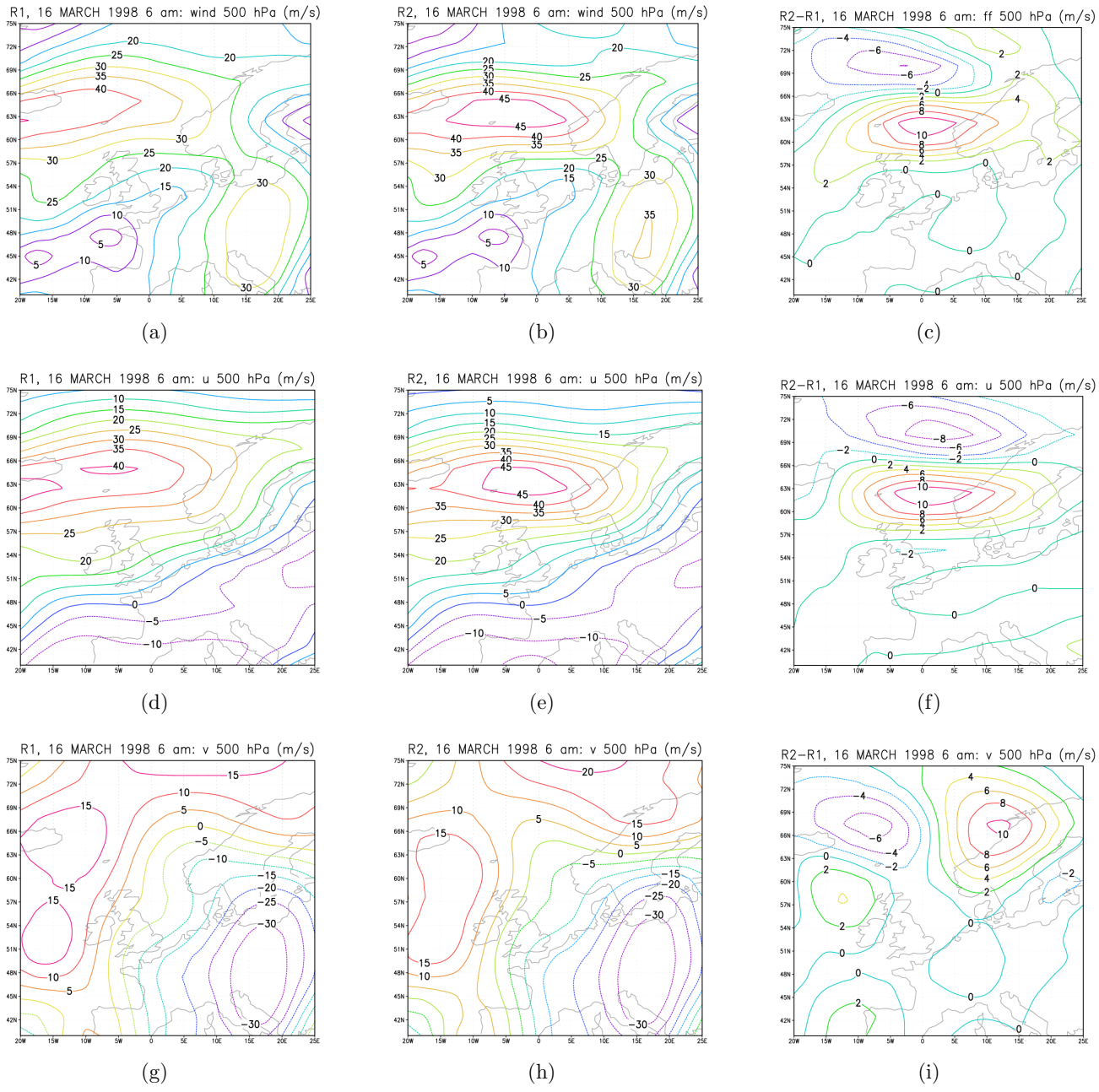

Figure B.3: *Wind speed (top row) and its u (middle) and v (bottom) components at 500 hPa from NRA_R1 (left panel) and NRA_R2 (middle panel) reanalyses on 16th March at 6am. The right panel shows the differences.*

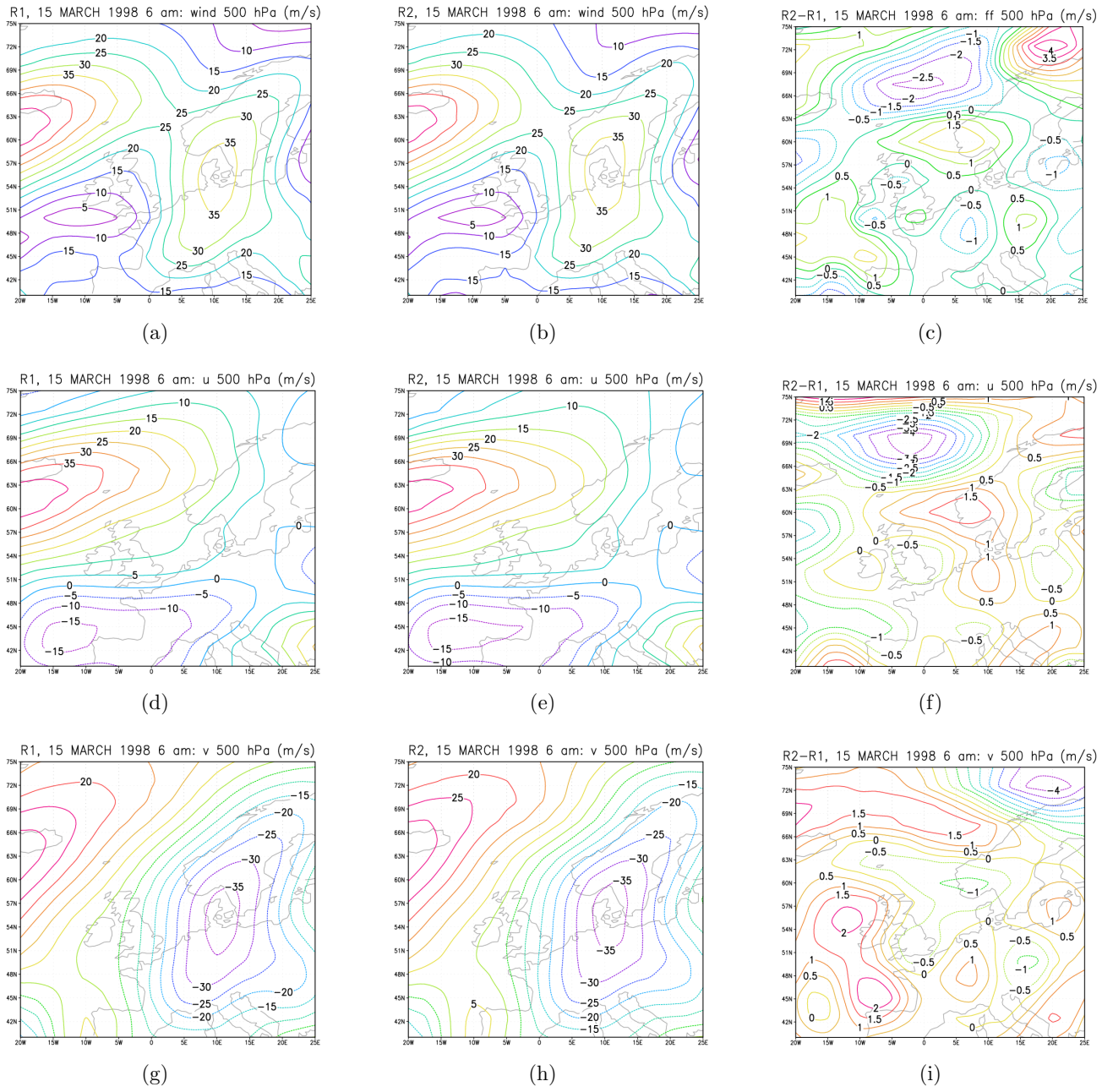

Figure B.4: *wind speed (top row) and its u (middle) and v (bottom) components at 500 hPa from NCEP/NCAR (left panel) and NCEP/DOE II reanalyses (middle panel) on 15th March at 6am. The right panel shows the differences.*

***Wetzel, P*.** (2005): **Interannual and Decadal Variability in the Air-Sea Exchange of CO_2.**
Reports on Earth System Science, Max Planck Institute for Meteorology, No. 7/2004, pp. 77

Stier, P. (2005): **Towards the Assessment of the Aerosol Radiative Effects - A Global Modelling Approach.** Reports on Earth System Science, Max Planck Institute for Meteorology, No. 9/2004, pp. 111

Zuo, X. (2005): **Annual Hard Frosts and Economic Growth.**
Department of Economics, University of Hamburg, Hamburg, pp. 112

Jung, M. (2005): **Carbon sequestration options in the international climate regime.**
Department of Economics, University of Hamburg, Hamburg, pp. 119

Zhou, Y. (2005): **Economic Analysis of Selected Environmental Issues in China**
Department of Economics, University of Hamburg, Hamburg, pp. 101

Devasthale, A. (2005): **Aerosol Indirect Effect in the Thermal Spectral Range as Seen from Satellites**
Reports on Earth System Science, Max Planck Institute for Meteorology, No. 16/2005, pp. 70

Zandersen, M. (2005): **Aerosol Valuing Forest Recreation in Europe: Time and Spatial Considerations**
Department of Economics, University of Hamburg, Hamburg, pp. 125

Xuefeng Cui (2005***): Interactions between Climate and Land Cover Changes on the Tibetan Plateau***
Reports on Earth System Science, Max Planck Institute for Meteorology, No. 17/2005, pp. 125

Stehfest, Elke (2005***): Modelling of global crop production and resulting N_2O emissions***
Zentrum für Umweltsystemforschung Universität Kassel pp. 125

Kloster, Silvia (2006***): DMS cycle in the ocean-atmosphere system and its response to anthropogenic perturbations.*** Reports on Earth System Science, Max Planck Institute for Meteorology, No. 19/2006, pp. 82

Criscuolo, Luca (2006***): Assessing the Agricultural System and the Carbon Cycle under Climate Change in Europe using a Dynamic Global Vegetation Model***
Reports on Earth System Science, Max Planck Institute for Meteorology, No. 21/2006, pp. 140

Tiwari, Yogesh Kumar (2006***): Constraints of Satellite Derived CO_2 on Carbon Sources and Sinks***
Technical Reports, Max-Planck-Institut für Biogeochemie, No.7/2006, pp.125

Schurgers, Guillaume (2006***): Constraints Long-term interactions between vegetation and climate - Model simulations for past and future -*** Reports on Earth System Science, Max Planck Institute for Meteorology, No. 27/2006, pp. 135

Ronneberger, Kerstin Ellen (2006***): The global agricultural land-use model KLUM - A coupling tool for integrated assessment -*** Reports on Earth System Science, Max Planck Institute for Meteorology, No. 26/2006, pp. 123

Woth, Katja (2006***): Regionalization of global climate change scenarios: An ensemble study of possible changes in the North Sea storm surge statistics***
Department for Earth Sciences, University of Hamburg, Hamburg, pp. 97

Hoelzemann, Judith Johanna (2006***): Global Wildland Fire Emission Modeling for Atmospheric Chemistry Studies***
Reports on Earth System Science, Max Planck Institute for Meteorology, No. 28/2006, pp. 206

Gaslikova, Lidia (2006***): High-resolution wave climate analysis in the Helgoland area***
Department for Earth Sciences, University of Hamburg, Hamburg, pp. 90

Grossmann, Iris (2006***): Future perspectives for the Lower Elbe Region 2005–2030: Climate Trends and Globalisation***
GKSS-Forschungszentrum, Geesthacht, pp. 175

Narayan, Caroline (2006*)*: **CO2 fluxes and concentration patterns over Eurosiberia: A study using terrestrial biosphere models and the regional atmosphere model REMO**
Reports on Earth System Science, Max Planck Institute for Meteorology, No. 29/2006, pp. 242

Vizcaino, Miren (2006): **Long-term interactions between ice sheets and climate under anthropogenic greenhouse forcing Simulations with two complex Earth System Models**
Reports on Earth System Science, Max Planck Institute for Meteorology, No. 30/2006, pp. 187

Schwoon, Malte (2006): **Managing the Transition to Hydrogen and Fuel Cell Vehicles – Insights from Agent-based and Evolutionary Models –**
Reports on Earth System Science, Max Planck Institute for Meteorology, No. 32/2006, pp. 132

Link, Peter Michael (2006): **Modeling the economic impacts of changes in thermohaline circulation with an emphasis on the Barents Sea fisheries**
Reports on Earth System Science, Max Planck Institute for Meteorology, No. 33/2006, pp. 185

Li, Qian (2006): **Climatological analysis of planetary wave propagation in Northern Hemisphere winter**
Reports on Earth System Science, Max Planck Institute for Meteorology, No. 35/2006, pp. 153

Weis, Philipp (2006): **Ocean Tides and the Earth's Rotation - Results of a High-Resolving Ocean Model forced by the Lunisolar Tidal Potential**
Reports on Earth System Science, Max Planck Institute for Meteorology, No. 36/2006, pp. 115

Heistermann, Maik (2006): **Modelling the Global Dynamics of Rain-fed and Irrigated Croplands**
Reports on Earth System Science, Max Planck Institute for Meteorology, No. 37/2006, pp. 152

Kristina Trusilova (2006): **Urbanization impacts on the climate in Europe**
Technical Reports, Max Planck Institute for Biogeochemie, No. 9/2006, pp. 82

Xiuhua Zhu (2007): **Low frequency variability of the Meridional Overturning Circulation**
Reports on Earth System Science, Max Planck Institute for Meteorology, No. 39/2007, pp. 158

Christoph Müller (2007): **Climate Change and Global Land-Use Patterns — Quantifying the Human Impact on the Terrestrial Biosphere**
Reports on Earth System Science, Max Planck Institute for Meteorology, No. 41/2007, pp. 126

Sven Kotlarski (2007): **A Subgrid Glacier Parameterisation for Use in Regional Climate Modelling**
Reports on Earth System Science, Max Planck Institute for Meteorology, No. 42/2007, pp. 179

Daniela Matei (2007): **Decadal Variability: Internal Variability and Sensitivity to Subtropics**
Reports on Earth System Science, Max Planck Institute for Meteorology, No. 44/2007, pp. 107

Adetutu Aghedo (2007): **The impact of african air pollution: A global chemistry climate model study**
Reports on Earth System Science, Max Planck Institute for Meteorology, No. 45/2007, pp. 142

Melissa Anne Pfeffer (2007): **The Relative Influences of Volcanic and Anthropogenic Emissions on Air Pollution in Indonesia as Studied With a Regional Atmospheric Chemistry and Climate Model**
Reports on Earth System Science, Max Planck Institute for Meteorology, No. 46/2007, pp. 119

Felix Landerer (2007): **Sea Level and Hydrological Mass Redistribution in the Earth System: Variability and Anthropogenic Change**
Reports on Earth System Science, Max Planck Institute for Meteorology, No. 47/2007, pp. 115

Angelika Heil (2007): **Indonesian Forest and Peat Fires: Emissions, Air Quality, and Human Health**
Reports on Earth System Science, Max Planck Institute for Meteorology, No. 50/2007, pp. 142

Manu Anna Thomas (2008): **Simulation of the climate impact of Mt. Pinatubo eruption using ECHAM5**
Reports on Earth System Science, Max Planck Institute for Meteorology, No. 52/2008, pp. 161

Martin Jung (2008): **Uncertainties of terrestrial carbon cycle modelling: Studies on gross carbon uptake of Europe**
Technical Reports - Max Planck Institute for Biogeochemistry, No. 11/2008, pp. 142